1-1-1991

Modelling of flocculation kinetics in water treatment

Ningning Wang
Iowa State University

Modelling of flocculation kinetics in water treatment

by

Ningning Wang

A Thesis Submitted to the
Graduate Faculty in Partial Fulfillment of the
Requirement for the Degree of
MASTER OF SCIENCE

Department: Civil and Construction Engineering
Major: Civil Engineering (Sanitary Engineering)

Approved:

niversity
Ames, Iowa

1991

TABLE OF CONTENTS

LIST OF TABLES

LIST OF FIGURES

NOMENCLATURE

a	Radius of particle
B	Breakup constant
c	The unit of electrical charge
C_1	Constant
C_2	Constant
D	Diffusion coefficient of particle
d	Diameter of floc
D_T	Turbulent diffusion coefficient
D_{eff}	Effective turbulent diffusion coefficient
du	Change in fluid velocity per unit distance dz
E	Electric field strength
E_L	Largrangian energy spectrum
e_f	entrainment factor
$E(k,t)$	Kinetic energy
f	Frequency
f_λ	Eddy frequency
G	mean velocity gradient
k	Boltzmann's constant
k_a	Constant
k_b	Floc breakup constant
k_d	Wave number associated with the size of eddies that provide the main contribution to the total energy dissipation
k_e	Wave number associated with the size of eddies which contain the majority of the energy
k_F	Flocculation rate constant

k_0	Flocculation rate constant employed in new models
k_p	Constant
k_s	Proportionality coefficient
m	Floc breakup rate exponent
n	Particle number concentration
n_1	Primary particle number concentration
n_{10}	Initial primary particle concentration
n_F	Floc number concentration
p	Total energy input
R	Radius of particle
R_F	Radius of floc
R_1	Radius of primary particle
R_{ij}	Collision radius for the pair of particles i and j
SSA	Sum of squares due to factor A
SSAB	Sum of squares due to interaction of A and B
SSB	Sum of squares due to factor B
SSE	Sum of squares due to error
T	Absolute temperature
t	time
TSS	Total sum of squares
$\overline{u^2}(d)$	Square of difference of velocity between two points distance d apart
u_k	Eddy velocity
$\overline{u^2}$	Mean square velocity fluctuation
V	Water volume
v	Particle velocity

Y_{iA}	Average of observations receiving ith level of A
Y_{jB}	Average of observations receiving jth level of B
Y_{ij}	Average of observations receiving ith level of A and jth level of B
Yijk	Observations of kth replication at ith level of A and jth level of B

Greek Symbols:

α	Collision efficiency function
β	Size distribution function of the suspension
$\beta(i,j)$	Collision frequency function
ϵ	Total energy dissipation/unit time/unit mass
η	Kolmogorov microscale
λ	Size of the fluid mass moving with a frequency f
τ	Surface shear yield strength
τ_0	Characteristic time
Φ	Floc volume fraction
μ	Fluid absolute viscosity
ξ	Zeta potential
ρ	Density of the fluid
ρ_s	Density of the particle
υ	The kinematic viscosity of the fluid
λ	Eddy scale
ζ	Mean square velocity constant in viscous dissipation subrange

ABBREVIATIONS

Automatic image analysis	AIA
centimeter	cm
cubic centimeter	cm^3
cubic inch	in^3
cubic millimeter	mm^3
degree Celsius	^oC
feet	ft
gram(s)	g
liter(s)	l
milligram(s)	mg
pound(s)	lb
square inch	in^2
square centimeter	cm^2
square millimeter	mm^2

I. INTRODUCTION AND OBJECTIVES

The contaminants in surface water can be classified into settleable material, suspended material, colloidal material and dissolved material based on their physical characteristics.

The settleable and suspended substances can be removed by sedimentation and filtration processes in water treatment plants. The colloidal particles will not be separated from water by gravity sedimentation. They are so small (in the size range of 0.1 μm to 1 or 2 μm) that they pass through the pores of most common filtration media. To be removed, the individual colloids must aggregate and grow in size. In water treatment plants, coagulation and flocculation are specifically designed for the removal of those colloidal particles.

Coagulation is the process to destabilize colloidal particles in water by adding coagulants, thus inducing aggregation of the colloids. Flocculation is the process of forming flocs from the aggregation of small destabilized particles and aggregates.

Over the past several decades, the flocculation kinetics have been studied because of their practical importance in the design and operation of water clarification systems. The earliest and the most fundamental model was developed by Smoluchowski in 1917 (Smoluchowski, 1917). Later on, much work

has been done to modify and improve Smoluchowski's model.

Argaman and Kaufman (1968) developed a model for turbulent flocculation to describe the relationship between the rate of disappearance of primary particles and the system kinetic parameters - velocity gradient G and flocculation time t. Their model has been used as the guidelines for the design of coagulation and flocculation processes in water treatment (Montgomery, 1985). However, their model was derived under some assumptions that are not very reasonable (Huck and Murphy, 1978; Argaman, 1979). Argaman and Kaufman's model was tested using the flocculation data from completely mixed stirred tank reactors (CSTR) only. There are not enough supporting data from laboratory results of batch flocculation experiments. Argaman and Kaufman assumed there were only two classes of particles present in the suspension: primary particles and flocs. The flocculation rate is determined by the collision frequency between primary particles and flocs. A second thought on this issue would lead to the conclusion that the flocculation rate depends on the collision frequency between primary particles and flocs as well as on the collision rate among the primary particles themselves. The later situation is found especially true with some flocculation experiments in this study. It is therefore desirable to develop a flocculation kinetics model based on this reasoning.

The objectives of this research are as follows:

1. To verify the existing flocculation kinetics model of Argaman and Kaufman with the laboratory batch flocculation tests.

2. To develop new flocculation kinetic models based on an improvement of Argaman-Kaufman's model.

3. To verify the new models with various experimental data from the present research and data collected by other researchers.

4. To compare Argaman and Kaufman's model with the newly developed models using flocculation research data collected during this study and by other investigators.

The experimental data utilized to study the above objectives are from three different sources:

1. Experimental research of coagulation and flocculation conducted during this study.

2. Experimental results from Hanson's work (1989).

3. Experimental data collected by Argaman and Kaufman (1968).

Nonlinear data regression techniques are to be used for model verification. The job is done by using SAS - NLIN software which is available at Iowa State University Computation Center.

The following section will review some of the literature relevant to this research.

II. LITERATURE REVIEW

A. Introduction

This section discusses the background for coagulation and flocculation and modelling of flocculation kinetics. The first section of this chapter discusses briefly the literature related to coagulation and flocculation mechanisms. The second section discusses the literature related to modelling of flocculation kinetics.

B. Mechanisms of Coagulation and Flocculation

In order to better understand the mechanisms of coagulation and flocculation, the properties of the colloidal substances have to be reviewed first.

The stability of colloidal particles

The colloid is composed of one or more than one molecule. Because of its small size, it undergoes Brownian motion which makes it impossible to settle in water in a limited time. The colloidal surface takes on a net electrostatic charge (the primary charge), which may be negative or positive, due to one or more of the following:

(1) Imperfection in the crystal structure.

In certain cases, a colloidal particle may acquire a charge as a result of isomorphic replacements within the crystal lattice, resulting in a net negative charge on the particle (Fair, Geyer, and Okun, 1968). The clay particles acquire their negative charge in this manner (Van Olphen, 1977).

(2) Adsorption of ions onto the particle surface. Many colloidal particles acquire a charge as a result of the preferential adsorption of either positive or negative ions on their surface.

(3) Ion dissolution. Certain colloidal substances acquire an electric charge if the oppositely charged ions of which they are composed do not dissolve equally.

(4) Ionization of surface sites. Some proteins acquire their charge as a result of the ionization of carboxyl or amino groups. Ionization of these groups is pH dependent, and particles may exhibit a net positive charge at low pH, a net negative charge at high pH, and a net zero charge at some intermediate pH, known as the iso-electric point (Benefield, Judkins, and Weand, 1982).

The major source of colloidal particles in water is the clay particles which are usually negatively charged. To counterbalance this primary charge, opposite ions (counterions) gather around the surface of the colloid to form a cloud of counterions in the solution phase. Two opposite forces are exerted on the counterions that surround the

colloidal particle: electrostatic attraction and diffusion due to the tendency of ions to diffuse in direction of decreasing concentration (Fick's Law). These two forces produce a diffuse cloud of ions surrounding the particles which can extend up to 300 nm into the solution. The primary charge forming ions and some counterions are adsorbed to the surface of the colloidal particle surface to form a Stern layer which moves with the particle. While some other counterions outside the Stern layer tend to diffuse into solution and form the diffuse layer. The two layers are known as the electrical double layer (Montgomery, 1985; Kruyst, 1952).

A maximum electrical potential exists on the surface of colloidal material. The potential decreases as the distance from the particle surface increases. The surface of the double layer and the electrical potential curves are shown in Figure 1.

The attraction force exerted on the counterions in the diffuse layer by the colloid is very weak. When the colloid moves in solution, most counterions in the diffuse layer will not follow the movement. This give rise to the shear plane. Usually, the shear plane lies in the diffuse layer, some distance beyond the Stern layer. But in colloidal chemistry, the surface of the Stern layer is considered the shear plane. The electrical potential at shear plane is crucial to the stability of the particle. This potential is called the zeta

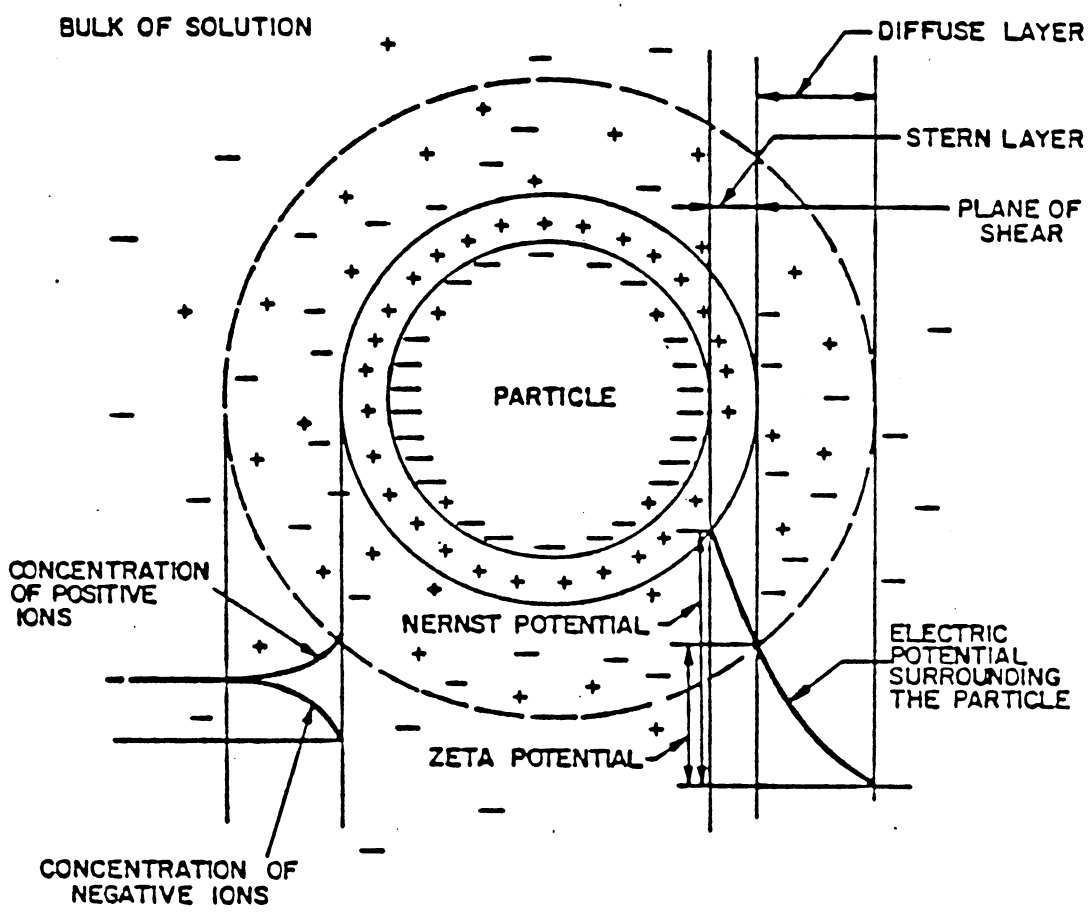

Figure 1. Theoretical representation of the double layer and the electrical potential curves (As quoted by Hanson, 1989)

potential and can be determined by electrophoresis measurement (measurement of rate of movement of the particle in an electric field) (Montgomery, 1985).

Zeta potential is calculated from the experimental measurements of the steady motion of particles under the influence of the electric field, and the following formula is used for the zeta potential calculation (van Olphen, 1977).

$$\xi = 4\pi \mu v/\epsilon E \qquad (1)$$

where

E = electric field strength (vm^{-1})

μ = liquid viscosity ($Nm^{-2}s$)

v = particle velocity (ms^{-1})

ϵ = media dielectric constant ($cv^{-1}m^{-1}$)

ξ = zeta potential (v)

c = the unit of electric charge Q

The zeta potential is usually considered as the surface charge responsible for electrostatic repulsion that prevents colloidal particles from aggregating into bigger particles. High zeta potentials suggest strong forces of separation and stable colloidal systems, whereas lower zeta potentials are associated with less stable systems.

In addition to this electrostatic repulsion, particles may also be quite stable due to the presence of adsorbed water molecules that provide a liquid barrier to successful particle collisions.

The stability of colloidal particles can be analyzed from the interaction forces between the two particles when they collide. As two similarly charged particles approach each other, their diffuse counterion atmospheres begin to interfere and cause the particles to be repulsed. The amount of work required to overcome this repulsion and bring the particles from infinite separation to a given distance apart is called the repulsive energy or the repulsive potential, V_R, at that distance. The electric potential for an individual particle decreases with distance from the particle as shown in Figure 1. Consequently, the repulsive energy between two particles decreases roughly exponentially with increasing particle separation as shown in Figure 2 (Benefield, 1982). On the other hand, an attraction force, van der Waals attraction energy (V_A), exists between the two particles and is inversely proportional to the second power of the distance separating the particles and decreases very rapidly with increasing interparticle distance (O'Melia, 1969). The combination of the two opposing forces determines the stability of colloidal particles. The curves of repulsion and attraction forces and their combinations are shown in Figure 2.

The resultant curve indicates that repulsion force predominated at certain distance of the separation, but if the particles can be brought close enough together, the van der Waal's attraction forces will predominate and the particles

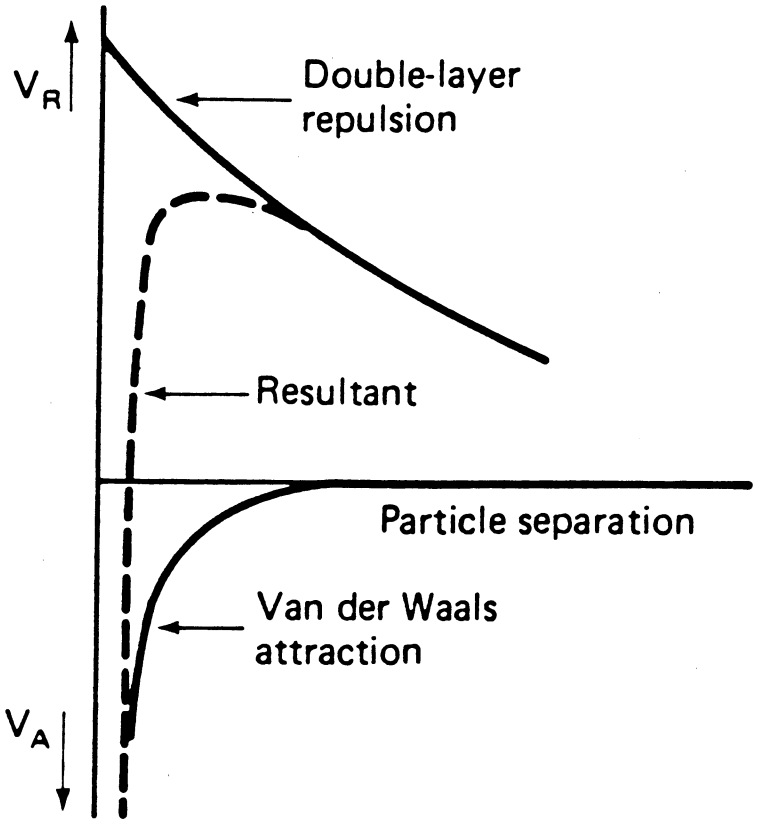

Figure 2. The relationship between the double layer repulsion and van der Waals attraction forces and the particle separation distance

will coalesce. To come together, the particles must possess enough kinetic energy to overcome the so-called energy hump on the total energy curve.

Destabilization of colloidal particles in water

As discussed in the previous section, colloidal particles remain stable in water due to the electrostatic repulsion resulting from the double layer or due to the water envelope surrounding the particles which prevent them from aggregating. In order to achieve destabilization of colloidal system, two distinct steps must occur: (1) the repulsion forces must be reduced; and (2) particle transport must be achieved to provide contacts between the destabilized particles (Benefield, Judkins, and Weand, 1982). The second step, transportation, is usually realized by stirring the suspension to the extent to provide particle interaction. And the first step, destabilization, is achieved by the following four mechanisms:

(1) Double-layer compression. The addition of electrolyte into a colloidal suspension results in the increase ionic strength in the solution and thus decreases the thickness of the diffuse layer. Due to the concentration diffusion and electrostatic attraction between opposite ions, more counterions will move inside the shear plane. As a result, the zeta potential is decreased. This process is

called double layer compression.

An interesting aspect of double layer compression is that it will not cause charge reversal, regardless of how much electrolyte is added. The charge reversal is only possible by the adsorption and charge neutralization mechanism for particle destabilization.

(2) Adsorption and charge neutralization. Some chemical species are capable of being adsorbed at the surface of colloidal particles. If the adsorbed species carry a charge opposite to that of the colloid's, such adsorption causes a reduction of surface potential and a resulting destabilization of the colloids. Unlike double layer compression, it is possible to overdose a system and cause restabilization as a result of a reversal of charge on the colloidal particle. Another distinction between adsorption and double layer compression is that destabilization by adsorption is stoichiometric. Thus the required dosage of coagulant increases as the concentration of colloids increases. While the amount of electrolyte required to achieve coagulation by double layer compression is not stoichiometric and is practically independent of colloid concentration.

(3) Interparticle bridging. Many different natural compounds such as starch, cellulose and proteineous materials as well as a wide variety of synthetic polymeric compounds are known to be effective coagulating agents. It is impossible to

explain their destabilization mechanism by double layer compression or adsorption and neutralization, because both positive (cationic) and negative (anionic) polymers are capable of destabilizing negatively charged colloidal particles. Ruehrwein & Ward (1952) and LaMer & Healy (1963) have developed a chemical bridging theory that is consistent in explaining the observed behavior of those polymeric compounds. The chemical bridging theory indicates that long-chain polymers carrying negative charges can adsorb on the particles and form bridges between particles, thus aggregating the suspension.

(4) Enmeshment (Sweep flocculation). If certain metal salts are added to water in sufficient amounts, rapid formation of precipitates will occur. Colloids may serve as condensation nuclei for these precipitates or may become enmeshed as the precipitates settle. Coagulants such as $Al_2(SO_4)_3$, $FeCl_3$, and $Ca(OH)_2$ can induce coagulation through the formation of insoluble $Al(OH)_3$, $Fe(OH)_3$, and $CaCO_3$. This mechanism is often referred to as sweep-flocculation coagulation (Benefield, et al., 1982).

Frequently, the removal mechanism in a certain colloidal-coagulant system is the combination of two or more mechanisms discussed above. According to Stumm and O'Melia (1968), aluminum (III) and iron (III) accomplish destabilization by two mechanisms: (1) adsorption & charge neutralization and (2)

enmeshment in sweep flocculation. If an aluminum (III) or iron (III) salt is added to water in concentration less than the solubility limit of the metal hydroxide, the hydrolysis products can form and adsorb onto the particles, causing destabilization by charge neutralization. When aluminum (III) or iron (III) is sufficient to exceed the solubility of the metal hydroxide, the hydrolysis products will form as kinetic intermediates in the formation of the metal hydroxide precipitates. In this situation, both charge neutralization and enmeshment contribute to coagulation. Adsorption destabilization (A/D) and sweep flocculation are probably the most frequently used mechanisms in the destabilization of colloids in water and wastewater treatment.

C. Modelling of Flocculation Kinetics

The function of coagulation is to destabilize colloidal particles in water to induce aggregation among these small particles. The aggregation rate, or the rate of flocculation (small colloidal particles grow into big flocs) depend on the successful collisions which result in aggregation among destabilized particles.

The collision rate depends on the following three major physical processes which affect the transport of small particles in water suspension: (i) Brownian or molecular

diffusion; (ii) fluid shear; (iii) and differential sedimentation.

Current understanding of flocculation kinetics stems directly from the early work of Smoluchowski (1917). The following is a summary of the major results from recent presentations (Amer. Water Works Assoc., 1990; Lawler and Han, 1989; Lawler et al., 1983; O'Melia, 1980; Gregory, 1989; Hanson, 1989).

Smoluchowski (1917) considered the binary collision between particles in an suspension and described the expected change in the number concentration of particles of any particular size. For discrete particle sizes, Smoluchowski's equation can be expressed as:

$$\frac{dn_k}{dt} = \frac{1}{2}\alpha\sum\beta(i,j)n_i n_j - \alpha n_k\sum\beta(i,k)n_i \qquad (2)$$

The two terms on the right hand side (Lawler and Han, 1989) represent the creation of particles of size k by the collision of two smaller particles (of size i and j) and the loss of such particles by their collision with others. Here, n is the number concentration of particles; i, j and k are the subscripts denoting particular particle sizes and t is time. α is a collision efficiency function. β(i,j) and β(i,k) represent the sum of collision frequency functions for different mechanisms of collision that will be discussed

later. $\beta(i,j)$ is defined as the number of collisions in unit volume per unit time.

Particle collisions occur because of Brownian motion, fluid shear, and differential sedimentation. The collision rate depends on those major processes and the collision frequency function $\beta(i,j)$ can be expressed as follows for each of the modes of particle contact:

Brownian or molecular diffusion (perikinetic flocculation)

The Smoluchowski's approach is to imagine a stationary central particle and to calculate the number of particles colliding with it in unit time by Brownian diffusion. The $\beta(i,j)$ for Brownian diffusion is thus written as:

$$\beta(i,j) = 4\pi R_{ij}(D_i+D_j) \qquad (3)$$

The term D_i, D_j are the diffusion coefficients. R_{ij} is the collision radius for the pair of particles and represents the center-to-center distance at which particles may be assumed to be in contact. Smoluchowski assumed spherical particles, radii a_i and a_j, and that $R_{ij}=a_i+a_j$. Also, for the diffusion coefficients, the Stokes-Einstein expression is used: $D_i = kT/(6\pi a_i\mu)$ in which μ is the viscosity of the fluid. Hence, $\beta(i,j)$ becomes:

$$\beta(i,j) = \frac{2kT}{3\mu}\frac{(a_i+a_j)^2}{(a_i a_j)} \qquad (4)$$

where

k = is Boltzmann's constant

T = is absolute temperature

Fluid shear (orthokinetic flocculation)

In Smoluchowski's treatment of orthokinetic flocculation, the fluid motion is laminar, the particles are assumed to follow fluid streamlines and the collision frequency depends on the size of the particles and on the velocity gradient or shear rate, du/dz. The collision frequency can be expressed as:

$$\beta(i,j) = \frac{4}{3}\frac{du}{dz}(a_i+a_j)^3 \qquad (5)$$

where

du = change in fluid velocity per unit distance, dz.

Differential settling

Particles of different size or density will settle at different rates and the resulting relative motion can cause particle collisions and hence flocculation.

According to Gregory (1989), the collision frequency can be calculated very simply, assuming that Stokes law applies

and that particle motion is linear up to contact with another particle. The result, for spherical particles of equal density is

$$\beta(i,j) = \frac{2\pi g}{9\mu}(\rho_s-\rho)(a_i+a_j)^3(a_i-a_j) \qquad (6)$$

where g is the acceleration due to gravity, ρ_s is the density of the particle and ρ is the density of the fluid.

Comprehensive flocculation kinetic models

For monodisperse suspension where particles are of the same size, an explicit form of particle number concentration vs. time can be written for each particle contact motion - Brownian, fluid shear and differential sedimentation by substituting equations 4, 5, and 6 into equation 2.

Gregory (1989) gave such explicit form of expressions for perikinetic flocculation (Brownian flocculation) as follows.

Consider an initially monodisperse suspension of particles of radius a_1, the initial collision rate can be calculated easily from equation 4 since only one type of collision (1-1, i=1, j=1) is involved. Also, the initial rate of decrease of the total particle concentration, n_T, follows directly from the collision rate since each collision reduces the number of particles by one (two primary particles lost, one aggregate gained, $dn_T/dt = 1/2\ dn_1/dt$). The result is:

From equation 4:

$$\beta(1,1) = \frac{2kT}{3\mu}\frac{(a_1+a_1)^2}{a_1 a_1} = \frac{8kT}{3\mu} \qquad (7)$$

From equation 2 whose first term is eliminated in this case and $\alpha = 1$

$$\frac{dn_T}{dt} = \frac{1}{2}\frac{dn_1}{dt} = \frac{1}{2}(-n_1\sum\beta(1,1)n_1) = -(\frac{4kT}{3\mu})n_1^2 = -k_F n_1^2 \qquad (8)$$

where $k_f(=4kT/3\mu)$ is known as the flocculation rate constant and has a value of $6.13*10^{-8}$ m^2s^{-1} for aqueous dispersions at 25 °C. Lichtenbelt et al. (1974) determined the rate constant for rapid flocculation of latex particles and found the k_f to be half of the value. This is known to be a result of hydrodynamic interaction between approaching particles. This effect will be discussed later.

Gregory (1989) also gave the expression of the initial rate of decline of the total particle concentration, n_T, for a monodisperse suspension for orthokinetic flocculation by solving equation 2 and 5 for particle size of a, and du/dz in equation 5 is replaced by G:

$$-\frac{dn_T}{dt} = (\frac{16}{3})n_1^2 G a^3 \qquad (9)$$

Here, Gregory introduced the concept of volume fraction of particles, Φ ($=4\pi a^3 n_1/3$), thus,

$$-\frac{dn_T}{dt} = 4G\Phi n_1/\pi \qquad (10)$$

Φ is assumed to remain constant during flocculation.

Harris et al. (1966) derived an equation similar to equation 10:

$$\frac{dn_T}{dt} = -\frac{\alpha\beta a^3}{\pi} G\Phi n_1 \qquad (11)$$

where

α = collision efficiency

β = size distribution function of the suspension

a = ratio of the collision radius of a floc to its physical radius

Thus, according to these formulations, orthokinetic flocculation is a first-order rate expression with respect to n_1, with a rate constant directly proportional to velocity gradient and the floc volume fraction. When the suspension is heterogeneous, with a wide size distribution, the rate of aggregation is increased (Swift and Friedlander, 1964) to some extent. Hence, the kinetic model for monodispersed suspension is conservative.

Certain limitations apply to the previous discussion of

Smoluchowski's work. They are summarized below:

a. The fluid flow is limited to the laminar region.

b. No hydrodynamic or van der Waals forces are considered.

c. All particles and aggregates are assumed to be solid spheres.

d. No floc breakup is assumed (Bratby, 1981).

To address the first problem, Camp and Stein (1943) proposed that the mean velocity gradient, $\bar{G}$, could be calculated from the power input, P, to be used in place of velocity gradient.

$$\bar{G} = (p/\mu V)^{(1/2)} = (\epsilon/\upsilon)^{(1/2)} \qquad (12)$$

where

p = total power input

V = water volume

ϵ = total energy dissipated/unit time/unit mass

μ = the absolute viscosity of the water

υ = the kinematic viscosity of the water

This value can be inserted into equation 5 to give modified Smoluchowski result for collision frequency function:

$$\beta(i,j) = \frac{4}{3}\left(\frac{\epsilon}{\upsilon}\right)^{(\frac{1}{2})}(a_i+a_j)^3 \qquad (13)$$

Saffman and Turner (1956) developed a model for turbulent flocculation of raindrops in a cloud. Their result is very like the expression of Camp and Stein, which differs only in the numerical constant (1.29 rather than 4/3=1.33).

It has long been observed that even if the particles are fully destabilized, the collision efficiencies are usually less than unity. Many researchers (Adler, 1981; Lawler et al., 1983; Casson and Lawler, 1990) agree that it is hydrodynamic forces that prevent those completely destabilized particles from collision. Gregory (1989) gave the following vivid description of the hydrodynamic phenomenon:

> "When two particles approach each other in a medium such as water, the no-slip boundary condition at the particle surfaces means that it becomes increasingly difficult for the water to be removed from the narrow gap between them. In the limit of contact (zero separation), an infinite force would have to be applied to squeeze out the last layer of water. At greater distances (up to many particle diameters), this hydrodynamic or viscous interaction can still have an effect in retarding the approach of particles." (212)

The hydrodynamic or viscous interaction can occur in all mechanisms of particle motion, Brownian (perikinetic coagulation), and fluid shear (orthokinetic, and turbulent) and differential sedimentation.

According to Spielmen's (1970) investigation of hydrodynamic interactions in Brownian coagulation, the hydrodynamic effects can produce a retardation of the coagulation rate by an additional factor of about ten for thin double layers.

Adler (1981) addressed the issue of hydrodynamic interaction in heterocoagulation in shear flow. The results demonstrated that in most cases, homocoagulation is favored over heterocoagulation. Although this result is contrary to traditional theory, it is proved by some recent flocculation research. Casson and Lawler (1990) performed flocculation experiments for monodisperse, bimodal, and trimodal latex suspensions in a controlled turbulent flow field. The research with multiple particle sizes indicated little or no influence of the larger particles on the growth of the smaller particles.

By including hydrodynamic effects, Lawler and Han (1989) calculated the collision frequency functions $\beta(i,j)$ for each type of collision (i.e., by Brownian motion, fluid shear, or differential sedimentation). The models which include hydrodynamic forces are called curvilinear models in contrast to the rectilinear models without the hydrodynamic interactions. Their curvilinear models were applied to calculate the collision frequency function for particle sizes between 0.1 μm and 100 μm. The results are shown in Figure 3.

The shaded regions in the figure indicate where each mechanism dominates in the curvilinear model. The Brownian motion can be seen to be the dominant mechanism for collisions when at least one of the two particles is small (approximately less than 1 μm). Differential sedimentation is dominant when at least one of the two particles is large (approximately

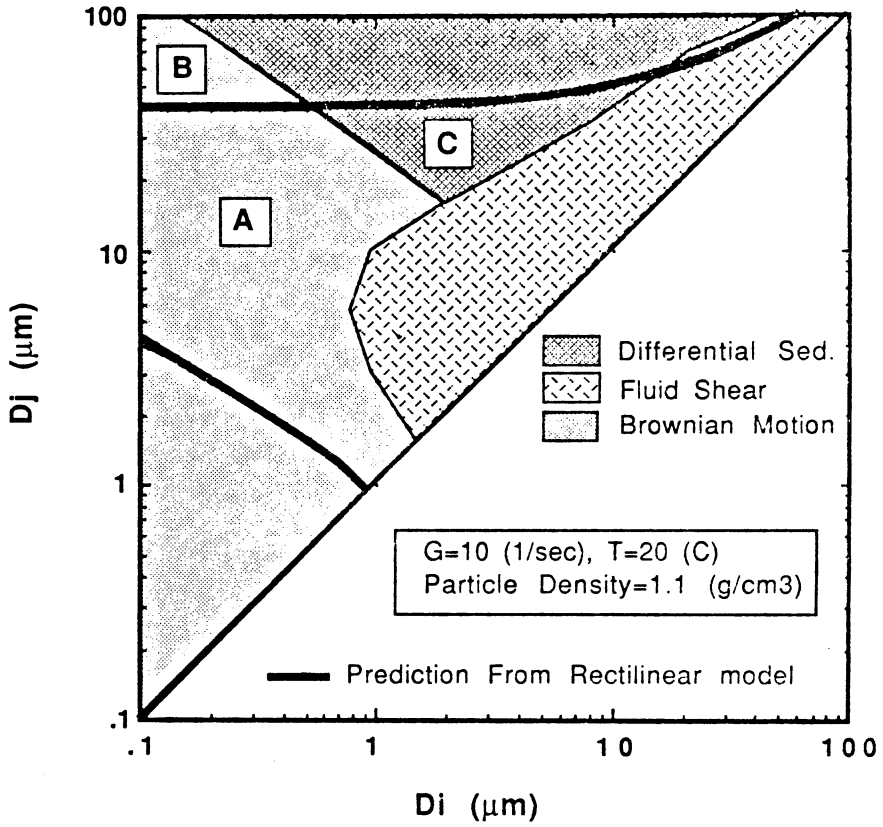

Figure 3. Dominant regions for each mechanism: Comparison between rectilinear and curvilinear models (Lawler and Han, 1989)
(Shaded areas represent regions dominated by each mechanism in curvilinear model; Regions A, B, and C show regions of difference between the two models.)

larger than 20 μm) and the other is dissimilar in size (i.e., has a significantly different settling velocity). Collision by fluid shear only are dominant between particles that are similar in size and both greater that 1 μm.

The regions of dominance of each type of collision are also shown for the rectilinear model in the same figure, delineated by the thick lines. For this model, Brownian motion is dominant when both particles must be small. Differential sedimentation is dominant when one of the particles must be quite large (> 40 μm).

Fluid shear dominance switches to Brownian dominance (as indicated by letter A) for curvilinear model which represents the reality of particle collisions. This curvilinear model as shown in Figure 3 suggests that fluid shear is not as important in bringing about collisions and flocculation as thought before. Lawler and Han (1989) further concluded that the primary purpose of mixing is to keep large particles in suspension so that they can cause flocculation by Brownian motion and differential sedimentation rather than to cause collisions directly. Therefore, the commonly used velocity gradient, G, which represents the fluid shear, is relatively insignificant in flocculation. This conclusion is further strengthened by the experimental work of Lawler et al. (1983).

The use of G value as the important flocculation

parameter has also been criticized by other researchers (Cleasby, 1984; Clark, 1985).

In order to better understand this issue, it is necessary to have a brief discussion about turbulent flow first.

Turbulence is frequently described as an energy cascade (or eddy cascade), where energy is put into the system at large length scales. It then cascades down to small length scales through the mechanism of vortex stretching, and finally leaves the system through viscous dissipation (Hanson, 1989).

A typical energy spectrum for a high Reynolds number flow shown in Figure 4 represents the relationship between eddy size and the energy contained in each eddy size (Hinze, 1975).

The y-axis in Figure 4 is the kinetic energy $\{E(k,t)\}$ contained in a specific eddy size at a fixed point in time. The x-axis is the wave number, which is the inverse of the vortex size (1/d). The variables k_e and k_d represent the eddy size which contains the majority of the energy, and dissipate the majority of the energy respectively.

The range of wave-numbers around k_e is called the range of energy containing eddies (Frost and Moulden, 1977). The structure of the turbulence in this region is determined by (Hinze, 1975):

- energy/unit mass-time
- t, time
- kinematic viscosity, υ

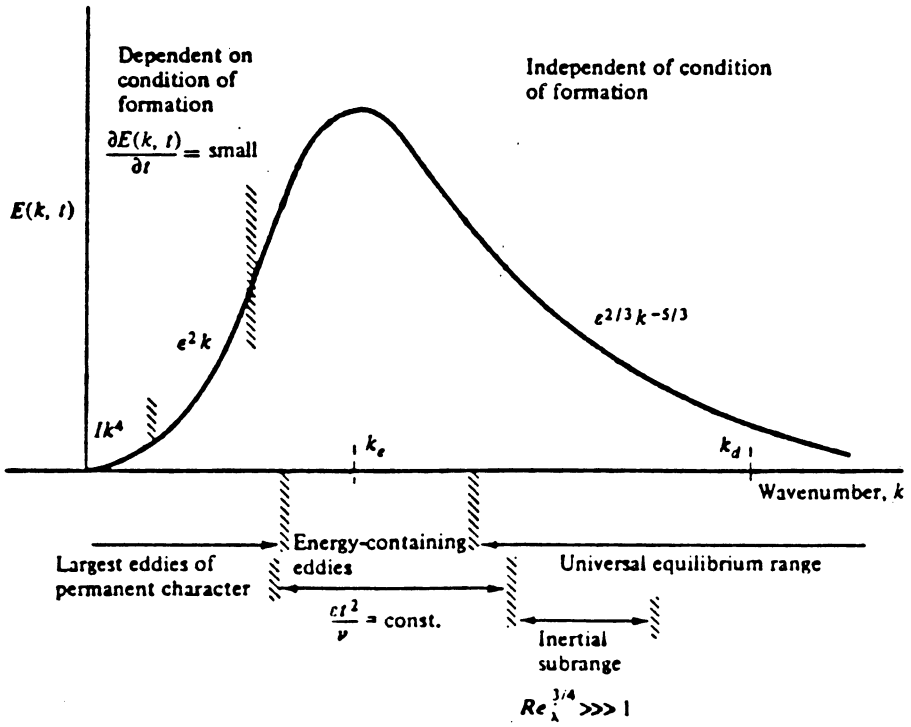

Figure 4. Form of the three dimensional spectrum E (k,t) in the various wave number ranges (As quoted by Hanson, 1989)

The majority of energy dissipation takes place in the universal equilibrium subrange which is often called the "dissipation subrange." The k_d in Figure 4 is the wave number associated with the size of eddies that provide the main contribution to the total energy dissipation (Hinze, 1975). Kolmogorov used dimensional reasoning to derive the length scale (η) which corresponds to k_d, i.e., $k_d = 1/\eta$. This special length scale is referred to as the Kolmogorov microscale, and is defined as:

$$\eta = \left(\frac{\upsilon^3}{\epsilon}\right)^{(1/4)} \qquad (14)$$

where

υ = kinematic viscosity

ϵ = energy/unit mass-time

Parker et al. (1972) stated that the microscale eddies in the universal equilibrium subrange are further divided into a low eddy region, the viscous dissipation subrange, and a larger eddy size range, the inertial convection subrange. The two subranges are divided by the Kolmogorov microscale. For the range of eddy scales in the inertial convection subrange, it has been shown (Batchelor, 1958) that when $L > d > \eta$, the energy spectrum is

$$E(k,t) = k_1 \epsilon^{2/3} d^{5/3} \qquad (15)$$

in which k_1 = constant. For eddies in the viscous dissipation

subrange, Obukhoff et. al. (1951) obtained for d < η, the relationship

$$E(k,t) = k_2 \epsilon d^3 \qquad (16)$$

in which k_2 = constant.

The turbulent energy dissipation does not reach far below the kolmogorov microscale and the lower scale of turbulence has been reached. Below this scale, all particle transport is caused by localized shear fields.

Figure 5, which is based on Argaman and Kaufman's (1968) work, contains calculated values for Kolmogorov's microscale at various G values and temperatures. The smallest eddies, according to the graph, are in the size around 50 μm which are much larger than the particle diameter of 1.8 μm used in this research.

It is thought that the particles in a turbulent field move together with the eddies of the fluid. Therefore, the collision between particles is determined by the movement of those eddies. Casson and Lawler (1990) pointed out that the flocculation is induced by eddies of approximately the same size as the particles. Therefore, it is unlikely that even the smallest turbulent eddies will play a direct role in turbulent flocculation until the floc have grown very large (Koh et al., 1984). But how does flocculation occur in a turbulent field? Hanson (1989) explains the phenomenon in his thesis. Each eddy, or vortex, contains homogeneously dispersed primary

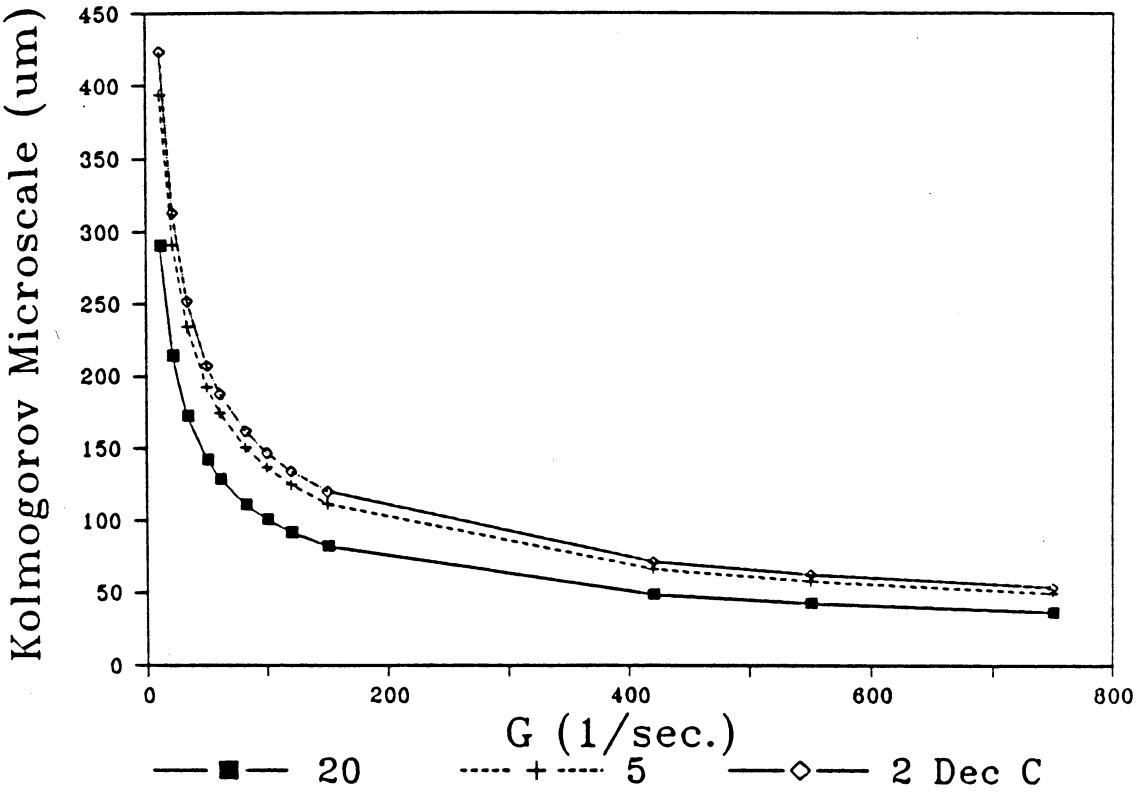

Figure 5. G versus the Kolmogorov microscale of turbulence η at various temperatures, G is from Argaman and Kaufman (1968), η is calculated based on G (Hanson, 1989)

particles which follow the movement of the vortex. Before vortex stretching, the particles are moving relatively to the bulk flow, but are stationary with respect to each other. As the vortex undergoes stretching, a localized velocity gradient (i.e., shear gradient) is induced in the fluid contained in the vortex, and this localized velocity gradient induces particle collisions. Therefore, the flocculation is caused by the localized shear fields formed by the turbulent eddies. It is important to note that the smaller the Kolmogorov microscale of turbulence, the more intense the localized velocity gradient. From this reasoning, we can say that flocculation rate is determined by the localized velocity gradient in the turbulent field. Engineers and researchers, however, have employed root-mean-square of velocity gradient, G, as the indicator of flocculation. The weakness of G in representing flocculation is discussed here.

G is defined as (sometimes expressed as $\bar{G}$):

$$G = \sqrt{\frac{p}{\mu V}} = \sqrt{\frac{\epsilon}{\upsilon}} \qquad (12)$$

where

p = power input

V = fluid volume in which power is introduced

μ = the absolute viscosity of the water

ϵ = energy input/unit time/unit mass of water

υ = the kinematic viscosity of the water

The G value calculated as above for a given energy input is a definite value for the whole reactor. However, the localized velocity gradient, which causes flocculation is not homogeneous within the reactor.

Lawler et al. (1983) tested Smoluchowski's model by conducting a series of batch flocculation experiments. The flocculation modes include the three basic mechanisms (Brownian motion, fluid shear and differential sedimentation). The model predicts a substantial difference between their two experimental conditions based on the different velocity gradients, with more rapid and extensive coagulation at higher velocity gradient. The dissimilarity between the model predictions and experimental results suggests that the importance of velocity gradient, G, on rate of flocculation was greatly overestimated by the model.

Delichatsios and Probstein (1975) developed a mathematical models of flocculation for destabilized particles in an isotropic turbulent flow. Their models considered particle sizes both larger and smaller than the Kolmogorov microscale and were tested experimentally. The interparticle collision rate was found to depend on the particle number concentration, particle diameter, and relative velocity between the particles during collision. Expressions for the relative velocity were developed for particle sizes less than

the Kolmogorov microscale, greater than the Kolmogorov microscale, and equal to the Eulerian macroscale of turbulence.

An important contribution of Delichatsios and Probstein was the realization that a single parameter, such as G, was not adequate to describe the interparticle contacts resulting from fluid motion in flows containing different eddy sizes and particle diameters. Another interesting result from their work was that they found the coagulation efficiency for partially destabilized systems appeared to be independent of the particle transport mode, that is, Brownian or turbulent, as had been observed by previous investigators (Hahn and Stumm 1968). Casson et al. (1990) developed a method for estimating the velocity gradients in eddies of different sizes in the turbulent flow and incorporated into the corrected Smoluchowski's model which included hydrodynamics of particle interactions as well. The preliminary modelling of interparticle contacts in flocculation using the velocity gradients of the eddies indicated that they adequately described the interparticle contacts from mixing.

Clark (1985) critiqued the RMS velocity gradient based on fundamental concepts from continuum mechanics. Clark's criticism of the velocity gradient was that Camp and Stein's (1943) conceptualization of an "absolute velocity gradient" and "RMS velocity gradient" were fundamentally incorrect,

since they essentially require that a three dimensional flow in general be replaced by a single two dimensional flow. Cleasby (1984) investigated the validity of G as a turbulent flocculation parameter. He pointed out that G was valid only for particles smaller than the Kolmogorov microscale, and above that, power input per unit mass to the two thirds power ($\epsilon^{2/3}$) would be a more appropriate flocculation parameter than the parameter G.

All the discussions so far about the modelling of flocculation kinetics have not included the effects of floc breakup. Because of the lack of suitable quantitative techniques, most of the experimental and analytical work in this area has been of an empirical nature (Gregory, 1989). A couple of imaginary floc breakage mechanisms have been proposed. Thomas (1964) suggested that floc breakup was principally the result of dynamic pressure differences on opposite sides of the floc which resulted in bulgy deformation and ultimately in floc splitting. In summary of Thomas's work, Parker et al. (1972) gave the rate of floc disruption as follows:

$$\frac{dn_F}{dt} = -f_\lambda n_F = -\frac{u_\lambda}{\lambda} n_F \qquad (17)$$

where

n_F = floc concentration

t = time

f_k = eddy frequency

u_k = eddy velocity

λ = eddy scale

In equation 17 the eddy size of interest was assumed equal to the floc diameter.

For the eddy frequency in the inertial convection subrange, Thomas obtained:

$$f_\lambda = \frac{\beta^{1/2}\epsilon^{1/3}}{\lambda^{2/3}} \tag{18}$$

and for viscous dissipation subrange:

$$f_\lambda = \zeta^{1/2}(\epsilon/\upsilon)^{1/2} \tag{19}$$

where

β = Mean square velocity constant in inertial convection subrange

ζ = Mean square velocity constant in viscous dissipation subrange

υ = Kinematic viscosity

Substituting equation 18 and 19 into 17 respectively, we get the following equations:

For inertial convection subrange:

$$\frac{dn_F}{dt} = -\frac{\beta^{1/2}\epsilon^{1/3}}{\lambda^{2/3}} n_F \qquad (20)$$

For viscous dissipation subrange:

$$\frac{dn_F}{dt} = -\zeta^{1/2}\left(\frac{\epsilon}{\upsilon}\right)^{1/2} n_F \qquad (21)$$

Another floc breakup theory was proposed by Argaman and Kaufman (1968) who suggested that the principal mode of breakup was surface erosion of flocs by turbulent drag. The corresponding floc breakup rate was proposed as:

$$\frac{dn_1}{dt} = BR_F^2 \frac{n_F}{R_1^2} \overline{u^2} \qquad (22)$$

where

n_1 = primary particle concentration

B = breakup constant

R_F = Radius of floc

R_1 = Radius of primary particle

$\overline{u^2}$ = mean square velocity fluctuation

Parker et al. (1972) derived a general floc breakup model for activated sludge floc:

$$\frac{dn_1}{dt} = k_B x G^m \qquad (23)$$

in which k_B is floc breakup rate coefficient, m is floc breakup rate exponent, and x is MLSS concentration. For the inertial convection subrange, m=4; for the viscous dissipation subrange, m = 2.

Matsuo and Unno (1981) studied the strength of flocs and the forces which cause floc breakup in the turbulence. They developed the following equations to calculate the forces acting on flocs:

For the viscous dissipation subrange:

$$\tau = C_1 \mu \left(\frac{\epsilon}{\upsilon}\right)^{1/2} \tag{24}$$

For the inertial convection subrange:

$$\tau = C_2 \rho \overline{u^2}(d) \tag{25}$$

where

τ = surface shear yield strength

μ = viscosity coefficient

ρ = density of water

$\overline{u^2}(d)$ = square of difference of velocity between two points distance d apart

d = diameter of floc

Pandya and Spielman (1981) developed a population balance equation that governs the floc size distribution in turbulent flow incorporating both splitting and erosion mechanisms of

floc breakage. It was found that the splitting frequency of parent flocs varied as the 0.33 power of the parent floc volume and 0.71 power of the shear rate. The average number of daughter fragments produced upon splitting of individual flocs was found to be about 2.5.

Hogg et al. (1985) studied floc density and breakup mechanisms experimentally by using suspensions of mineral particles flocculated with commercial polymeric flocculants. They found that floc density decreases as its size increases, and that a majority of breakage events are of erosive type.

For the purpose of practical design, equation 23 is often suggested. A disccusion of the appropriate exponent (m) on G in equation 23 is presented later.

The aggregation of colloidal particles in the presence of flocculants is a highly complex process. Floc growth results from particle-particle collisions promoted by Brownian motion, fluid shear and differential settling. At the same time, agitation and turbulence causes shearing and breakage of flocs. Consequently, flocculation is a process of simultaneous growth and size reduction.

Argaman and Kaufman (1968) developed a model for turbulence flocculation which consists of both floc aggregation and floc breakup terms. The model has been applied to the flocculation process design (Montgomery, 1985). It was developed based on the hypothesis that particles which are

suspended in a turbulent fluid experience a random motion, which may be characterized by a diffusion coefficient, D_{eff}, that can be expressed in terms of the energy spectrum, E_L, of the turbulent field. The derivation of the model is discussed briefly in the following paragraphs.

The form of equation 3 for Brownian flocculation (presented earlier) was adopted by Argaman and Kaufman for turbulent flocculation. The diffusion coefficient in the model was replaced by a turbulent diffusion coefficient relating the energy spectrum of the turbulent field. The diffusion coefficient was first derived by Corrsin (1962):

$$D_T(t) = \int_0^\infty E_L(f) \frac{\sin(2\pi ft)}{2\pi f} df \tag{26}$$

in which D_T is the turbulent diffusion coefficient of fluid particles; E_L, the largrangian energy spectrum; f, the frequency; and t is the time.

$E_L(f)$ is defined by the equation:

$$\overline{u^2} = \int_0^\infty E_L(f)\, df \tag{27}$$

in which $\overline{u^2}$ is the mean square velocity fluctuation.

Since equation 26 was considered applicable for particles much smaller than the smallest scale of the turbulent field,

Argaman and Kaufman employed an "entrainment factor", e_f, to modify equation 26 so that it would be applicable for particles both smaller and larger than the microscale of turbulent field.

$$e_f = \frac{\lambda}{2R+\lambda} \tag{28}$$

where λ is the size of the fluid mass moving with a frequency f, and R is the radius of the particle. For λ, Levich (1962) gave the form:

$$\lambda = Af^{-\frac{3}{2}} \tag{29}$$

Here A is a constant which depends on the total power dissipation, ϵ.

Another modification to Equation 26 accounted for the fact that the mutual diffusion of the colliding particles is governed by eddies which are smaller than the particles' spectrum. This correction is introduced by setting a lower limit to the integral of Equation 26. Therefore, we have:

$$\because \quad D_{eff} = D_{eff}(i) + D_{eff}(j) \tag{30}$$

$$\therefore \quad D_{eff} = \int_{f_{R_{ij}}}^{\infty} E_L(f) \frac{\sin 2\pi ft}{2\pi f} \frac{Af^{-3/2}}{2R_i + Af^{-3/2}} df$$

$$+\int_{f_{Rij}}^{\infty} E_L(f)\,\frac{\sin 2\pi ft}{2\pi f}\,\frac{Af^{-3/2}}{2R_j+Af^{-3/2}}\,df \qquad (31)$$

in which f_{Rij} is the frequency of eddy of size R_{ij}. Here, several simplification have been made by Argaman and Kaufman.

1. In a continuous flow flocculation reactor, primary particles are removed from the suspension, principally through their collision with previously formed flocs. It is assumed that there are only two categories of particles in the suspension, i.e., the primary particle with size R_1 and floc with size R_F. Any particles or aggregates in the intermediate sizes are neglected. Therefore, the primary particle radius R_1 and the floc radius R_F are used instead of R_i and R_j.

2. Since $R_F >> R_1$, the second term of equation 31 can be neglected. Also $R_{1F} = R_1 + R_F \cong R_F$.

3. $\mathrm{Sin}(2\pi ft) / 2\pi f$ was replaced by a characteristic time, τ_0.

4. The entrainment factor $Af^{-3/2}/(2R_1+Af^{-3/2})$ was approximated by a mean value $\bar{e}_f$ over the range f_{RF} to ∞. Therefore, we get:

$$D_{eff} = \tau_0 \bar{e}_f \int_{f_0}^{\infty} E_1(f)\,df \qquad (32)$$

Noting that $\int_0^\infty E_L(f)df = \overline{u^2}$ (equation 27), the integral of equation 32 can be replaced by $k_4\overline{u^2}$ where k_4 is the fraction of $\overline{u^2}$ contributed by fluid motions of frequencies higher than f_0. Finally, they argue that k_4 is proportional to some fraction of f_0 which in turn depends on R_F. And k_4 can be replaced by $k_5R_F^2$ where k_5 is a dimensional constant which reflects the properties of the spectrum function in the region $f > f_0$. With these assumptions the effective diffusivity can be approximated by

$$D_{eff} = k_s\overline{u^2}R_F^2 \qquad (33)$$

where $k_s = k_5\overline{e}_f\tau_0$. It is a proportionality coefficient expressing the effect of turbulence energy spectrum on the diffusion coefficient.

The rate of collisions between primary particles and flocs may now be obtained from equation 3 and 33:

$$\beta(1,F) = 4\pi k_s(R_F)^3\ \overline{u^2} \qquad (34)$$

By applying Smoluchowski's approach and considering floc breakup, the differential form of the flocculation equation can be written as:

$$\frac{dn_k}{dt} = \frac{1}{2}\sum 4\pi\alpha R_{ij}D_{ij}n_in_j - \sum 4\pi\alpha R_{ik}D_{ik}n_in_k - n_kB_k\overline{u^2} + \left(\frac{dn_k}{dt}\right)_{BK} \qquad (35)$$

The first term represents the formation of k-fold particles by collision and aggregation of two smaller particles. The second term is the elimination of k-fold particles due to their collision with other particles to form larger flocs. The third term is the elimination of k-fold particles by their breakup, and the last term represents formation of k-fold particles by breakup of larger particles. As the performance of a flocculation reactor is most simply measured by the reduction of primary particles, (k=1), the flocculation equation for primary particle is of most significance. Equation 35 becomes simpler as its first and third terms vanish:

$$\frac{dn_1}{dt} = -4\pi\alpha\sum R_{1i}D_{eff}n_1n_i + \left(\frac{dn_1}{dt}\right)_{BK} \qquad (36)$$

In the derivation of Argaman and Kaufman model, only two categories of suspended solids in water are considered, the primary particles and flocs which are represented by R_1 and R_F, respectively as their radii. Particles or aggregates in other sizes are not included in the model. Only the change in the concentration of primary particles during flocculation is considered. This approach greatly simplified the problem. Thus, equation 36 becomes:

$$\frac{dn_1}{dt} = -4\pi\alpha R_{1F}D_{eff}n_1n_F + \left(\frac{dn_1}{dt}\right)_{BK} \qquad (37)$$

Floc breakup is also included in the final model of Argaman and Kaufman. The rate of formation of primary particles due to floc breakup is given by

$$(\frac{dn_1}{dt}) = BR_F^2 \frac{n_F}{R_1^2} \overline{u^2} \tag{22}$$

in which B is the breakup constant.

The rate of change in the concentration of primary particles in a flocculation reactor is obtained by combining Equation 37 and 22 and 33:

$$\frac{dn_1}{dt} = -4\pi\alpha k_s R_F^3 n_F n_1 \overline{u^2} + B\frac{R_F^2}{R_1^2} n_F \overline{u^2} \tag{38}$$

in which α is the collision efficiency constant.

From their experimental results, Argaman and Kaufman found the relationship between u^2 and G as:

$$\overline{u^2} = k_p G \tag{39}$$

Furthermore, the total volume of the flocs in a reactor is given by

$$\Phi = \frac{4}{3}\pi n_F R_F^3 \tag{40}$$

Here Φ is the floc volume fraction.

Substituting Equations 39 and 40 into 38, we get:

$$\frac{dn_1}{dt} = -k_F k_s k_p G n_1 + k_B G^2 n_{10} \tag{41}$$

or

$$\frac{dn_1}{dt} = -k_a G n_1 + k_b G^2 n_{10} \tag{42}$$

in which the flocculation and breakup constants, k_f and k_b, are given by

$$k_F = 3\alpha\Phi \tag{43}$$

$$k_b = \frac{3}{4\pi}\frac{B}{n_{10}}\frac{\Phi k_p^2}{R_1^2 k_1} \tag{44}$$

and

$$k_a = k_F k_s k_p \tag{45}$$

Here n_{10} is the initial primary particle concentration.

Equations 42 can be solved for single CSTR: (Argaman and Kaufman, 1968):

$$\frac{n_{10}}{n_1} = \frac{1+k_a G t}{1+k_b G^2 t} \qquad (46)$$

For plug flow reactor, or a batch reactor (Bratby, 1981):

$$\frac{n_{10}}{n_1} = \frac{-k_a G e^{k_a G t}}{-k_a G + k_b G^2 (1-e^{k_a G t})} \qquad (47)$$

Equations 46 and 47 are frequently used as the guidance of flocculation process design.

III. IMPROVEMENT OF FLOCCULATION KINETIC MODELLING

Argaman and Kaufman's model deals with only two classes of suspended solids, primary particles (size d_1) and flocs (size d_F). The rate of decline of primary particle concentration is controlled by the collision frequency between primary particles and flocs which is expressed by equation 34. In fact, the dispearance of primary particles depends not only on their collisions with flocs, but more importantly on the collision among the primary particles. This is especially true during the early stage of flocculation where primary particles dominate and very few flocs have been formed. If this is true, the rate of change of primary particles, dn_1/dt is proportional to n_1^2, instead of to $n_1 n_F$.

Gregory developed the similar equation (equation 9 presented earlier) for orthokinetic flocculation:

$$-\frac{dn_T}{dt} = (\frac{16}{3}) n_1^2 G a^3 \qquad (9)$$

Then he introduced the concept of volume fraction of particles Φ ($= 4\pi a^3 n_1/3$) to simplify the equation and to thereby produce equation 10 in which dn_T/dt is proportional to n_1, instead of n_1^2.

Harris et al. (1966) also derived this form of equation with the same assumption that Φ remains constant during

flocculation. This assumption has been criticized by some researchers (Huck and Murphy, 1978; Argaman, 1979). But because of its simplicity, it is still being widely utilized.

According to Lawler and Han (1989), the dominant collision mode switches from fluid shear to Brownian motion when hydrodynamic interaction is considered. It is well known that Brownian collision frequency is proportional to the square of particle concentration (Equation 8). Consequently, the flocculation rate is more likely to be proportional to n_1^2 instead of n_1, especially during the early stage of flocculation.

In an attempt of improving the existed model of flocculation kinetics, i.e., Argaman and Kaufman's model expressed as equation 42, several revisions have been made in this study as follows:

(1) The revised model replaces n_1 with n_1^2 in its floc formation term;

(2) The flocculation process is divided into two stages. No floc breakup is assumed during the first stage of flocculation when $(Gt) \leq (Gt)_{cr}$. $(Gt)_{cr}$ is the critical Gt product beyond which floc breakage begins to occur. During the second stage of flocculation when $Gt > (Gt)_{cr}$, floc breakup is considered.

Applying the law of substance conservation for the flocculation system, equation 48 can be written for the mass

balance of primary particles:

Inflow = Outflow + Accumulation

± (Utilization, Generation) (48)

Equation 48 will be used as the basis describing the primary particle concentration changes in the flocculation system. There are usually two type of flocculation systems. One is the complete stirred tank reactor (CSTR) system; the other is the batch reactor (BR) system. Most actual coagulation and flocculation processes are of the CSTR type. The BR is employed more often in laboratory flocculation studies. The experimental work reported here was done with a BR flocculation system.

In this research, two new models of flocculation kinetics are proposed as follows.

A. New Model 1

As we discussed, this new model is based on the assumption of two stage flocculation, with one sub-model in each stage.

First stage of flocculation

During the first stage of flocculation where $Gt \leq (Gt)_{cr}$, the primary particle concentration change rate is proportional to G and n_1^2, and there is no floc breakup occurring.

The declining rate of primary particle concentration is proposed as:

$$\frac{dn_1}{dt} = -\frac{k_0}{n_{10}} G n_1^2 \qquad (49)$$

in which k_0 is the flocculation constant (dimensionless).

For a BR system, since there is no inflow nor outflow of substance (i.e., primary particles), equation 48 thus is simplified as:

$$0 = 0 + \frac{d(Vn_1)}{dt} + \left(\frac{k_0}{n_{10}} G n_1^2\right) V \qquad (50)$$

in which V is the suspension volume in the reactor and V remains constant during flocculation.

For constant volume, dividing equation 50 by V, we have:

$$\frac{dn_1}{dt} = -\frac{k_0}{n_{10}} G n_1^2 \qquad (51)$$

Integration of equation 51 for the boundary conditions $n_1=n_{10}$ at $t = 0$, and $n_1 = n_1$ at $t = t$ gives:

$$\int_{n_{10}}^{n_1} \frac{dn_1}{n_1^2} = -\int_0^t \frac{k_0}{n_{10}} G dt \qquad (52)$$

$$-\left(\frac{1}{n_1}-\frac{1}{n_{10}}\right) = -\frac{k_0}{n_{10}}Gt \tag{53}$$

$$\frac{1}{n_1} = \frac{1}{n_{10}}+\frac{k_0}{n_{10}}Gt \tag{54}$$

Rearranging equation 54, we get the New Model 1, first stage sub-model for a BR flocculation system:

$$\frac{n_{10}}{n_1} = 1+k_0Gt \tag{55}$$

For a CSTR system, equation 48 can be written as:

$$n_{10}Q = n_1Q+\frac{d(n_1V)}{dt}+\left(\frac{k_0}{n_{10}}Gn_1^2\right)V \tag{56}$$

At steady-state, $d(n_1V)/dt = 0$, therefore, equation 56 becomes:

$$(n_{10}-n_1)Q = \frac{k_0}{n_{10}}Gn_1^2V \tag{57}$$

$$\therefore \quad n_{10}-n_1 = \frac{k_0}{n_{10}}Gn_1^2\frac{V}{Q} \tag{58}$$

Since V/Q is the hydraulic detention time t, equation 58 is written as:

$$n_{10} = n_1 + \frac{k_0}{n_{10}} G n_1^2 t \qquad (59)$$

The above equation is a quadratic equation for n_1, which can be solved for n_1:

$$n_1 = \frac{n_{10}(\sqrt{1+4k_0Gt}-1)}{2k_0Gt} \qquad (60)$$

Equation 60 can be rewritten with respect of n_{10}/n_1 as follows:

$$\frac{n_{10}}{n_1} = \frac{1}{2}(1+\sqrt{1+4k_0Gt}) \qquad (61)$$

Second stage of flocculation

The second stage of flocculation is defined as its (Gt) > $(Gt)_{cr}$ where floc breakup takes place. In this stage, it is assumed that the rate of change in primary particle concentration is governed by the collision rate between floc and the primary particle. Furthermore, the floc breakup term will be included in the model.

As discussed in Chapter II, particles generated by floc

breakup can be expressed as a certain exponential function of G (or ϵ). The exponent, takes the values of 1/3 for ϵ according to equations 20 for the inertial convection subrange, and 1 for G according to equation 21 (Thomas, 1964). The exponent can also take the value of 2 for G (Argaman and Kaufman, 1968) and 4 for activated sludge flocculation (Parker et al., 1972). In order to decide which exponential function to be adopted in the new model, extensive flocculation data from Hanson (1989) were used in testing Argaman and Kaufman's flocculation kinetic model by setting different exponents for G in the floc breakup term. The exponent value in which the model produced the least mean of squares of error from model regression was taken as the exponent of G in the floc breakup term in the new models. The model regression was performed by using SAS NLIN software which will be discussed in Chapter V. The results showed that value of 2 would always give better prediction of Hanson's flocculation data. Therefore, Argaman and Kaufman's floc breakup term $dn_1/dt = k_b G^2 n_{10}$ has been adopted as the floc breakup term for new models.

For the New Model 1, stage 2, the assumption is the same as that made by Argaman and Kaufman. Therefore, Argaman and Kaufman's model is adopted as the second stage flocculation sub-model for New Model 1:

$$\frac{dn_1}{dt} = -k_a G n_1 + k_b G^2 n_{10} \qquad (42)$$

For the BR system, substitute equation 42 into equation 48:

$$0 = 0 + \frac{d(Vn_1)}{dt} + (k_a G n_1 - k_b G^2 n_{10})\, V \qquad (62)$$

$$\therefore \quad \frac{dn_1}{dt} = -k_a G n_1 + k_b G^2 n_{10} \qquad (42)$$

For BR system, the equation derived from mass balance takes the same form of its original differential equation. Integration of equation 42 for the boundary conditions of $n_1 = n_{1cr}$ at $t = t_{cr}$ at the end of first stage, and $n_1 = n_1$ at time $t = t$ during second stage of flocculation:

$$\int_{n_{1cr}}^{n_1} \frac{dn_1}{-k_a G n_1 + k_b G^2 n_{10}} = \int_{t_{cr}}^{t} dt \qquad (63)$$

$$\therefore \quad \ln \frac{-k_a G n_1 + k_b G^2 n_{10}}{-k_a G n_{1cr} + k_b G^2 n_{10}} = -k_a (Gt - (Gt)_{cr}) \qquad (64)$$

Rearranging equation 64:

$$\frac{n_{10}}{n_1} = \frac{-k_a G e^{k_a(Gt-(Gt)_{cr})}}{-k_a G \frac{n_{1cr}}{n_{10}} + k_b G^2 (1-e^{k_a(Gt-(Gt)_{cr})})} \tag{65}$$

n_{1cr}/n_{10} is obtained from equation 55:

$$\frac{n_{1cr}}{n_{10}} = \frac{1}{1+k_0(Gt)_{cr}} \tag{66}$$

Substituting equation 66 to equation 65, we have the second stage sub-model of New Model 1 for BR system:

$$\frac{n_{10}}{n_1} = \frac{-k_a G e^{k_a(Gt-(Gt)_{cr})}}{-\frac{k_a G}{1+k_0(Gt)_{cr}} + k_b G^2 (1-e^{k_a(Gt-(Gt)_{cr})})} \tag{67}$$

A detailed development of equation 67 is given in Appendix A.

For CSTR system, since the suspension is assumed to be homogeneous over the whole reactor, and the flocculation time remains stable, therefore, the flocculation falls in either stage 1 when $Gt \leq (Gt)_{cr}$, or stage 2 when $Gt > (Gt)_{cr}$. The corresponding flocculation kinetic models for CSTR system at stage 1 and 2 are given by equation 61 and 46, respectively.

The selection of $(Gt)_{cr}$

Huck et al. (1978) found that for the flocculation with polymer as the primary coagulant, the critical Gt value is 80,000. The value is expected to be larger than it is for flocculation with alum, since the alum induced flocs are weaker and are more easily broken than the polymer induced flocs. Based on the experimental research of this study and the study of Hanson (1989), when Gt product is under 36,000 floc breakup is not significant. The value is empirical rather than a theoretical parameter. Above this critical level, floc breakup occurs. The flocculation time corresponding to the critical Gt of 36,000 for different G levels are listed in Table 1.

Table 1. The flocculation time and G when Gt=36000

G (s^{-1})	Time (min.)	G (s^{-1})	Time (min.)
4.2	143.0	90	6.7
22.6	26.0	120.0	5.0
30.0	20.0	144.3	4.0
42.2	14.0	160.0	3.7
45.0	13.3	180.0	3.3
60.0	10.0	240.0	2.5
65.7	9.0		

B. New Model 2

In this model, the flocculation process is no longer divided into stages. The overall primary particle concentration changing rate is expressed as:

$$\frac{dn_1}{dt} = -\frac{k_0}{n_{10}} G n_1^2 + k_b G^2 n_{10} \tag{68}$$

The similar procedure is applied here as in the previous section in integrating for n_{10}/n_1 from the mass balance for BR system. We get the following model for BR flocculation:

$$\frac{n_{10}}{n_1} = \frac{\sqrt{k_0 k_b G} - k_0 + (k_0 + \sqrt{k_0 k_b G})\, e^{2\sqrt{k_0 k_b G} Gt}}{\sqrt{k_0 k_b G} - k_b G + (k_b G + \sqrt{k_0 k_b G})\, e^{2\sqrt{k_0 k_b G} Gt}} \tag{69}$$

For CSTR, we can derived New Model 2 as:

$$\frac{n_{10}}{n_1} = \frac{1 + \sqrt{1 + 4 k_0 G t (1 + k_b G^2 t)}}{2 (1 + k_b G^2 t)} \tag{70}$$

The derivation of equation 69 and 70 are given in Appendix B.

Tables 2 and 3 summarize the Argaman-Kaufman and the two new models proposed in this study for BR flocculation and CSTR flocculation systems, respectively.

Table 2. Summary of flocculation models for BR system

Argaman-Kaufman's model $$\frac{n_{10}}{n_1} = \frac{-k_a G e^{k_a G t}}{-k_a G + k_b G^2 (1 - e^{k_a G t})} \quad (47)$$
New Model 1 - First Stage $$\frac{n_{10}}{n_1} = 1 + k_0 G t \quad (55)$$ New Model 1 - Second Stage $$\frac{n_{10}}{n_1} = \frac{-k_a G e^{k_a (Gt - (Gt)_{cr})}}{-\frac{k_a G}{1 + k_0 (Gt)_{cr}} + k_b G^2 (1 - e^{k_a (Gt - (Gt)_{cr})})} \quad (67)$$
New Model 2 $$\frac{n_{10}}{n_1} = \frac{\sqrt{k_0 k_b G} - k_0 + (k_0 + \sqrt{k_0 k_b G})\, e^{2\sqrt{k_0 k_b G} G t}}{\sqrt{k_0 k_b G} - k_b G + (k_b G + \sqrt{k_0 k_b G})\, e^{2\sqrt{k_0 k_b G} G t}} \quad (69)$$

Table 3. Summary of flocculation models for CSTR system

Argaman-Kaufman' Model $$\frac{n_{10}}{n_1} = \frac{1+k_a G t}{1+k_b G^2 t} \quad (46)$$
New Model 1 - First Stage $$\frac{n_{10}}{n_1} = \frac{1}{2}\left(1+\sqrt{1+4k_0 G t}\right) \quad (61)$$ New Model 1 - Second Stage $$\frac{n_{10}}{n_1} = \frac{1+k_a G t}{1+k_b G^2 t} \quad (46)$$
New Model 2 $$\frac{n_{10}}{n_1} = \frac{1+\sqrt{1+4k_0 G t\left(1+k_b G^2 t\right)}}{2\left(1+k_b G^2 t\right)} \quad (70)$$

IV. EXPERIMENTAL INVESTIGATION

A. Objectives of Experiments

The objectives of the experimental work are to test the general validity of the proposed new flocculation kinetic models and to compare them with the existing models.

The experiments were designed to evaluate the relationship between the flocculation energy input and primary particle change rate as expressed by the existing and new models. Five levels of flocculation energy input were investigated with 3 to 4 replications at each level. The layout of the experimental scheme is illustrated by Table 4.

Table 4. Layout of the experimental scheme

Level of G (s^{-1})	Number of Experiments
4.2	4
22.6	3
42.2	3
65.7	4
144.3	3

Except for the energy input, other experimental conditions were kept the same.

The experiments were conducted in a constant temperature room with its temperature controlled by a personal computer system. The flocculation work was performed in a bench scale batch reactor identical to the reactor used by Argaman and Kaufman (1968).

Argaman and Kaufman conducted flocculation experiments in the sweepfloc region of coagulation with alum dosage of 25 mg/l (as $Al_2(SO_4)_3.14H_2O$) for clay concentration of 25 mg/l. Unlike their work, this research was performed in the adsorption/destabilization region of coagulation. The alum dosage was 5 mg/l (as $Al_2(SO_4)_3.18H_2O$) for the flocculation experiments with clay concentration of 25 mg/l.

In each run of the experiments, 11 samples were taken during the course of flocculation and particle concentration and size distribution were analyzed by using an Automatic Image Analyzer (AIA).

After all the data were collected, standard statistical procedure were adopted to analyze the variance of the experiments. The following information from statistical analysis was desired:

a. Was the experimental error too big to make it impossible to draw inferences from experimental work?

b. If there was no significant experimental error, were there

significant performance difference among flocculation experiments receiving different levels of flocculation energy input G?

Once this preliminary statistical process was done, more sophisticated procedures were followed for the comparison of different flocculation kinetic models. This portion of work will be discussed in detail in Chapter V.

B. Experimental Equipment and Material

The experimental equipment and material preparation are same to those employed by previous researchers at Iowa State University (Hanson, 1989; Srivastava, 1988).

Reactor

The flocculation experiments were carried out in a bench scale batch reactor identical to the reactor used by Argaman and Kaufman (1968). A flat, two-blade turbine impeller was used as the only mixing device. Essential features of the plexiglass reactor used in the study are shown in Figure 6.

The electric mixing motor was mounted on a wooden support which was attached to the top of the reactor. The wooden support for the motor also held the pH probe and thermocouple for temperature data acquisition and control.

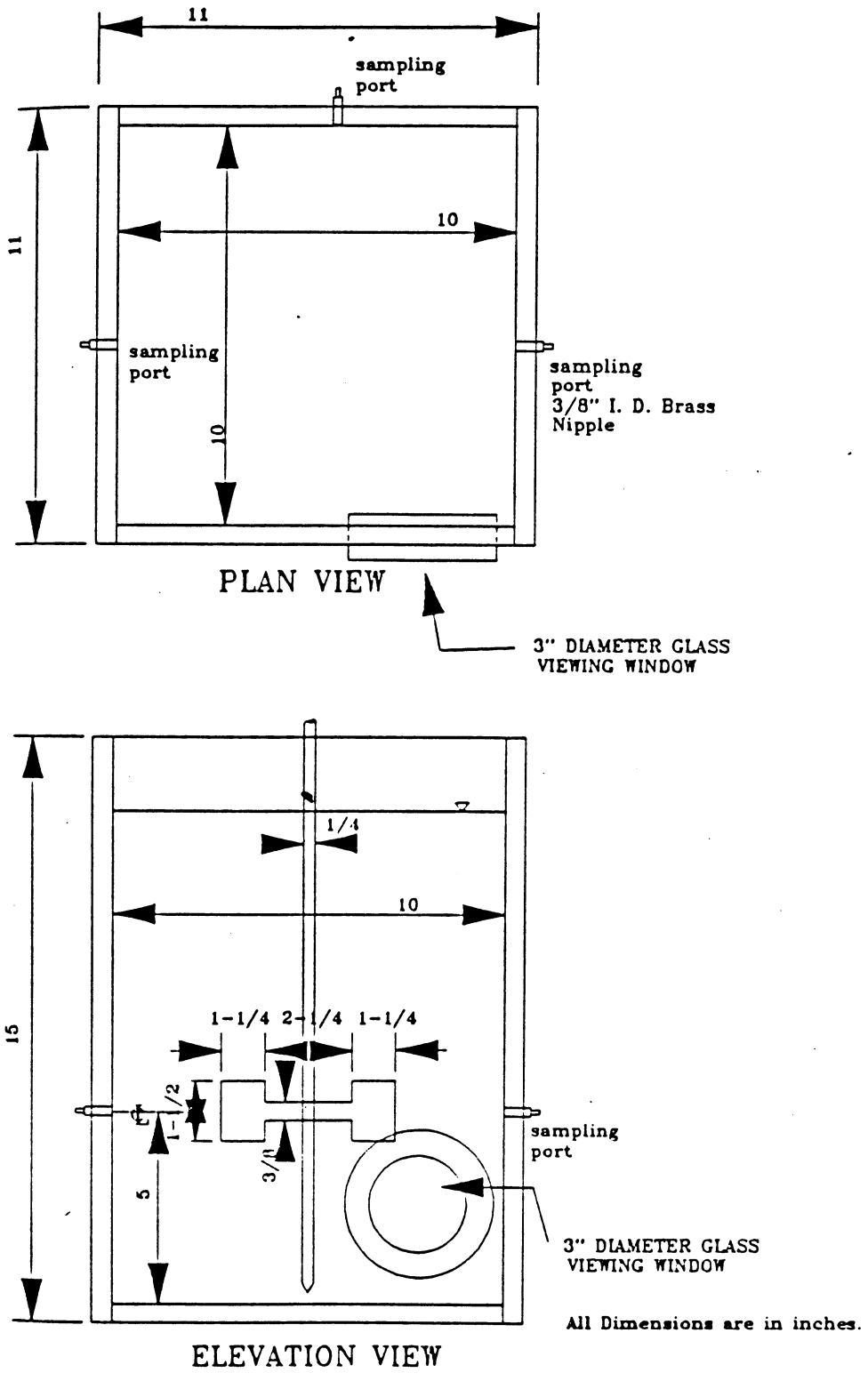

Figure 6. Schematic of the batch reactor (Hanson, 1989)

Clay

Kaolinite clay was used as the primary particle source. The kaolinite clay had a log mean diameter of 1.8 μm. In this study, a primary particle has been defined arbitarily as a particle with an equivalent circular diameter smaller than 2.5 μm.

Forty five liters of 800 mg/l clay stock solution were prepared at a time. The stock solution was thoroughly mixed by its circulation system for 40 minutes before each experiment. Once the suspension was completely mixed, the sample hose was purged briefly to waste, and a 562.5 ml of clay stock suspension was collected in a graduated cylinder. The 562.5 ml of stock suspension was added to the reactor which was previously filled with 17.5 liter of buffered tap water. The final volume of liquid and clay stock suspension in the reactor was 18 liters for each experiment. The motor was then turned on and the mixing speed was adjusted to 250 rpm for 3 minutes before taking the homogenized sample.

Buffered dilution water

The suspension dilution water was Ames, IA tap water buffered with 100 mg/l $NaHCO_3$. The buffer stock solution was 1 molar, that is 84.01 g/l of $NaHCO_3$. A day before the experiment, 17.5 liter buffered tap water was stored in the reactor inside the constant temperature room to achieve

temperature equilibrim.

Coagulant

Alum ($Al_2(SO_4)_3$ $18H_2O$) was used as coagulant in this study. A 0.25 M stock solution was prepared by weighing 166.6025 g of alum and dissolving it in distilled water to a total volume of one liter. The stock solution was stored in room temperature for about two months without any aging problem. The day before each experiment, 15 ml of 0.25M stock alum was transferred into 250 ml flask to prepare 10 mg/ml diluted solution. The solution was mixed by shaking the flask, and placed in the constant temperature room at 20°C for the next day's experiment.

Acid

All pH adjustments were made by using reagent grade HCl diluted volumetrically to 0.1N with distilled water.

C. Experimental Methods and Procedures

Temperature measurement

The temperature measurement and control was done automatically by a personal computer data collection and control system. The sensor of the system was a type "T" thermocouple which was placed in a cup of water in the

temperature room and was connected with the computer system.

The temperature goal for all experiments was 20 ± 0.1°C. However, due to the influence of clay stock suspension whose temperature fluctuated from day to day, the water temperature in the reactor was found to be in the range of 19.2 to 20.4 °C.

Tachometer

The mixing speed was measured using an Ametek Model 1736 tachometer with an encoder type sensor.

Motor controller

The Master Servodyne motor and motor controller were used to mix the batch reactor at a fixed, reproducible speed. The energy input, however, was not recorded from the Servodyne due to its inaccuracy in reading. Rather, it was calibrated from the work done by Argaman and Kaufman (1968) based on mixing speed. Their equation correlating rpm and G was expressed as:

$$G = 0.12(rpm)^{1.54} \qquad (71)$$

The water temperature for their experiments was kept at 20 ± 1 °C.

The following table illustrates the corresponding G value for each mixing speed.

Table 5. The relationship between mixing rpm speed and G at 20 ± 1 °C water temperature

Mixing Speed (rpm)	G Value (s^{-1})
10	4.2
30	22.6
45	42.2
60	65.7
100	144.3

Turbidity measurement

The turbidity of the homogenized suspension was checked on a Hach Model 18900 Ratio Turbidimeter at the beginning of the experiments and recorded. Initial turbidities of the 17 experiments are shown in Figure 7. Those initial turbidities have a mean of 22.8, and estimated standard deviation of 2.1.

pH adjustment and monitoring

The pH of the system was monitored using a 12 mm diameter pH probe, and a Fisher Accumet #610 pH meter. The pH meter was standardized using first a 4.0 pH buffer, then a 7.0 pH buffer. The pH meter was checked at the beginning of each experiment.

An optimal pH value of 6.8 after rapid mixing was

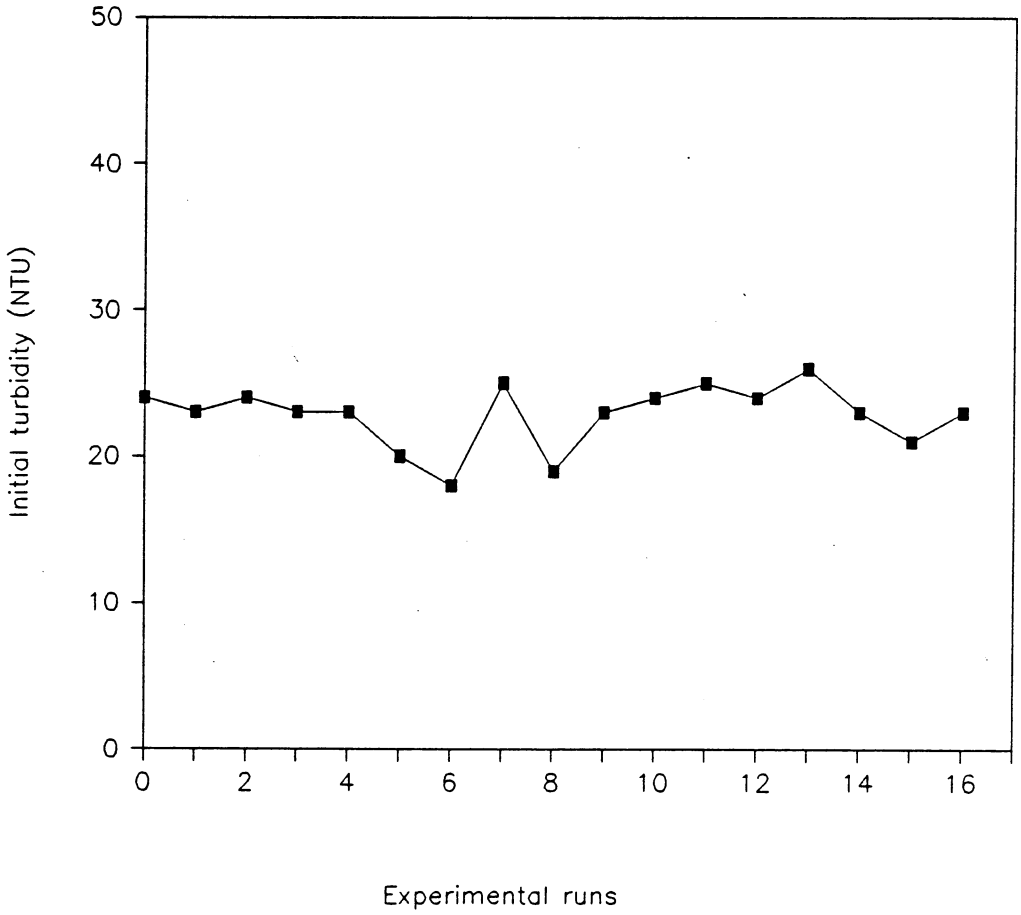

Figure 7. Initial turbidities of the flocculation experiments

selected in this study based on Hanson's work (1989) for alum dosage of 5 mg/l. Prior to all experiments, preliminary tests were conducted to find the amount of acid needed for to achieve the desired pH during flocculation. The results of those preliminary tests indicated that 90 ml of 0.1 HCl was needed to achieve a stable pH of 6.8 during flocculation. Before the addition of the acid, clay suspension was mixed at 250 rpm for 3 minutes and the homogenized sample was taken. Then, 90 ml HCl was added through the sample port on the side of the reactor, using a 60 ml syringe with a #13 gauge needle. This would bring the pH down to around 6.6, but the pH values would recover gradually. Once pH went up to 6.85, 9 ml of alum was injected immediately through the sample port using 10 ml syringe with a # 13 gauge needle. This would produce pH after rapid mixing right at 6.8. The pH profile during rapid mixing is illustrated in Figure 8. During the slow mixing process, pH continued to drift up slightly. The extent of the pH increase was determined by the flocculation intensity. A high flocculation intensity was accompanied by a higher pH shift. Figures 9 and 10 show the two extreme examples of pH changes during slow mixing for flocculation G values at 4.2 and 144.3 s^{-1}, respectively.

A detailed discussion about the cause of pH changes during the flocculation process can be found in Hanson's work (1989).

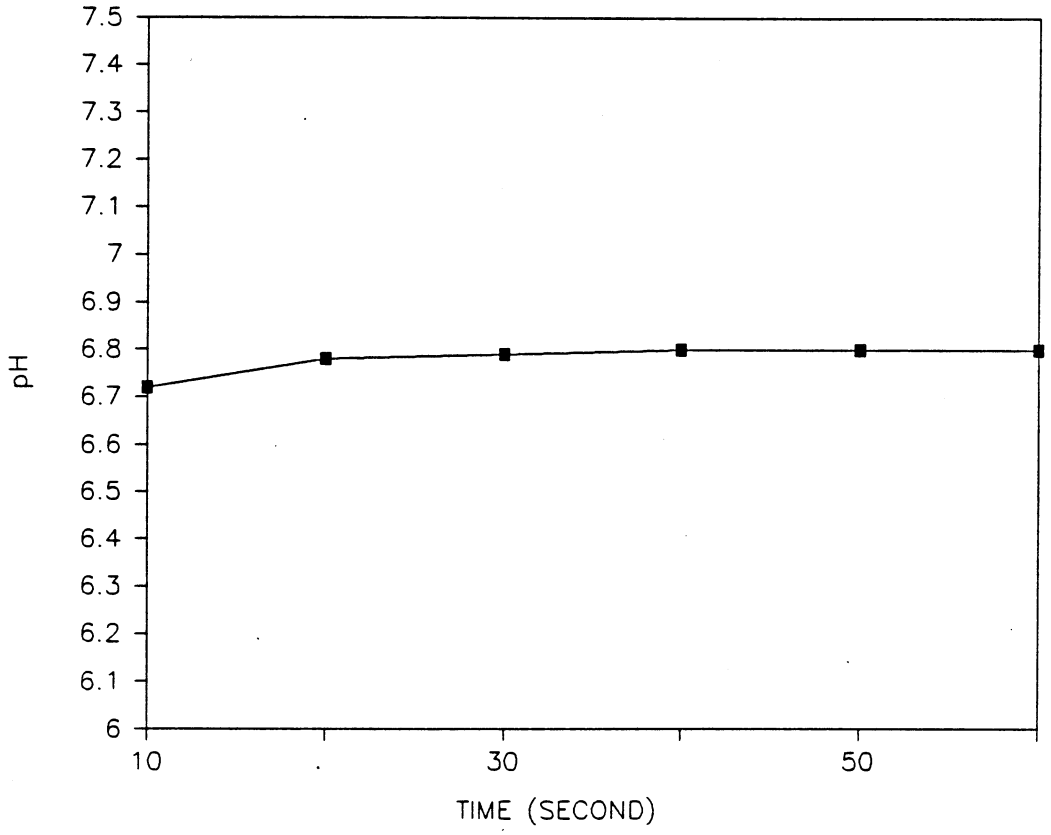

Figure 8. pH profile during rapid mixing at G = 500 s^{-1}

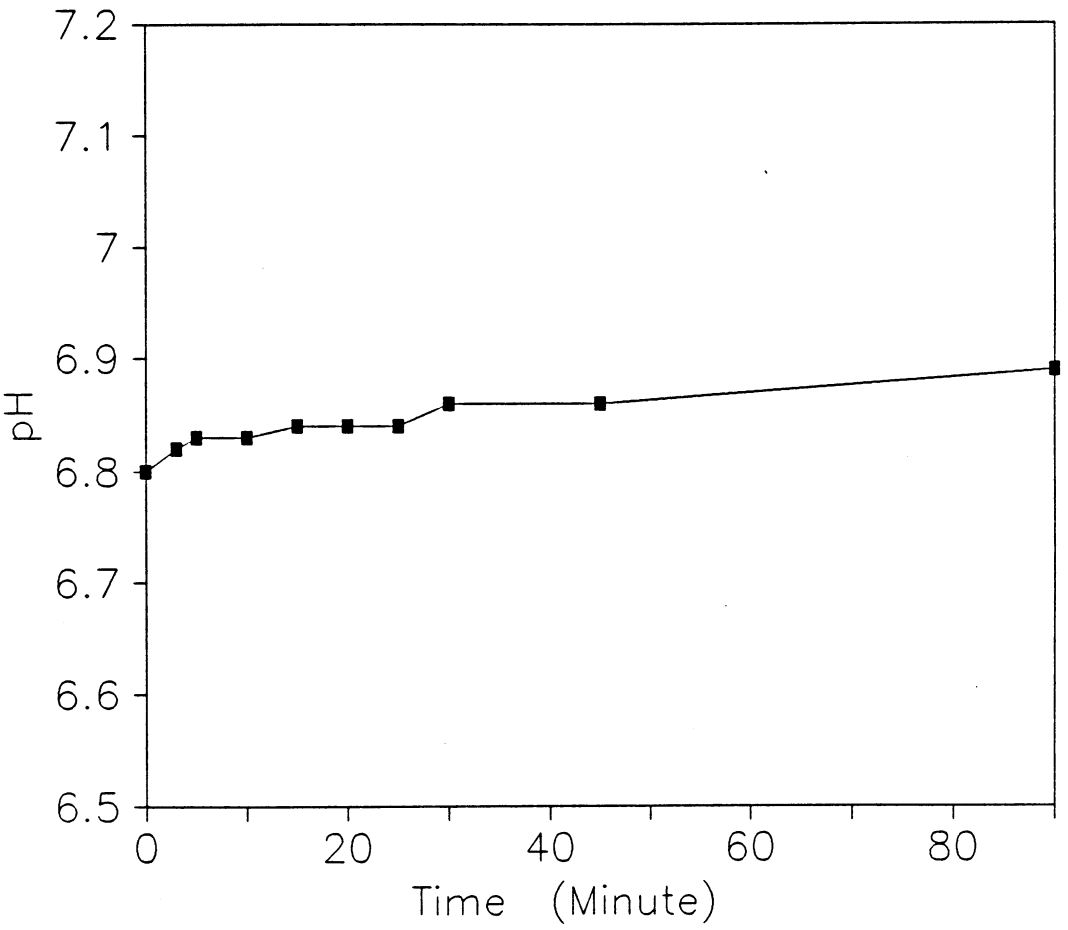

Figure 9. pH profile during slow mixing at G = 4.2 s^{-1}

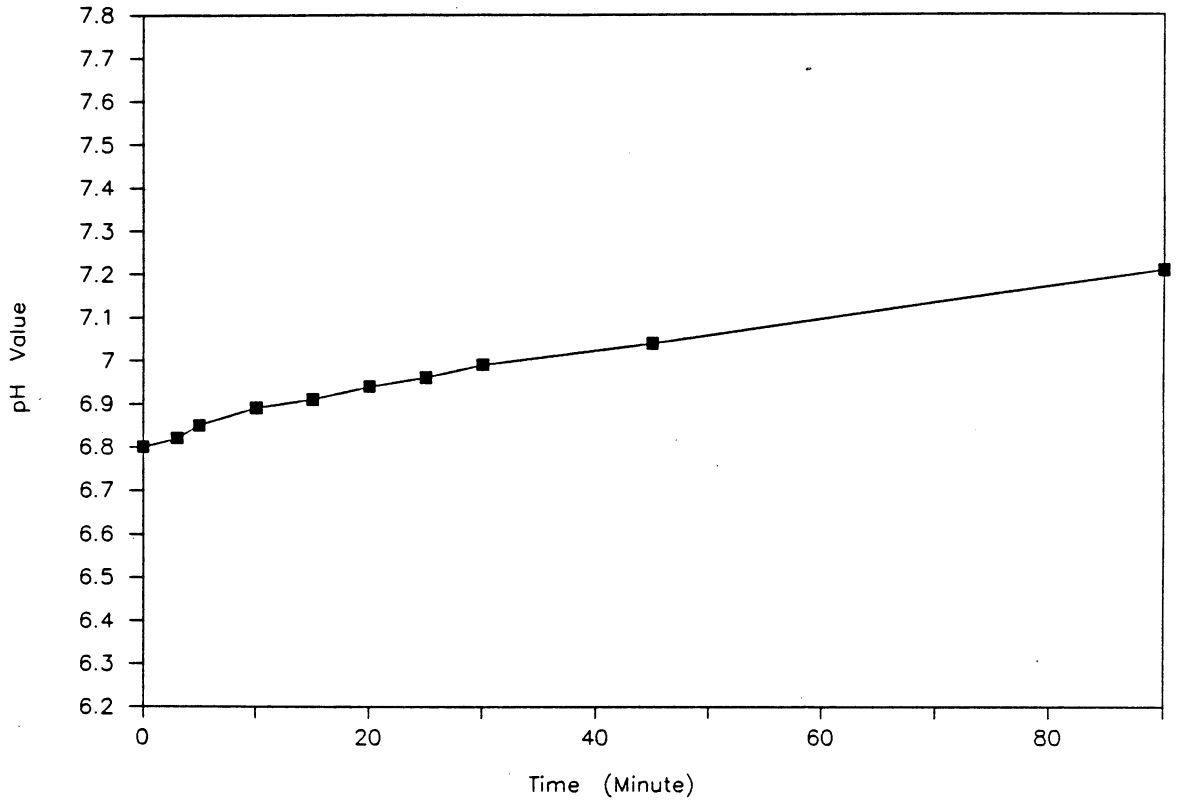

Figure 10. pH profile during slow mixing at G = 144.3 s^{-1}

Sample collection

During the flocculation work, samples were collected at the following times for analysis of the particle size distributions:

- Prior to coagulant addition, called the homogenized sample
- Immediately following rapid mixing, time zero
- 3, 5, 10, 15, 20, 25, 30, 45 and 90 minutes after slow mixing began

The samples were withdrawn from the reactor through sample port using a 1-ml syringe with a #13 gauge Perfectum PS 13 Hospileur 4-1/2 stainless steel hypodermic needle. The sample was collected carefully over a time period of 15 seconds. It was immediately placed in a specially constructed counting cell. Each sample cell was covered with 45×50 mm Number 1-1/2 Fisher brand Microscope Cover Glass. The procedure of filling a cell with sample is described by Hanson (1989).

Once the cell was filled, it was allowed to sit overnight for particles to settle down to the bottom of the cell which is also the focal plane of the microscope.

Before this study, the cell depth for each sample cell had been measured by a previous researcher (Hanson, 1989) using a handheld micrometer. There are three major disadvantages for using a micrometer in measuring cell depth:

(1) The micrometer has to contact the cell floor for the measurement. This will inevitably result in some scratches to the floor of the cell. The image of the scratches will be picked up by AIA camera and be counted as particles.

(2) The configuration of the micrometer limits its reach to only the annular area of the cell near the cell edge. Readings were not possible near the center of the cell. Therefore, the readings do not represent the average depth of the cell. This problem is especially critical for some of the cells whose floors are not very flat.

(3) The accuracy of a micrometer is 10 micro meters.

In this study, the measurement of the cell depth was conducted by means of an Olympus BH-2 optical microscope.

The Olympus BH-2 optical microscope has a very special feature - the scales on the focus knob make it possible to measure the position of the focused objective plane. There are 100 units scaled around the focus knob. Each unit represents a 2 μm distance adjustment by the knob. One revolution of the knob will lower or raise the focused objective plane $100 \times 2 = 200$ μm.

To measure the cell depth using this microscope, a cell was covered with a cover glass tightly by moisturing the cell edge with some water. Place the cell with the cover glass under the objective lens of the microscope and the focus the bottom of the cover glass. The position was recorded by

writing down the focus knob reading. Then focus on the floor of the cell and the second focus knob reading was recorded. The difference between the two readings gave the exact cell depth on that point of the cell. In order to get more accurate cell depth, depths were measured at ten to twelve different locations in the cell and an average cell depth was calculated.

The cell depth measured in this way did not leave any scratches on the cell floor. Furthermore, the measurement is more accurate and representative of the entire cell area than that previously measured with the micrometer.

Lemont OASYS automatic image analysis

The automatic image analysis (AIA) system, consisting of an Olympus BH-2 optical microscope (Olympus Corporation, Lake Success, NY) and the Lemont Image Analysis System (Lemont Scientific Inc., State College, PA), were used to analyze particle size distribution from the flocculation samples. A schematic of the system can be seen in Figure 11. A video camera, which is mounted to the top of the microscope, collects the sample image from the microscope and transmits it to the image analyzer, where the live image is digitized. Based on the information from the digitized image, the image analysis software estimates parameters such as the particle projected area, equivalent circular diameter, perimeter, angle

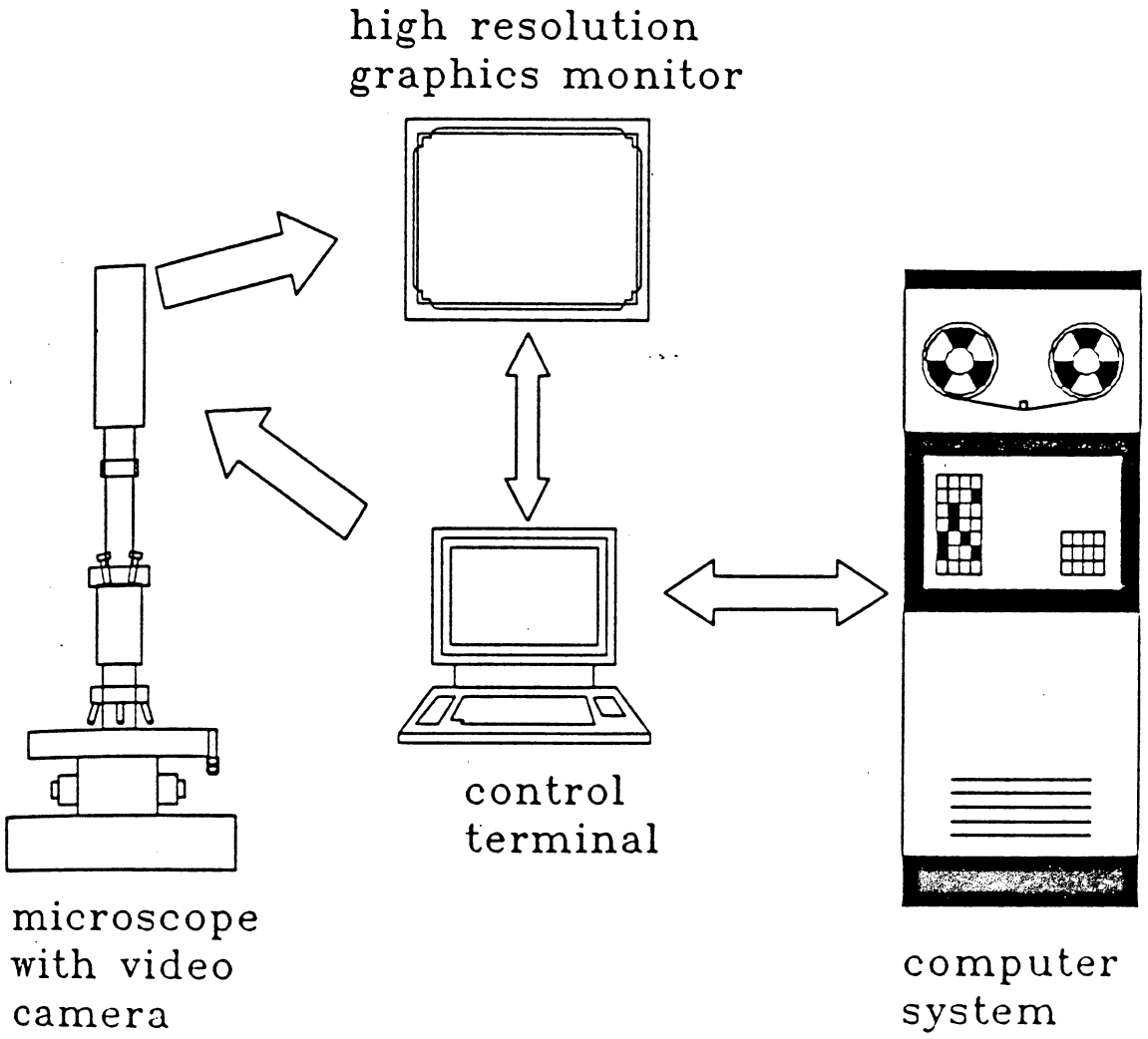

Figure 11. Schematic of the fully automatic image analysis system (AIA) (Hanson, 1989)

of repose, etc., and then divides the particles into classes based on this information. The particles projected area class, or histogram, was used to classify the particles analyzed in this study.

A detailed instruction on the system is given by Hanson (1989). The only difference was that the magnification of the system was calibrated each time before sample analysis in this study. This was done by using an objective micrometer which is scaled to 0.01 mm. The image of the scales on the objective micrometer was collected by the camera and was shown in the screen of the monitor. Then a certain length of the scale was selected for the calibration of the magnification by inputing the actual distance corresponding to that length. The calculation of the magnification was done automatically by the computer and the value was shown on the screen of the computer.

Summary of experimental procedure

Having discussed the experimental equipment and material preparation, let's have an overview of the experimental procedure.

The day before the experiment, the buffered tap water was introduced into the reactor and allowed to come to thermal equilibrium with the surroundings. The stock 0.25 Molar alum solution was diluted using distilled water to create a

10 mg/ml dosing solution, which was stored in the constant temperature room.

On the day of experiment, the clay stock suspension was mixed by its circulating pump for 40 minutes. Then 562.5 ml of the clay stock suspension was transferred to the reactor. More buffered tap water is added, if necessary, to adjust the volume to 18 liters in the reactor. The suspension in the reactor was then stirred at 250 rpm ($G = 500\ s^{-1}$) for 3 minutes. After 50 ml of homogenized sample was withdrawn, 90 ml 0.1 N HCl was injected into suspension through sample port and the pH was monitored constantly during its recovery. Once the pH value reached 6.85, 9 ml of alum dosing solution was injected in to the suspension through the sample port. The rapid mixing lasted for 60 seconds at $G=500\ s^{-1}$. During the rapid mixing, the pH values were recorded every 10 seconds.

A sample was taken after 60 seconds of rapid mixing. The turbine mixer was turned down to the desired speed for slow mixing. During the course of flocculation, samples were taken at time intervals of 3, 5, 10, 15, 20, 25, 30 45, and in many cases, 90 minutes of flocculation.

The 1 ml syringe with #13 stainless steel needles were used to extract samples from the reactor through its sample port. The plunger of the syringe was slowly withdrawn over about 15 seconds so that the sample was gradually induced into the body of the syringe. The sample was then transferred into

the sample cell by slowly filling the cell, starting from one end of the cell, and covering the cell with the microscope glass cover as the cell was gradually filled. When this was done, the glass cover was then gently pressed down around the edges using kimwipes and excess sample, which emerged from under the cover slip, was absorbed and wiped off. Then the sample cell was placed in a container to sit overnight for particle size distribution analysis.

After the flocculation experiment was done, the reactor and sample syringes and needles were washed thoroughly and saved for the next experiment.

The flocculation experiments were conducted at five different G levels: 4.2, 22.6, 44.2, 65.7, 144.3 s^{-1}. Three to four replications of each level were performed. The other experimental conditions for this research were listed in Table 6.

Table 6. Summary of experimental conditions

Water temperature	20 ^{0}C
Primary particles	Kaolinite clay, 25 mg/l, 23 NTU
Water	Ames, IA tap water buffered with 100 mg/l $NaHCO_3$
Coagulant	Alum as $Al_2(SO_4)_3.18H_2O$; 10 mg/ml aged at 20 ^{0}C overnight; Dosage: 5 mg/l
Rapid mixing intensity	500 s^{-1}
Rapid mixing time	60 s

V. RESULTS AND DISCUSSION

A. Introduction

Experiments were conducted at five different level of flocculation energy input, G, with three to four replications for each level. The flocculation data are presented by n_{10}/n_1 versus time, as used by Argaman & Kaufman (1968). n_{10} is the primary particle concentration at the beginning of flocculation (immediately after rapid mixing), and n_1 is the primary particle concentration at time t. Here, samples at times of 3, 5, 10, 15, 20, 25, 30, 45, and in some cases, 90 minutes of flocculation were analyzed.

According to the proposed New Model 1, the flocculation process can be divided into two stages, the first stage where primary particles dominant and the flocculation rate is determined by the collision rate between primary particles, and the second stage where the flocculation rate is controlled by the collision frequency between a primary particle and floc. In the following section of this thesis, the particle size distribution during the flocculation process will be analyzed to test the validity of the New Model 1 - two stage flocculation theory. In section C, the experimental variance will be analyzed according to the standard statistical procedures. The analysis of variance will give us such

information as the pure experimental error, the significance of the flocculation energy input and time on the flocculation performance. Model verification and comparison will be performed in section D.

B. Particle Size Distribution Analysis

The particles size distribution was analyzed based on their projected area distribution which was then transformed into geometric mean diameter distribution.

Figures 12 to 16 show the particle size (geometric mean diameter which is calculated based on equivalent spherical diameter) distribution at each flocculation time for five levels of energy input. The vertical axis is the cumulative percentage of primary particle number concentration, while the horizontal axis is the geometric mean of primary particle diameter based on equivalent spherical diameter. The data represent the replication means of the experiments.

Figures 12 and 13 demonstrates that more than 85% of particles are primary particles for flocculation time less than 25 minutes. As the flocculation process goes on, the percentage of the primary particle concentration declined. In Figure 14, the primary particle concentration represents 85% of the total particles' for flocculation times less than 15 minutes at flocculation energy G = 42.2 s^{-1}. At G = 65.7 s^{-1} as

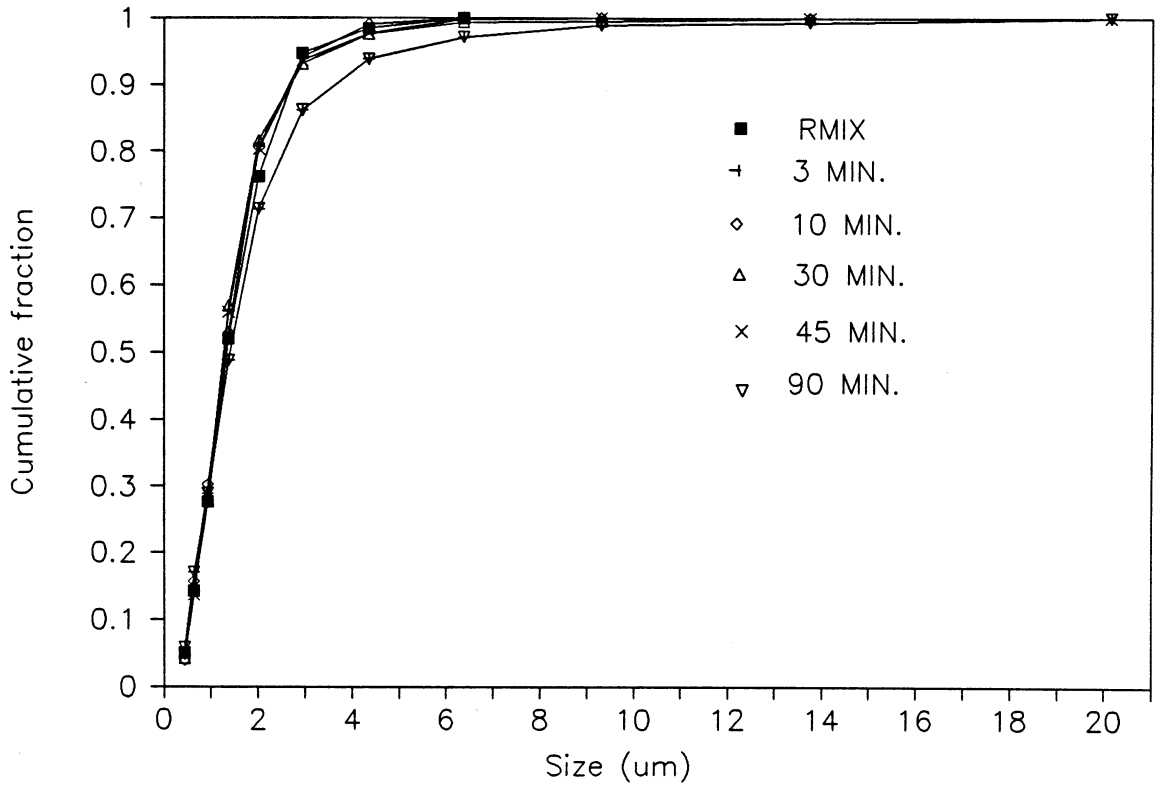

Figure 12. Cumulative particle size distribution versus time during flocculation, rapid mixing $G = 500\ s^{-1}$ for 1 minute, slow mixing $G = 4.2\ s^{-1}$

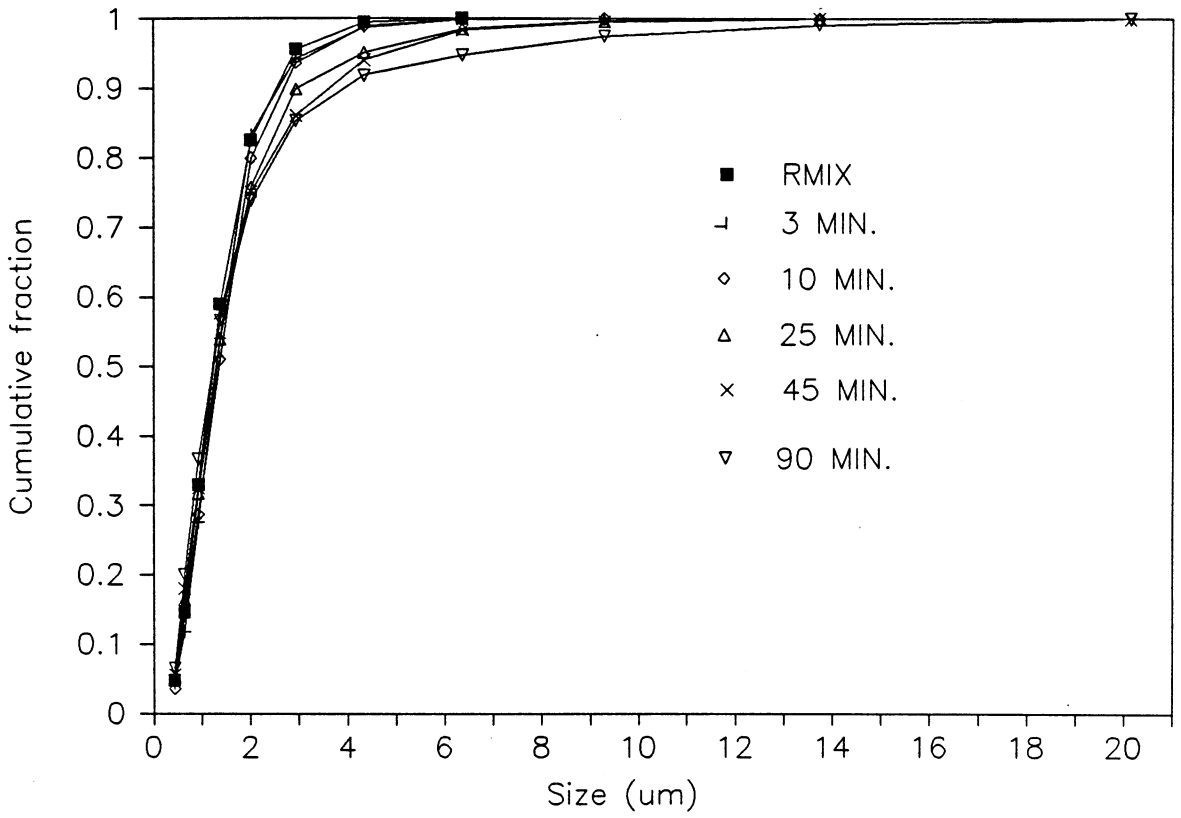

Figure 13. Cumulative particle size distribution versus time during flocculation, rapid mixing $G = 500\ s^{-1}$ for 1 minute, slow mixing $G = 22.6\ s^{-1}$

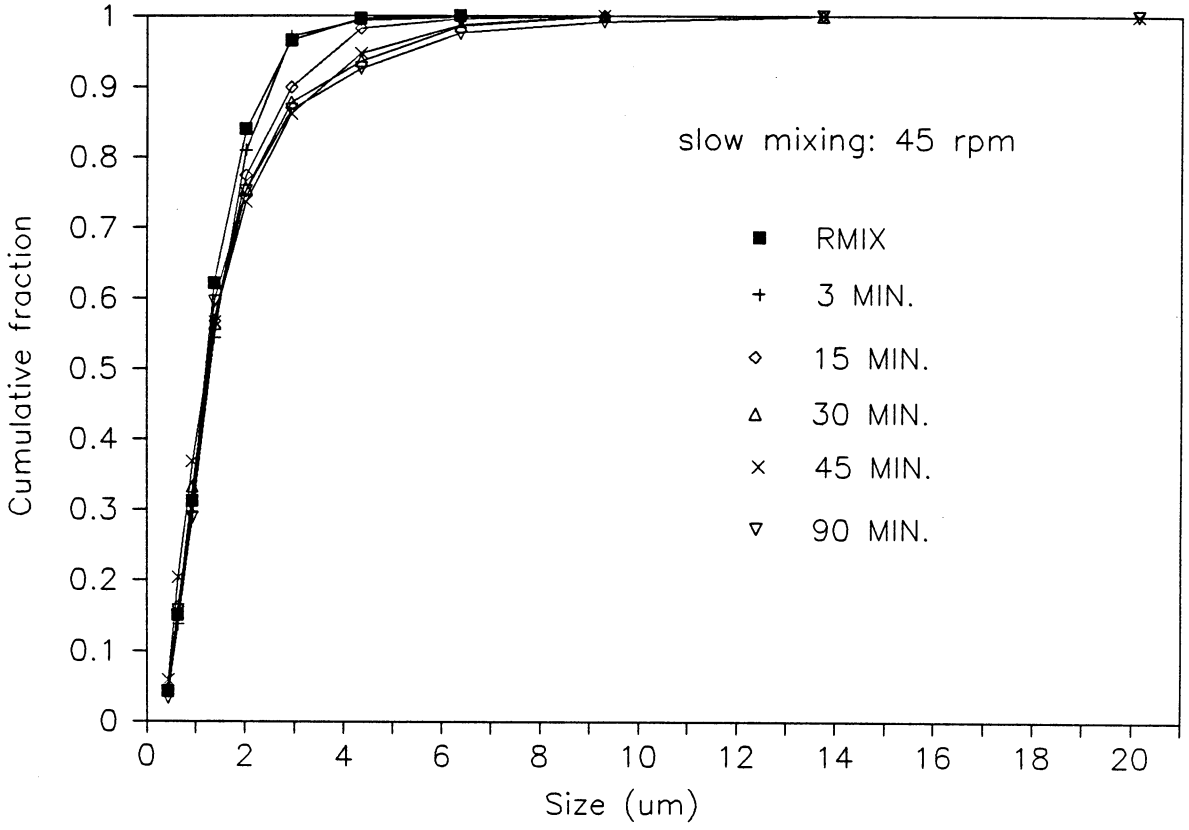

Figure 14. Cumulative particle size distribution versus time during flocculation at rapid mixing $\underline{G}_1$ = 500 s^{-1} for 1 minute, slow mixing G = 42.2 s^{-1}

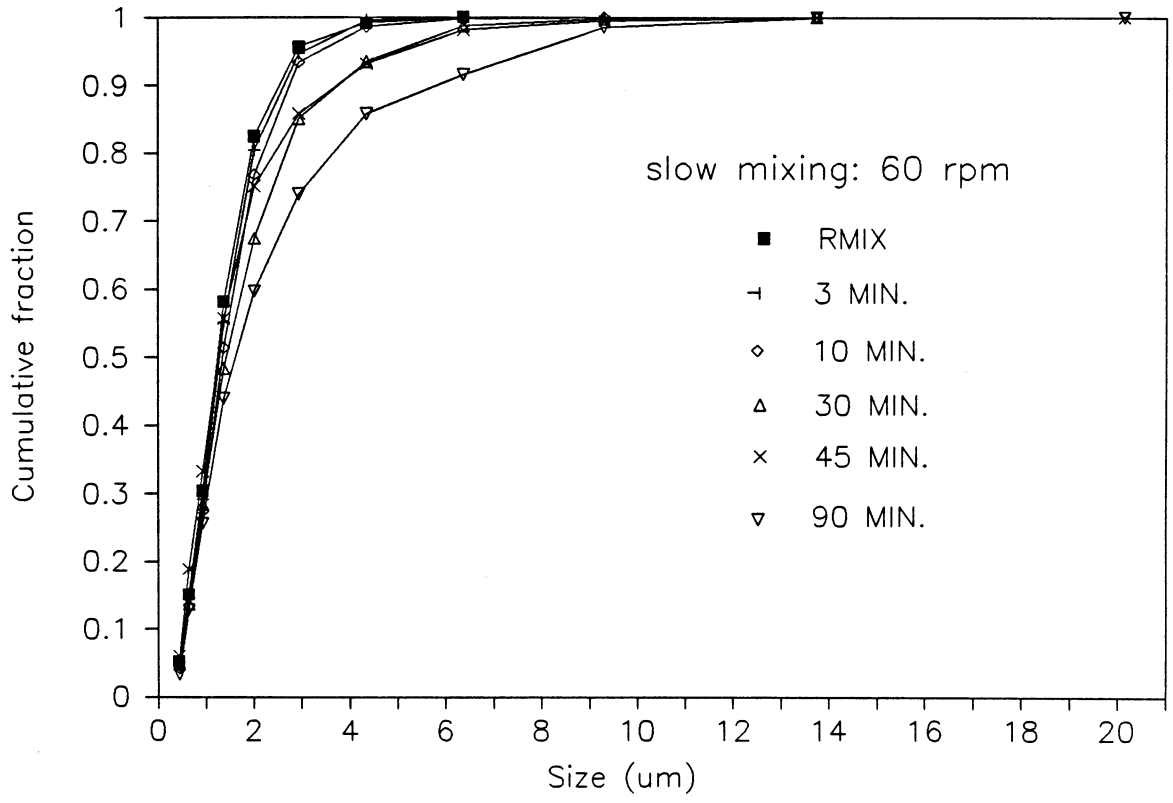

Figure 15. Cumulative particle size distribution versus time during flocculation, rapid mixing G = 500 s^{-1} for 1 minute, slow mixing G = 65.7 s^{-1}

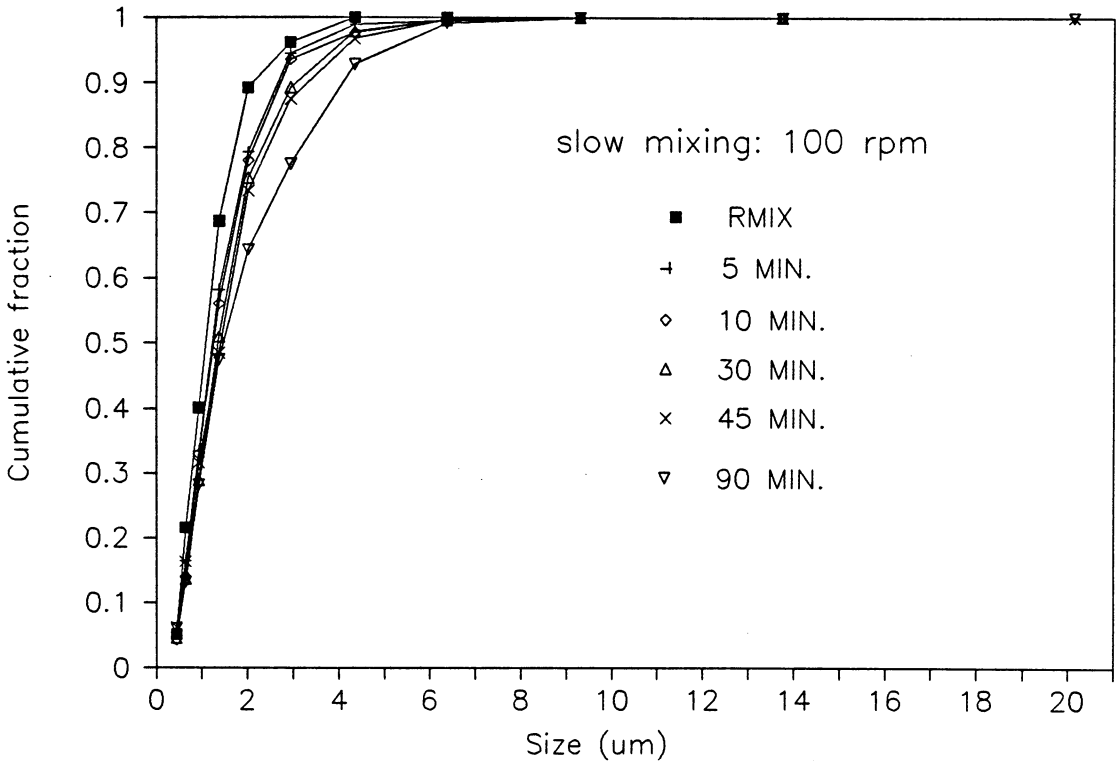

Figure 16. Cumulative particle size distribution versus time during flocculation, rapid mixing G = 500 s^{-1} for 1 minute, slow mixing G = 144.3 s^{-1}

seen in Figure 15, the primary particle consists 85% when flocculation time is less than 10 minutes.

Based on this information, the (Gt)cr of 36,000 was taken as the critical Gt product to separate the two stages of flocculation. The first stage of flocculation was defined when $Gt \leq (Gt)cr$, and second stage was assumed with $Gt > (Gt)cr$. The experimental results support the values of critical t values at different G levels as presented in Table 1.

C. Analysis of Variance for Flocculation Experiments

The purpose of our flocculation experiments was to test the existing and proposed kinetic flocculation models described in Chapter III.

The experiments were designed to investigate quantitatively the impact of two factors - flocculation intensity G and flocculation time on the flocculation performance which is expressed as the ratio of initial primary particle concentration to the primary particle concentration at any time, n_{10}/n_1.

Factors G and t are independent variables whose values were selected based on the actual flocculation practices in the water treatment industry. The ranges for G and t were beyond current practical values to make their impacts appear more pronounced and easily discernible. n_{10}/n_1 is a dependent

variable or response variable whose values depends on G and t.

One assumption of experimental science is that each experimental unit is unique. Under this study, an experimental unit is the 18-liter jar of clay suspension to be flocculated. It is impossible for two units under the same experimental conditions to give identical results. In some cases, a high degree of control is used and this, combined with crude measurement, can give an impression of exact replication of results over experimental units. However, if the measurement is sufficiently refined, no two suspension samples will give the same particle distribution profile, and no two experimental units will yield identical responses no matter how much care is taken to standardize techniques, control conditions and to select uniform experimental material. The consequence of this basic assumption is an unavoidable requirement for replication of experimental units within a set of flocculation conditions, or a set of treatment conditions, so that the magnitude of variability of the experimental error or, the pure experimental error can be estimated.

The experimental treatments employed in this study are five levels of flocculation intensity (G at 4.2, 22.6, 42.2, 65.7 and 144.3 s^{-1}) and ten levels of flocculation time (t at 0, 3, 5, 10, 15, 20 25, 30, 45 and 90 minutes). To examine the effects of these two factors (G and t) on the flocculation response, the standard factorial experimental design should be

employed in the study. A factorial experiment is an experiment in which the response is observed in all factor-level combinations of independent variables.

Factorial experiment is usually expressed by $n_1*n_2*...*n_k$, which means the experiments contains k factors, n_1 levels for the first factor, n_2 levels for the second factor,..., and n_k levels for the kth factor. An experiment produces a k-way classification of the data if all factor-level combinations of the k independent variables are observed at least once. Therefor, our flocculation tests can be written as a two-way classification, 5*10 factorial experiments, indicating 5 levels of factor G, and 10 levels of factor t.

A special ingredient in this factorial experimental design is the randomization which requires that treatments (i.e., the factor-level combinations) should be assigned to the experimental unit (i.e., 18-liter clay suspension) at random. By a random assignment of the treatments to the units one assumes that one of the possible outcomes has been selected for examination and, in the selection, all the outcomes had an equal chance of being examined.

The randomization of the experimental design in this study also assures that the impact on flocculation performance caused by any changes in unknown experimental conditions (for example, tap water quality) could be "averaged" over all experiments. Since we could not randomize the time factor in

our study, the randomization enters the design by insisting that the assignment of G levels to the experimental units be done by some random order. Since G has five levels (4.2, 22.6, 42.2 65.7, and 144.3 s^{-1}) and we want to have 3 replications for each level, than we need to run 5×3=15 experiments. The order or the sequence of the 15 experiments has to be selected randomly.

The question we are going to answer is whether the two factors G and t have significant impact on flocculation performance. The answer to the question seems to be obvious. Nevertheless, the procedure is necessary from the statistical point of view. If there is no impact from either G or t, or their interaction, it is meaningless to construct a kinetic model which includes their effects. The procedure we are going to use for this test is called the analysis of variance (Ott, 1988). A typical table illustrating the results from analysis of variance is given by Table 7. Table 7 illustrates the analysis of variance from the a×b factorial experiment with "a" levels of factor A and "b" level of factor B and r replications for each level-factor combination.

The first column of Table 7 shows the sources of variability, factor A, factor B, and their interaction expressed as AB. The rest of the variance not counted by A or B or AB is due to experimental error. We call this variance the pure experimental error. The second column of the table

Table 7. Analysis of variance

Sources	df	Sum of Squares	Mean Squares
A	a-1	SSA	MSA = SSA/(a-1)
B	b-1	SSB	MSB = SSB/(b-1)
AB	(a-1)×(b-1)	SSAB	MSAB = SSAB/((a-1)×(b-1))
Error	ab×(r-1)	SSE	MSE = SSE/(ab×(r-1))
Totals	abr-1	TSS	

shows the degree of freedom associated with each source. The third column is the sum of squares due to each source. The fourth column gives us the mean squares which are calculated from sum of squares divided by the corresponding degree of freedom. The calculation for sum of squares are given as follows:

$$SSA = rb\sum_i (\bar{y}_{iA}-\bar{y}) \tag{72}$$

$$SSB = ra\sum_j (\bar{y}_{jB}-\bar{y})^2 \tag{73}$$

$$SSAB = \frac{1}{r}\sum_{ij}(\sum_{k} y_{ijk})^2 - SSA - SSB - \frac{1}{abr}(\sum_{ijk} y_{ijk})^2 \qquad (74)$$

$$SSE = \sum_{ijk}(y_{ijk} - \bar{y}_{ij})^2 \qquad (75)$$

$$TSS = SSA + SSB + SSAB + SSE \qquad (76)$$

where

$\bar{y}_{iA}$ is the average of observations receiving ith level of A;

$\bar{y}_{jB}$ is the average of observations receiving jth level of B;

$\bar{y}_{ij}$ is the average of observations receiving ith level of A and jth level of B;

y_{ijk} is the observation of kth replication at ith level of A and jth level of B;

i = 1,2, ..., a

j = 1,2, ..., b;

k = 1,2, ..., r.

To test if there is difference among factor A, i.e., if factor A is significant, the standard F test is used.

$$F_A = \frac{MSA}{MSE} \qquad (77)$$

with $df_1 = a-1$, $df_2 = ab\times(r-1)$

$$F_B = \frac{MSB}{MSE} \tag{78}$$

with $df_1 = b-1$, $df_2 = ab\times(r-1)$

$$F_{AB} = \frac{MSAB}{MSE} \tag{79}$$

with $df_1 = (a-1)\times(b-1)$, $df_2 = ab\times(r-1)$

If we select confidence coefficient, $(1-\alpha)$ of 95%, i.e., $\alpha = 0.05$, as the probability, we can find tabulated F values in a statistical table of percentage points of the F distribution with the corresponding df_1 and df_2. If our calculated F value is larger than the tabulated value, we reject the hypothesis of the factor is not significant and conclude that we have sufficient evidence to indicate that the factor has significant effect. The hypothesis is often denoted as H_0:

H_0: No difference among levels of the factor (A, B, or AB interaction)

Next, we are going to follow these statistical procedures to test the following hypotheses:

$(H_0)_1$: No difference in flocculation performance among 5 different G levels;

$(H_0)_2$: No difference in flocculation performance among 10 time intervals;

$(H_0)_3$: Flocculation time and energy input do not have interactive effects.

Table 8 gives the data from our 5×10 factorial experiments. The analysis of variance of the experimental data was performed by executing SAS GLM procedure. The program is given in the Appendix C and its result of ANOVA table is listed in Table 8.

Table 8. Analysis of variance of flocculation data (5×10 factorial experiments)

Source	df	SS	MS	F
Energy, G	4	10.038	2.510	2.510/0.172=14.57
Time, t	9	114.513	12.724	12.724/0.172=73.89
G×t	36	27.316	0.759	0.759/0.172=4.41
Error	110	18.937		
Total	159	170.8044		

With significance level = 0.05, $df_1 = 36$ for AB interaction, $df_2 = 110$, we find out that the tabulated values of $F(36,110) = 2.10 < F$ for interaction which is 4.41. This indicates that strong interactive effect between energy input

G and time t exists. For the main effects of energy G and time t:

$F(4,110) = 13.6 < F$ for G which is 14.57 and

$F(9,110) = 2.76 < F$ for t which is 73.89,

Therefore, we have sufficient evidence to indicate that G and t have significant effects on flocculation performance.

Figure 17 shows the relationship between flocculation performance with flocculation time at different G levels. If such a figure showed approximately parallel curves, there would be no interaction. Since the curves in Figure 17 were far from parallel, a strong interaction between G and t is indicated.

So far we have discussed the significance of G and t for flocculation experiments through the analysis of variance. We conclude that the interaction of G and t as well as their main effects on flocculation performance are all significant. But remember that all these discussions just give us an qualitative information. We are more interested in estimating quantitatively the effects of G and t on flocculation performance. This work will be done in the next section, Model Verification, via standard statistical analysis of the fitness of the models to our experimental data.

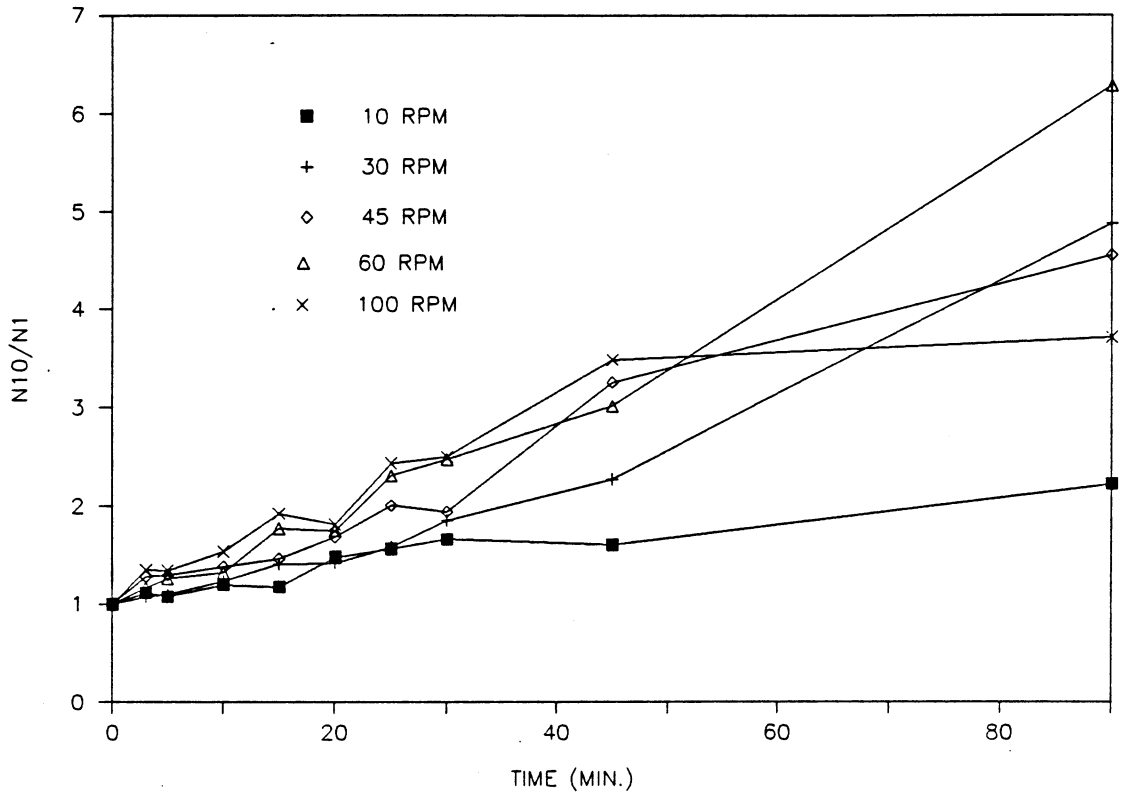

Figure 17. Relationship between flocculation performance and flocculation time at different G levels (Points on the curve represent experimental means from 3 to 4 replications of experiment at each G level)

D. Model Verification and Comparison

The analysis in the previous section indicated that there is significant interaction of velocity gradient G and flocculation time t in their effects on flocculation experiments. The flocculation kinetic models which were discussed in Chapter III represent quantitatively how the two factors G and t affect flocculation performance. In this section, model verification and comparison will be conducted through some statistical analyses.

In order to make model application more general, some experimental results from other researchers (Hanson, 1989; Argaman and Kaufman, 1968) are also utilized for model verification and comparison. Therefore, we have three set of data set 1, set 2, and set 3, representing data from current study, Hanson's work (1989), and Argaman and Kaufman's research (1968), respectively. The data sets are given in appendix D, E, and F, respectively.

Data set 2 was obtained in the following experimental conditions:

- Batch reactor flocculation;
- Water temperature = 20°C;
- Clay suspension concentration = 25 mg/l;
- Alum dosage = 5 mg/l;

and two G levels (22.6 and 65.7 s^{-1}), with three replications

for each level. Samples were taken at 0, 1, 3, 5, 10, 15, 20, 25, and 30 minutes of flocculation.

Data set 3 was obtained in the following conditions:

. Single CSTR flocculation;

. Water temperature = 20 ± 1°C;

. Clay suspension concentration = 25 mg/l;

. Alum dosage = 25 mg/l;

with G at 30, 45, 60, 90, 120, 180, 240 s^{-1} for flocculation time of 8, 12, 16, 24 minutes. No replications of the experiments were conducted. Cautions should be given in interpreting Argaman and Kaufman's data. The primary particle concentration in their flocculation tests was not measured by AIA system as it was in experiments from which data sets 1 and 2 were collected. Argaman and Kaufman used light scattering photometer to measure absolute turbidity of their samples. The relative concentration of primary particles in the sample was determined by measuring the turbidity after 30 minutes of settling, and by using a calibration curve relating the primary particles concentration and the absolute turbidity.

The models of Tables 2 and 3 are use to fit our three sets of data to estimate such parameters as k_0, k_a, k_b using least square methods. This work was done by running "NLIN" - nonlinear procedure and REG procedure in SAS. The letters of SAS stand for Statistical Analysis System which is a software system for data analysis. It provides all the tools needed for

data analysis (SAS Institude, Inc., 1979):

. information storage and retrieval

. data modification and programming

. report writing

. statistical analysis

. file handling

A wide variety of statistical analysis can be performed by SAS procedures. AS shown in Tables 2 and 3, the models to be tested in this study are non-linear with respect to parameters k_0, k_a, and k_b, except for equation 55 which is linear with respect to k_0. For non-linear regression models, the NLIN procedure in SAS was selected for parameters estimations. Procedure of REG in SAS was used for linear model regression and parameter estimation.

NLIN (Non-LINear regression) procedure produces least-squares or weighted least squares estimates of the parameters of a non-linear model. A complete NLIN program employed in this study consisted of two parts: i) data input step and ii) SAS NLIN procedure step (PROC step). In the data input step, the experimental data of n_{10}/n_1 with its corresponding flocculation time, t, and flocculation energy level, G, were sent into the SAS data set. A hundred and sixty such data points from 17 flocculation tests (which were conducted under five different G levels during this study shown in Table 4) were sent to the SAS data set as data set 1. Data sets 2 and 3

were also sent to the SAS data set for separate analysis as the first step for model regression. In the PROC step, the name of NLIN procedure was given in a PROC statement. SAS called this NLIN program from its library to analyze one data set. The followings explains how NLIN program works:

NLIN first performs a grid search to determine starting values for the parameters to be estimated, and then uses one of these three iterative methods:

. modified Gauss-Newton method

. Marquardt method

. gradient or steepest-descent method

to find the best estimation of the parameters.

The steepest descent method converges very slowly and uses more machine time than the other methods. The Marquardt method is a compromise between Gauss-Newton and the steepest descent. It is equivalent to performing ridge regressions and is most useful when the parameters are highly correlated. Since the parameters k_0, k_a, and k_b were shown to be correlated (correlation in the range of 0.8 to 0.9), The Marquardt method was selected as the iterative method in the NLIN program to be used in this study.

For each non-linear model to be estimated, the following items must be specified in the program:

. the names and the range of starting values of the parameters to be estimated (in this research, k_0 and

k_a are in the range of 10^{-6} to 10^{-4} and k_b in the range of 10^{-8} to 10^{-7})

- the models (expressed by equations 47, 67, 69 for data sets 1 and 2 and equations 46, 61, 70 for data set 3)
- partial derivatives of the model with respect to each parameter

During this study, Argaman and Kaufman's model and New Model 1, stage 2, and New Model 2 were fitted the three sets of data by NLIN regression program. The output from the NLIN procedures gave the following information:

- a list of residual sum of squares (SSE) associated with all or some of the combinations of possible starting values of parameters
- the estimates of the parameters and the residual sum of squares determined in each iteration performed
- if the convergence criterion was met, an analysis of variance table (including the sources of variation due to "regression" and "residual", "uncorrected total", and the "corrected total"); the estimates of the parameters; the asympotically valid standard error of the estimates; the asymptotically valid .95 confidence interval for the estimates; and the asymptotically valid estimated correlation matrix of the parameter estimates.

For the purpose of model comparision, the estimates of

the parameters and their estimated standard errors and the .95 confidence intervals are listed in Tables 9 through 11.

For the regression of New Model 1 which is separated into two satges, each data set was divided into two parts according to the critical Gt product of 36,000. The specific separating "t" values for different G levels were shown in Table 1. Since equation 55 is linear with respect to k_0, the linear program (REG in SAS) was employed to analyze the first parts of data set 1 and 2 for the first stage of flocculation in the batch reactor system from which data sets 1 and 2 were collected.

Table 9. Estimation of k_0 by least square analysis

Data Set	k_0	Est. σ	95% Confidence Intervals
New Model 1, Stage 1			
1	$1.590*10^{-5}$	$1.860*10^{-6}$	N/A*
2	$6.335*10^{-5}$	$3.810*10^{-6}$	N/A
3	$8.156*10^{-5}$	$2.841*10^{-6}$	$(7.426*10^{-5},8.887*10^{-5})$
New Model 2			
1	$1.689*10^{-5}$	$1.182*10^{-6}$	$(1.455*10^{-5},1.922*10^{-5})$
2	$7.360*10^{-5}$	$5.429*10^{-6}$	$(6.269*10^{-5},8.451*10^{-5})$
3	$1.157*10^{-5}$	$1.047*10^{-6}$	$(9.360*10^{-5},1.378*10^{-4})$

* means not available by the SAS program.

For CSTR system from which data set 3 was collected, the equation for New Model 1, stage 1 is non-linear (as shown by equation 61), NLIN program was used for parameter estimation.

Table 10. Estimation of k_a by least squares analysis

Data Set	k_a	Est. σ	95% Confidence Intervals
Argaman and Kaufman's model			
1	$1.000*10^{-5}$	$4.140*10^{-7}$	$(9.184*10^{-6}, 1.082*10^{-5})$
2	$3.744*10^{-5}$	$1.649*10^{-6}$	$(3.413*10^{-5}, 4.076*10^{-5})$
3	$4.265*10^{-5}$	$2.997*10^{-6}$	$(3.649*10^{-5}, 4.880*10^{-5})$
New Model 1, Stage 2			
1	$8.241*10^{-6}$	$6.953*10^{-7}$	$(6.851*10^{-6}, 9.631*10^{-6})$
2	$2.945*10^{-5}$	$9.812*10^{-6}$	$(8.075*10^{-6}, 5.083*10^{-5})$
3	$3.856*10^{-5}$	$3.217*10^{-6}$	$(3.185*10^{-5}, 4.527*10^{-5})$

Like the NLIN program, the REG program also needed data input as its first step, and in the second step, the name of REG was given in the PROC statement followed by the model specification. The REG is a linear model regression procedure in SAS. Its output gave information on the analysis of variance due to regression (model) and residual, the estimate of the parameter and its standard error. Unlike the NLIN

program, the REG did not give .95 confidence interval of the estimate parameter. The data input sets for the SAS NLIN and REG programs are given in Appendix G,H, and I for each data set.

The flocculation constants k_0, k_a values calculated from all the three models remain quite stable as seen from Tables 9

Table 11. Estimation of k_b by least squares analysis

Data Set	k_b	Est. σ	95% Confidence Intervals
Argaman and Kaufman's model			
1	$2.070*10^{-8}$	$1.745*10^{-9}$	$(1.721*10^{-8}, 2.411*10^{-8})$
2	$5.270*10^{-8}$	$4.826*10^{-8}$	$(4.301*10^{-8}, 6.241*10^{-7})$
3	$1.199*10^{-7}$	$1.288*10^{-8}$	$(9.342*10^{-8}, 1.464*10^{-7})$
New Model 1, Stage 2			
1	$1.628*10^{-8}$	$2.431*10^{-9}$	$(1.143*10^{-8}, 2.114*10^{-8})$
2	$3.640*10^{-8}$	$2.213*10^{-8}$	$(-1.18*10^{-8}, 8.463*10^{-8})$
3	$1.049*10^{-7}$	$1.305*10^{-8}$	$(7.769*10^{-8}, 1.321*10^{-7})$
New Model 2			
1	$9.600*10^{-9}$	$1.658*10^{-9}$	$(6.350*10^{-9}, 1.290*10^{-8})$
2	$0.000*10^{-9}$	$3.199*10^{-9}$	$(-6.43010^{-9}, 6.430*10^{-9})$
3	$1.767*10^{-7}$	$1.378*10^{-8}$	$(1.483*10^{-7}, 2.050*10^{-7})$

to 10. A higher estimation of parameters k_0, k_a and k_b were obtained from Argaman's experiments which were done under sweep flocculation conditions. The flocculation in the sweep floc region is expected to proceed faster than it is in the adsorption and destabilization (A/D) region which was utilized for data sets 1 and 2. A higher estimation in k_b from Argaman's research also (data set 3, Table 11) indicates more rapid floc breakup rate for sweep flocculation than for A/D flocculation. As stated previously, Argaman and Kaufman's data were collected by measuring absolute turbidity of the sample, rather by measuring the primary particles concentration directly by AIA system, as it was in this study and Hanson's. Thus, cautions should be given in explaining Argaman and Kaufman's data. Tables 9 through 11 also showed higher values of k_0, k_a, and k_b for data set 2 than data set 1. This indicates that floc aggregation and breakup rates in Hanson's experiments proceeded faster than they did during this study. This is confirmed by the experimental observation in this study, that flocculation proceeded very slowly with few big flocs formed after considerable time of slow mixing (as long as 30 minutes on average).

In order to evaluate the fitness of the models to the experimental data from this study, the observed and predicted n_{10}/n_1 are plotted against flocculation time for different G levels in Figures 18 through 22.

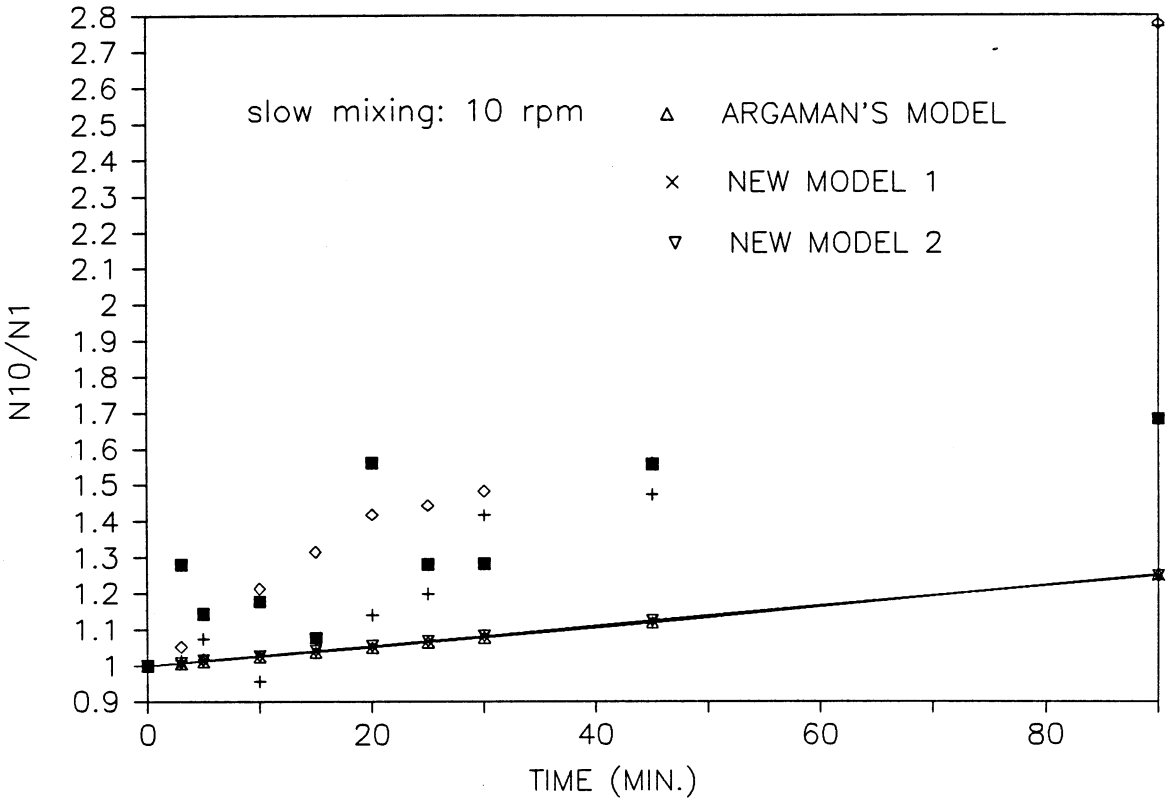

Figure 18. Comparison of experimental observations of the flocculation performance with three model predictions (Each type of symbol not shown in the legend represents the experimental data from one experiment at $G = 4.2\ s^{-1}$ for slow mixing. The lines represent the three model predictions)

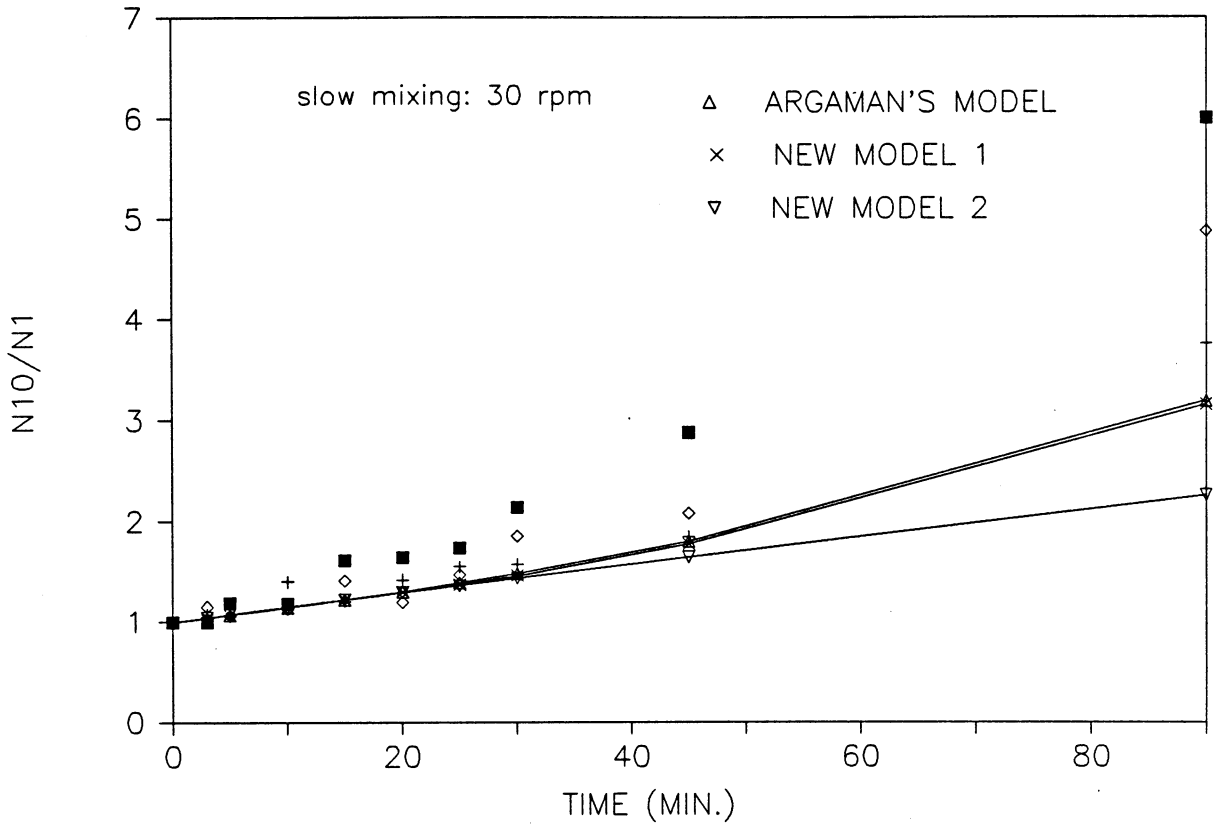

Figure 19. Comparison of experimental observations of the flocculation performance with three model predictions (Each type of symbol not shown in the legend represents the experimental data from one experiment at $G = 22.6\ s^{-1}$ for slow mixing. The lines represent the three model predictions)

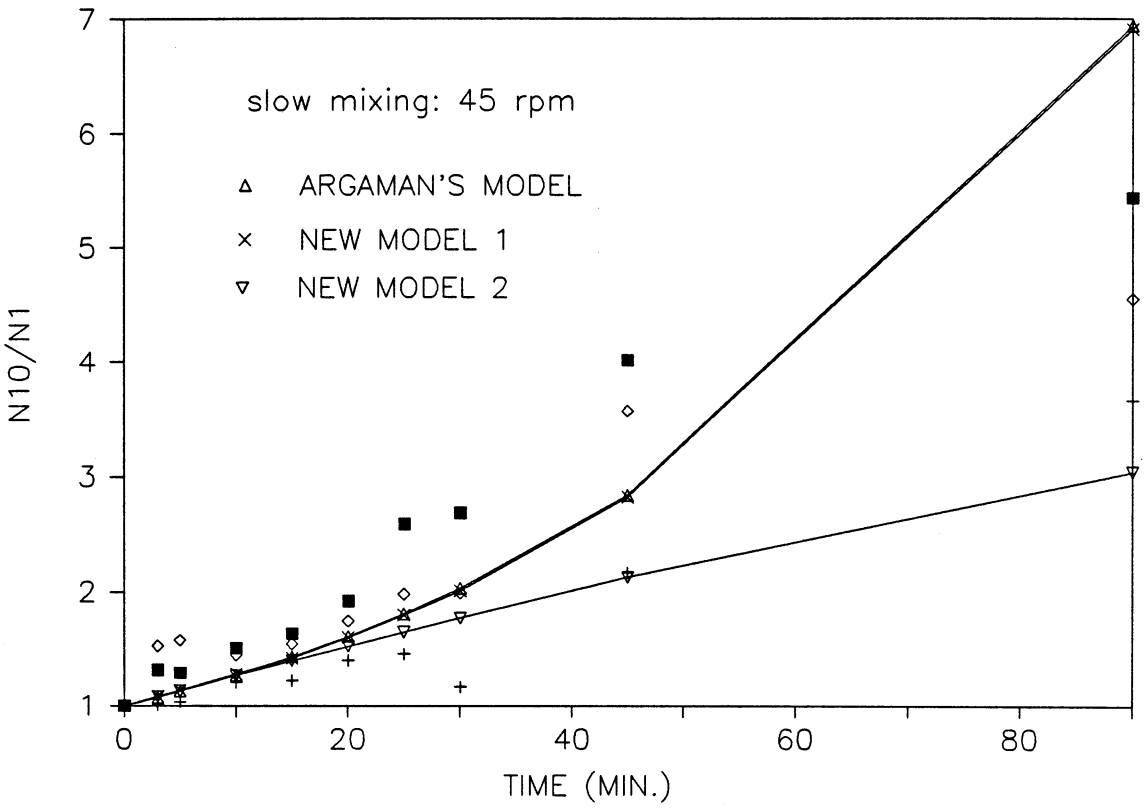

Figure 20. Comparison of experimental observations of the flocculation performance with three model predictions (Each type of symbol not shown in the legend represents the experimental data from one experiment at $G = 42.2\ s^{-1}$ for slow mixing. The lines represent the three model predictions)

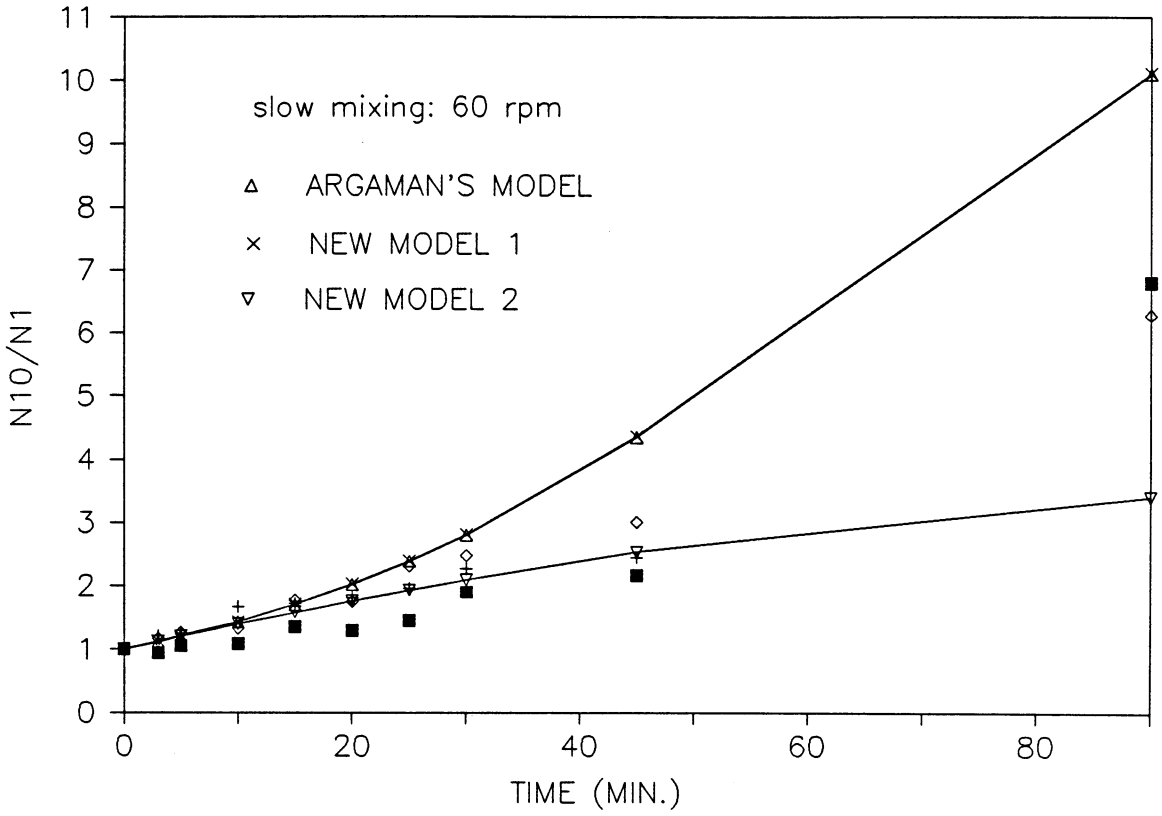

Figure 21. Comparison of experimental observations of the flocculation performance with three model predictions (Each type of symbol not shown in the legend represents the experimental data from one experiment at G = 65.7 s^{-1} for slow mixing. The lines represent the three model predictions)

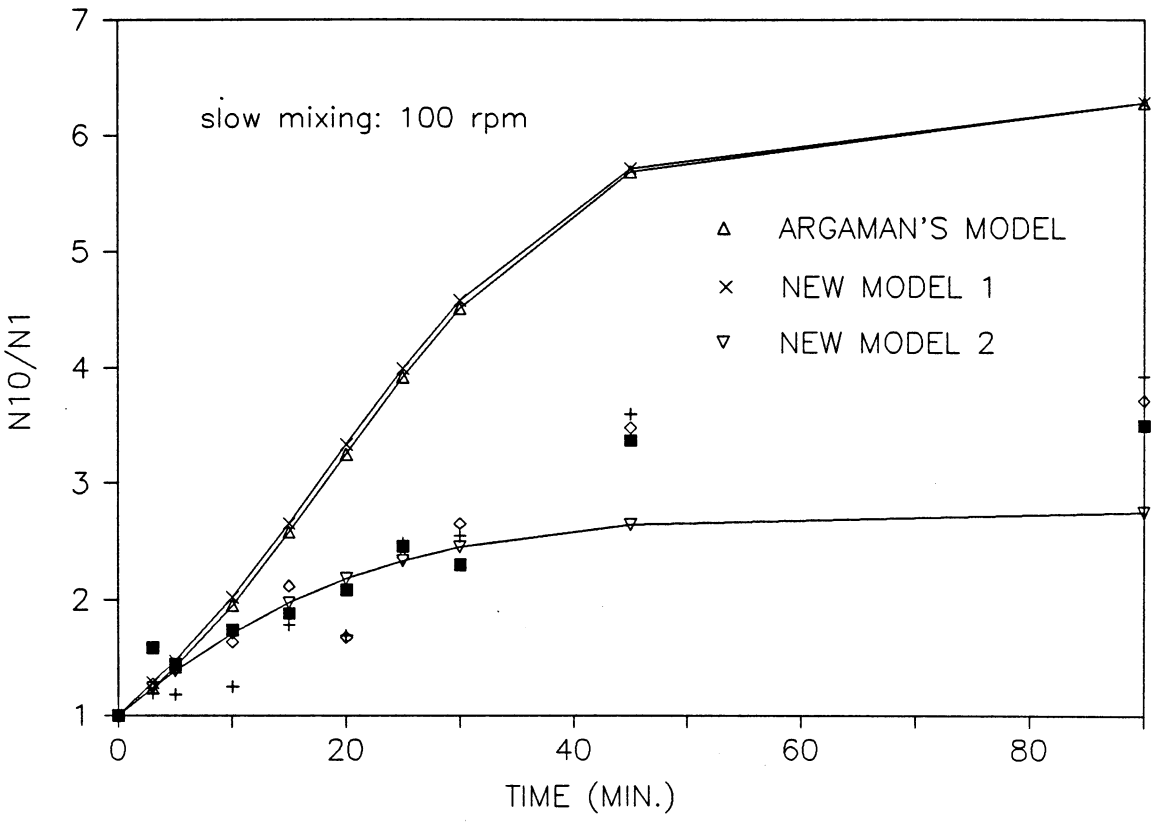

Figure 22. Comparison of experimental observations of the flocculation performance with three model predictions (Each type of symbol not shown in the legend represents the experimental data from one experiment at $G = 144.3\ s^{-1}$ for slow mixing. The lines represent the three model predictions)

Since the models were supposed to give an optimal fit to the data over the whole range of G levels, it was expected that the models would not give optimal estimation under each individual G level, especially under low or high G levels. As seen by Figures 18 and 19, all three models underestimated the flocculation performance at low G levels. At higher G levels, Argaman and Kaufman's model and New Model 1 gave higher predictions than New Model 2 did, as shown in Figures 19 through 22. Figure 20 demonstrated a reasonably good fit of Argaman and Kaufman's model and Model 1 at G = 42.2 s^{-1}. Figures 21 and 22 showed Argaman and Kaufman's model and Model 1 greatly overestimated flocculation performance. But New Model 2 gave somewhat better prediction of the data, at high G levels, at least up to 30 minutes flocculation time.

It is clear that all three models tend to underestimate flocculation performance at low G level. New model 1 whose second stage was Argaman and Kaufman's model produced almost the same predictions as Argaman and Kaufman's model did. Both models greatly overestimated the experimental observations at high G levels. This conclusion is consistant with the findings made by Lawler et al. (1983) who considered G to be of less importance. The poor fit indicates that G is not appropriately incorporated in these two models. In contrast, New Model 2 tends to give more conservative prediction to the flocculation performance, especially at high G levels.

The comparison of the models can also be done by comparing the means of squared errors generated by each model.

Tables 12 through 14 list the sums of squared errors (SSE), also known as residual sum of squares and means of squared errors (MSE) produced by the models for each data set. The calculations of SSE and MSE are conducted by the NLIN and REG programs in SAS according to the following equation:

$$SSE = \sum_{ijk} (y_{ijk} - \hat{y}_{ij})^2 \qquad (80)$$

with the degree of freedom = n-m, where n is the total number of observations and m is the number of parameters to be estimated in the model.

Table 12. SSE and MSE for data set 1

Model	SSE	d.f.	MSE
Argaman-Kaufman	41.543	158	0.263
New model 1 - 1st stage	10.028	95	
New model 1 - 2nd stage	31.087	62	
Sub total	41.115	157	0.262
New model 2	55.831	158	0.353

Table 13. SSE and MSE for data set 2

Model	SSE	d.f.	MSE
Argaman-Kaufman	29.991	49	0.510
New model 1 - 1st stage	6.371	36	
New model 1 - 2nd stage	22.939	62	
Sub total	29.310	48	0.661
New model 2	32.415	49	0.662

Table 14. SSE and MSE for data set 3

Model	SSE	d.f.	MSE
Argaman-Kaufman	1.152	26	0.0443
New model 1 - 1st stage	0.0162	5	
New model 1 - 2nd stage	0.873	20	
Sub total	0.889	25	0.0356
New model 2	0.922	26	0.0355

First examine Table 12. The MSE generated from Argaman-Kaufman's model is 0.263, very close to the MSE of 0.262 due to new model 1, for data set 1. New model 2 gives higher MSE

which means it predicts poorer than the other models for this set of data. For Hanson's data (data set 2), Argaman-Kaufman's model makes the best fitness by showing the smallest MSE among the three models. Recall that Argaman and Kaufman's model considers the collisions between floc and primary particle only, while the New Model 1, first stage and New Model 2 take the collision frequency between the primary particles themselves as the only contribution to the flocculation rate. For a system with more flocs, the Argaman's model should be applied, and for a system with fewer flocs or principally small particles, the new models should give better simulation than Argaman's. Since Hanson's experiments (Data Set 2) generated more flocs (with higher n_{10}/n_1 in the range of 1.0 to 11.341) than were generated in this study (Data Set 1), n_{10}/n_1 in the range of 1.0 to 7.525, Argaman's model is expected to give better predictions for Data Set 2. The opposite argument would apply to Argaman's flocculation experiments in the CSTR system because the values of n_{10}/n_1 ranged from 1.01 to 2.54. Table 14 shows the better predictions by the two models than by the Argaman's model. The primary particle concentration in the flocculation experiments done by Argaman predominated in the system.

The MSEs shown in Tables 12 through 14 vary from each other by a small amount of ten to twenty percent. Strictly speaking, any interpretation based on this information is

tentative. Nevertheless, it is certain that the studies so far indicate that New Model 1 and New Model 2 yield as good prediction as the existing Argaman and Kaufman's model. Under the flocculation condition where primary particles predominate (as in the adsoption and destabilization region), the new models are prefered to Argaman and Kaufman's model. New Model 1 takes Argaman and Kaufman's form in its second stage and gives basically the same predictions to the flocculation performance as Argaman and Kaufman's model. New Model 1 has three unknown parameters, one more parameter than the other two models have. Both Argaman and Kaufman's model and New Model 1 greatly overestimate flocculation performance at high G levels. Therefore, New Model 2 is selected over New Model 1 for the future research evaluation.

The experiments conducted so far have been confined in the BR system. For CSTR system, New Model 2 takes much simpler form (as expressed by equation 70) than it does in a BR system. It is desirable that more flocculation experiments be conducted with the CSTR system and New Model 2 be tested with such data.

VI. CONCLUSIONS

The objective of this research is to verify and compare the existing flocculation kinetics model developed by Argaman and Kaufman with two new flocculation kinetic models.

The major difference between the new models and Argaman and Kaufman's model was the assumptions made regarding the collision mechanisms during flocculation. In the first stage of New Model 1 and New Model 2, it was assumed that the flocculation rate was determined by the collision frequency among the primary particles. In Argaman and Kaufman's model, the flocculation rate was determined by the collision frequency between the primary particles and flocs.

Flocculation experiments were conducted in a laboratary scale batch flocculation tank at controlled water temperature of 20°C, and at five levels of flocculation energy input, G. Particle size distribution was analyzed by AIA system. The data from similar experiments (Hanson, 1989) were also used in model evaluation. The third data source was from Argaman and Kaufman's flocculation experiments which were conducted in a CSTR system and the particle concentration was analyzed by measuring absolute turbidity of the samples.

SAS NLIN and REG software were utilized for model regression and evaluation.

The conclusions drawn from this study are as follows:

1. All three flocculation kinetic models - Argaman and Kaufman's model and two new models, showed comparable predictions of the experimental observations up to about 45 minutes of flocculation.

2. For the flocculation system where primary particles predominate, such as in the adsorption and destabilization region of coagulation, the new models are expected to yield better predictions of the flocculation performance than Argaman and Kaufman's model.

3. Argaman and Kaufman's model and New Model 1 greatly overestimate flocculation performance at high G levels. New Model 2 yields more reasonable and conservative estimations at high G levels. Thus New Model 2 is prefered to New Model 1.

4. It is suggested that more flocculation experiments be conducted in CSTR system to further verify New Model 2 and the conclusions made here.

VII. BIBLIOGRAPHY

Adler, P.M., (1981), "Heterocoagulation in Shear Flow," J. Colloid Int. Sci., Vol.83, No.1, 106-115.

Argaman, Y., and Kaufman, W.J., (1968), "Turbulence in Orthokinetic Flocculation," SERL Report No.68-5, San. Eng. Res. Lab., College of Eng. & School of Public Health, Univ. of Calif., Berkeley.

Argaman, Y., and Kaufman, W.J., (1970), "Turbulence and Flocculation," J. of Sani. Eng. Div., Amer. Soc. of Civ. Engr., Vol.96, No.Sa2, Proc. Paper 7201, 223-241.

Argaman, Y., (1979), "Kinetic Model for Flocculation with Polymers," J. Env. Eng. Div., Amer. Soc. Civ. Engr., Vol.105, EE4, 792-793.

Amer. Water Works Assoc., (1990), Water Quality & Treatment, 4th edition, McGraw-Hill, Inc., New York, N.Y., 310-365.

Benefield, L.D., Judkins, J.F., and Weand, B.L.,(1982), Process Chemistry for Water and Wastewater Treatment, Prentice-Hall, Inc., Englewood Cliffs, N.J.

Batchelor, G.K., (1958), The Theory of Homogeneous Turbulence, Cambridge Univ. Press, Cambridge, England.

Bratby, J.R., (1981), "Interpreting Laboratory Results for the Design of Rapid Mixing and Flocculation Systems," J. Amer. Water Works Assoc., Vol.73, No.6, 318-325.

Camp, T.R., and Stein, P.C., (1943), "Velocity Gradients and Internal Work in Fluid Motion," J. Boston Soc. Civ. Eng., Vol. 30, 219.

Casson, L.W., and Lawler, D.F., (1990), "Flocculation in Turbulent Flow: Measurement & Modeling of Particle Size Distribution," J. Amer. Water Works Assoc., Vol.82, No.8, 54-68.

Clark, M.M., (1985), "Critique of Camp and Stein's RMS Velocity Gradient," J. Env. Eng. Div., Amer. Soc. of Civ. Engr., Vol.111, No.6, 741.

Cleasby, J.L., (1984), "Is Velocity Gradient a Valid Turbulent Flocculation Parameter?" J. Env. Eng. Div., Amer. Soc. of Civ. Engr., Vol.110, No.5, 875.

Corrsin, S., (1962), "Theories of Turbulent Diffusion," Mechanique de la Turbulence, Edition du Centre National de la Res. Scientifique, Paris.

Delichatsios, M.A., and Probstein, R.F., (1975), "Coagulation in Turbulent Flow: Theory and Experiment," J. Colloid Int. Sci., Vol.51, No.3, 394-405.

Fair, G.M., Geyer, J.C., and Okun, D.A., (1968), Water and Wastewater Treatment and Disposal, John Wiley & Sons, Inc., New York, N.Y.

Frost, W., and Moulden, T.H., (1977), Handbook of Turbulence: Volume 1: Fundamentals and Applications, Plenum Press, New York, N.Y.

Gregory, J., (1989), "Fundamentals of Flocculation," Critical Reviews in Env. Control, Vol.19, Iss.3, 185-230.

Hahn, H.H., and Stumm, W., (1968), J. Colloid Int. Sci., Vol.28, 134.

Hanson, A., (1989), "The Effect of Water Temperature and Reactor Geometry on Turbulent Flocculation," Ph.D Thesis, Iowa State University Library, Ames, I.A.

Harris, H.S., Kaufman, W.J., and Krone, R.B., (1966), "Orthokinetic Flocculation in Water Purification," J. Sanit. Eng. Div., Proc. of Amer. Soc. of Civ. Engr., Vol.92, No.SA6, 95-109.

Hinze, J.O., (1975), Turbulence McGraw - Hill Series in Mechanical Engineering, McGraw - Hill, Inc., New York, N.Y.

Hogg, R., Klimpel, R.C., and Ray, D.T., (1985), "Structual Aspects of Floc Formation and Growth," Flocculation, Sedimentation and Consolidation, Moudgil, B.M., et. al., editors, Proc. of Eng. Foundation Conf. Held at the Cloister, Sea Island, Georgia, USA.

Huck, P.M., and Murphy, K.L., (1978), "Kinetic Model for Flocculation with Polymers," J. Env. Eng. Div., Amer. Soc. Civ. Engr., Vol. 106, EE2, 454-455.

Ives, K.J., and Bhole, A.G., (1973), "Theory of Flocculation for Continuous Flow System," J. Env. Eng. Div., Amer. Soc. of Civ. Engr., Vol.99, EE1, 17-34.

Koh, P.T.L., Andrews, J.R.G., and Uhlherr, P.H.T., (1984), "Flocculation in Stirred Tanks," Chem. Eng. Sci., Vol. 39, No.6, 975-985.

Kruyt, H.R., (1952), Colloid Science, Vol.1, Elsevier, N.Y.

LaMer, V.K., and Healy, T.W., (1963), "Adsorption-Flocculation Reactions of Macromolecules at the Solid-liquid Interface," Rev. Pure App. Chem., Vol.13, 112-132.

Lawler, D.F., and Han, M., (1989), "The (Relative) Insignificance of G in Flocculation," Amer. Water Works Assoc. 1989 Annual Conference Proc., Los Angeles, C.A., June 18-22, 1989 1327-1332.

Lawler, D.F., Izurieta, E., and Kao, C.H., (1983), "Changes in Particle Size Distribution in Batch Flocculations," J. Amer. Water Works Assoc., Vol.75, No.12, 604-612.

Levich, V.G., (1962), "Physicochemical Hydrodynamics," Prentice-Hall, Inc., Englewood Cliffs.

Lichtenbelt, J.M.Th., Pathmamanoharan, C., and Wiersema, P.H., (1974), "Rapid Coagulation of Polystyrene Latex in a Stopped Flow Spectrophotometer," J. Colloid Int. Sci., Vol. 49, 281.

Matsuo, T., and Unno, H., (1981), "Forces Acting on Floc and Strength of Floc," J. Env. Eng. Div., Amer. Soc. Civ. Engr., Vol.107, EE3, 527-545.

Montgomery, J. M. Consulting Engineers, Inc., (1985), Water Treatment Principles and Design, John Wiley & Sons, Inc., New York, N.Y.

Obukhoff, A.M., and Yaglom, A.M., (1951), Prikladnaya Matematika i Mekhanika, Vol. 15, No.3.

O'Melia, C.R., (1980), "Aquasols: the Behavior of Small Particles in Aquatic Systems," Env. Sci. and Tech., Vol.14, No.9, 1052.

O'Melia, C.R., (1969), "A Review of the Coagulation Process", Public Works, May, 1969.

Ott, L., (1984), An Introduction to Statistical Methods and Data Analysis, 2nd ed., Duxburg Press, Boston, Mass.

Pandya, J.D., (1981), Ph.D. Thesis, Dept. of Chem. Eng., Univ. of Delaware, Newark, Delaware.

Pandya, J.D., and Spielman, L.A., J. Colloid Int. Sci., Vol.92, No.2, 517.

Pandya, J.D., and Spielman, L.A., "Floc Breakage in Agitated Suspensions: Effect of Agitation Rate," Chem. Eng. Sci., Vol.38, No.12, 1983-1992.

Parker, D.S., Kaufman, W.J., and Jenkins, D., (1971), "Physical Conditioning of Activated Sludge Floc," J. of Water Pollution Control Federation, Vol. 43, No.9, 1817.

Parker, D.S., Kaufman, W.J., and Jenkins, D., (1972), "Floc Breakup in Turbulent Flocculation Processes," J. San. Eng. Div., Amer. Soc. of Civ. Eng., Vol.98, SA1, 79-99.

Ruehrwein, R.A., and Ward, D.W., (1952), "Mechanisms of Clay Aggregation by Polyelectrolytes," Soil Sci., Vol.73, 485-492.

Saffman, P.G., and Turner, J.S., (1956), "On the Collision of Drops in Turbulent Clouds," J. Fluid Mechanics, Vol.1, 16-30.

SAS Institute, Inc., (1979), SAS Users Guide, P.O. Box 10066, Raleigh, North Carolina 27605.

Smoluchowski, M., (1917), "Versuch Einer Mathematischen Theorie der Koagulationskinetic Kolloider Lösungen," Z. Phys. Chem., Vol.92, No.129.

Spielman, L.A., (1970), "Viscous Interaction in Brownian Coagulation," J. Colloid Int. Sci., Vol.33, No.4, 562-571.

Srivastava, R.V., (1988), "Impact of Rapid Mixing and Temperature on Flocculation of Clay Suspensions in Water," M.S. Thesis, Iowa State University Library, Ames, I.A.

Stumm, W., and O'Melia, C.R., (1968), "Stoichiometry of Coagulation," J. Amer. Water Works Assoc., Vol. 60, No.5, 514.

Swift, D.L., and Friedlander, S.K., (1964), "The Coagulation of Hydrosols by Brownian Motion and Laminar Shear Flow," J. Colloid Sci., Vol. 19, 621-647.

Thomas, D.G., (1964), "Turbulent Disruption of Flocs in Small Particle Size Suspensions," Amer. Inst. Chem. Eng. J., Vol.10, No.4, 517-523.

Van Olphen, H., (1971), An Introduction to Clay Colloid Chemistry, 2nd edition, Wiley-Interscience, New York, N.Y.

VIII. ACKNOWLEDGMENTS

The author of this thesis extends her sincere appreciation to Dr. John L. Cleasby, Anson Marston Distinguished Professor In Engineering, for his guidance, suggestion, encouragement and patience during the course of this study.

The author would also like to thank her friends and colleagues, especially Lim-Seok Kang and Rumana Riffat for their invaluable help.

Finally, the author wishes to thank her husband, Dongsheng Chang, for his patience, understanding and support throughout the duration of this research.

APPENDIX A. DERIVATION OF EQUATION 67

The differential equation of New Model 1, second stage is given by:

$$\frac{dn_1}{dt} = -k_a G n_1 + k_b G^2 n_{10} \qquad (42)$$

The mass balance for primary particles is expressed by:

Inflow = Outflow + Accumulation

± (Utilization, generation) (48)

For a BR system, there is no inflow or outflow, equation 48 becomes:

0 = 0 + Accumulation ± (Utilization, generation)

The accumulation term is written as $d(Vn_1)/dt$, the disappearance of primary particles due to flocculation process which is given by equation 42 is considered as the utilization in the above equation, we have:

$$0 = 0 + \frac{d(Vn_1)}{dt} + (k_a G n_1 - k_b G^2 n_{10})\, V \qquad (62)$$

The suspension volume V remains constant. Equation 62 is simplified by dividing V to both sides:

$$\frac{dn_1}{dt} = -k_a G n_1 + k_b G^2 n_{10} \qquad (42)$$

As stated in Chapter III, the equation derived from mass balance takes the same form of its original differential equation for the BR system.

Equation 42 is integrated for the boundary conditions of $n_1 = n_{1cr}$ at $t = t_{cr}$ at the end of the first stage, and $n_1 = n_1$ at time $t = t$ during the second stage of flocculation:

$$\int_{n_{1cr}}^{n_1} \frac{dn_1}{-k_a G n_1 + k_b G^2 n_{10}} = \int_{t_{cr}}^{t} dt \tag{63}$$

$$\int_{n_{1cr}}^{n_1} \left(-\frac{1}{k_a G}\right) \frac{d(-k_a G n_1 + k_b G^2 n_{10})}{-k_a G n_1 + k_b G^2 n_{10}} = \int_{t_{cr}}^{t} dt$$

$$-\frac{1}{k_a G} \int_{n_{1cr}}^{n_1} \frac{d(-k_a G n_1 + k_b G^2 n_{10})}{-k_a G n_1 + k_b G^2 n_{10}} = \int_{t_{cr}}^{t} dt$$

Remember that

$$\int_{x_1}^{x_2} \frac{df(x)}{f(x)} = \ln \frac{f(x_2)}{f(x_1)}$$

$$-\frac{1}{k_a G} \ln \frac{-k_a G n_1 + k_b G^2 n_{10}}{-k_a G n_{1cr} + k_b G^2 n_{10}} = \int_{t_{cr}}^{t} dt$$

Therefore:

$$\ln\frac{-k_aGn_1+k_bG^2n_{10}}{-k_aGn_{1cr}+k_bG^2n_{10}} = -k_aG\int_{t_{cr}}^{t} dt$$

$$\therefore \quad \ln\frac{-k_aGn_1+k_bG^2n_{10}}{-k_aGn_{1cr}+k_bG^2n_{10}} = -k_a(Gt-(Gt)_{cr}) \qquad (64)$$

Equation 64 is rearranged according to

$$\ln x_1/x_2 = -\ln x_2/x_1$$

$$\ln\frac{-k_aGn_{1cr}+k_bG^2n_{10}}{-k_aGn_1+k_bG^2n_{10}} = k_a(Gt-(Gt)_{cr})$$

Let $Gt - (Gt)_{cr} = A$

$$\frac{-k_aGn_{1cr}+k_bG^2n_{10}}{-k_aGn_1+k_bG^2n_{10}} = e^{k_aA}$$

Dividing the nominator and the denominator of the left hand side of the equation by n_{10}:

$$\frac{-k_aG\frac{n_{1cr}}{n_{10}}+k_bG^2}{-k_aG\frac{n_1}{n_{10}}+k_bG^2} = e^{k_aA}$$

$$-k_a G\frac{n_{1cr}}{n_{10}}+k_b G^2 = (-k_a G\frac{n_1}{n_{10}}+k_b G^2)*e^{k_a A}$$

$$-k_a G\frac{n_{1cr}}{n_{10}}+k_b G^2 = -k_a G\frac{n_1}{n_{10}}e^{k_a A}+k_b G^2 e^{k_a A}$$

$$-k_a G\frac{n_1}{n_{10}}e^{k_a A} = -k_a G\frac{n_{1cr}}{n_{10}}+k_b G^2-k_b G^2 e^{k_a A}$$

Dividing both sides of the equation by $-k_a G e^{kaA}$:

$$\frac{n_1}{n_{10}} = \frac{-k_a G\frac{n_{1cr}}{n_{10}}+k_b G^2(1-e^{k_a A})}{-k_a G e^{k_a A}}$$

Inverse the nominator and the denominator of the equation:

$$\frac{n_{10}}{n_1} = \frac{-k_a G e^{k_a A}}{-k_a G\frac{n_{1cr}}{n_{10}}+k_b G^2(1-e^{k_a A})} \qquad (65')$$

The initial boundary condition is given by equation 55 at $n_1 = n_{1cr}$ and $t = t_{cr}$:

$$n_{10}/n_{1cr} = 1 + k_0\ (Gt)_{cr} \qquad (55)$$

According to this equation, we have:

$$\frac{n_{1cr}}{n_{10}} = \frac{1}{1+k_0(Gt)_{cr}} \tag{66}$$

Substituting equation 66 into equation 65':

$$\frac{n_{10}}{n_1} = \frac{-k_a G e^{k_a A}}{-k_a G \frac{1}{1+k_0(Gt)_{cr}} + k_b G^2 (1-e^{k_a A})}$$

Since A = Gt - $(Gt)_{cr}$, we now get equation 67:

$$\frac{n_{10}}{n_1} = \frac{-k_a G e^{k_a A}}{-\frac{k_a G}{1+k_0(Gt)_{cr}} + k_b G^2 (1-e^{k_a (Gt-(Gt)_{cr})})} \tag{67}$$

APPENDIX B. DERIVATION OF EQUATIONS 69 AND 70

Derivation of Equation 69

The differential equation of New Model 2 is given by:

$$\frac{dn_1}{dt} = -\frac{k_0}{n_{10}} G n_1^2 + k_b G^2 n_{10} \qquad (68)$$

As it was shown in Appendix A, the equation derived from mass balance takes the same form of its differential equation for the BR system. Therefore, we can solve equation 68 directly for the boundary conditions of $n_1 = n_{10}$ at $t = 0$, and $n_1 = n_1$ at $t = t$:

$$\int_{n_{10}}^{n_1} \frac{dn_1}{-\frac{k_0}{n_{10}} G n_1^2 + k_b G^2 n_{10}} = \int_0^t dt$$

Let $k_0 G / n_{10} = a$, and $k_b G^2 = b$, then the equation is simplified as:

$$\int_{n_{10}}^{n_1} \frac{dn_1}{-a n_1^2 + b n_{10}} = t$$

$$\int_{n_{10}}^{n_1} \frac{dn_1}{-a\left(n_1^2 - \frac{b}{a} n_{10}\right)} = t$$

$$-\frac{1}{a}\int_{n_{10}}^{n_1}\frac{dn_1}{n_1^2-\frac{b}{a}n_{10}} = t$$

$$\int_{n_{10}}^{n_1}\frac{dn_1}{n_1^2-\frac{b}{a}n_{10}} = -at$$

Let $c^2 = b/a$ ($= k_b G^2/((k_0/n_{10})G) = k_b G n_{10}/k_0$), we have:

$$\int_{n_{10}}^{n_1}\frac{dn_1}{n_1^2-c^2 n_{10}} = -at$$

$$\int_{n_{10}}^{n_1}\frac{dn_1}{(n_1-c\sqrt{n_{10}})\,(n_1+c\sqrt{n_{10}})} = -at$$

$$\int_{n_{10}}^{n_1}\frac{1}{2c\sqrt{n_{10}}}\left(\frac{1}{n_1-c\sqrt{n_{10}}}-\frac{1}{n_1+c\sqrt{n_{10}}}\right)dn_1 = -at$$

$$\frac{1}{2c\sqrt{n_{10}}}\left(\int_{n_{10}}^{n_1}\frac{dn_1}{n_1-c\sqrt{n_{10}}}-\int_{n_{10}}^{n_1}\frac{dn_1}{n_1+c\sqrt{n_{10}}}\right) = -at$$

$$\int_{n_{10}}^{n_1} \frac{dn_1}{n_1 - c\sqrt{n_{10}}} - \int_{n_{10}}^{n_1} \frac{dn_1}{n_1 + c\sqrt{n_{10}}} = -2ac\sqrt{n_{10}}\,t$$

$$\ln \frac{n_1 - c\sqrt{n_{10}}}{n_{10} - c\sqrt{n_{10}}} - \ln \frac{n_1 + c\sqrt{n_{10}}}{n_{10} + c\sqrt{n_{10}}} = -2ac\sqrt{n_{10}}\,t$$

$$\therefore \quad \ln \frac{(n_1 - c\sqrt{n_{10}})\,(n_{10} + c\sqrt{n_{10}})}{(n_{10} - c\sqrt{n_{10}})\,(n_1 + c\sqrt{n_{10}})} = -2ac\sqrt{n_{10}}\,t$$

$$\therefore \quad \frac{(n_1 + c\sqrt{n_{10}})\,(n_{10} - c\sqrt{n_{10}})}{(n_{10} + c\sqrt{n_{10}})\,(n_1 - c\sqrt{n_{10}})} = e^{2ac\sqrt{n_{10}}\,t}$$

Substitute a, b and c into the equation, we have:

$$\therefore \quad \frac{\left(n_1 + \sqrt{\frac{k_b G n_{10}}{k_0}}\sqrt{n_{10}}\right)\left(n_{10} - \sqrt{\frac{k_b G n_{10}}{k_0}}\sqrt{n_{10}}\right)}{\left(n_{10} + \sqrt{\frac{k_b G n_{10}}{k_0}}\sqrt{n_{10}}\right)\left(n_1 - \sqrt{\frac{k_b G n_{10}}{k_0}}\sqrt{n_{10}}\right)} = e^{2\frac{k_0 G}{n_{10}}\sqrt{\frac{k_b G n_{10}}{k_0}}\sqrt{n_{10}}\,t}$$

$$\therefore \quad \frac{\left(n_1 + \sqrt{\frac{k_b G}{k_0}}\,n_{10}\right)\left(n_{10} - \sqrt{\frac{k_b G}{k_0}}\,n_{10}\right)}{\left(n_{10} + \sqrt{\frac{k_b G}{k_0}}\,n_{10}\right)\left(n_1 - \sqrt{\frac{k_b G}{k_0}}\,n_{10}\right)} = e^{2\sqrt{k_0 k_b G}\,Gt} = D$$

$$\therefore \quad \frac{(n_1+\sqrt{\frac{k_bG}{k_0}}\,n_{10})\,(1-\sqrt{\frac{k_bG}{k_0}})}{(1+\sqrt{\frac{k_bG}{k_0}})\,(n_1-\sqrt{\frac{k_bG}{k_0}}\,n_{10})} = D$$

$$\therefore \quad \frac{(1+\sqrt{\frac{k_bG}{k_0}}\,\frac{n_{10}}{n_1})\,(1-\sqrt{\frac{k_bG}{k_0}})}{(1+\sqrt{\frac{k_bG}{k_0}})\,(1-\sqrt{\frac{k_bG}{k_0}}\,\frac{n_{10}}{n_1})} = D$$

$$1-\sqrt{\frac{k_bG}{k_0}}+(1-\sqrt{\frac{k_bG}{k_0}})\sqrt{\frac{k_bG}{k_0}}\,\frac{n_{10}}{n_1} = (1+\sqrt{\frac{k_bG}{k_0}})\,D-(1+\sqrt{\frac{k_bG}{k_0}})\sqrt{\frac{k_bG}{k_0}}\,D\frac{n_{10}}{n_1}$$

$$\therefore \quad 1-\sqrt{\frac{k_bG}{k_0}}-(1+\sqrt{\frac{k_bG}{k_0}})\,D = (-\sqrt{\frac{k_bG}{k_0}}+\frac{k_bG}{k_0}-(\sqrt{\frac{k_bG}{k_0}}+\frac{k_bG}{k_0})\,D)\,\frac{n_{10}}{n_1}$$

$$\therefore \quad \frac{n_{10}}{n_1} = \frac{1-\sqrt{\frac{k_bG}{k_0}}-(1+\sqrt{\frac{k_bG}{k_0}})\,D}{-\sqrt{\frac{k_bG}{k_0}}+\frac{k_bG}{k_0}-(\sqrt{\frac{k_bG}{k_0}}+\frac{k_bG}{k_0})\,D}$$

$$= \frac{k_0-\sqrt{k_0k_bG}-(k_0+\sqrt{k_0k_bG})\,D}{-\sqrt{k_0k_bG}+k_bG-(\sqrt{k_0k_bG}+k_bG)\,D}$$

$$\because \quad D = e^{2\sqrt{k_0 k_b G}Gt}$$

Therefore, eq. 69 is derived:

$$\frac{n_{10}}{n_1} = \frac{\sqrt{k_0 k_b G} - k_0 + (k_0 + \sqrt{k_0 k_b G})\, e^{2\sqrt{k_0 k_b G}Gt}}{\sqrt{k_0 k_b G} - k_b G + (k_b G + \sqrt{k_0 k_b G})\, e^{2\sqrt{k_0 k_b G}Gt}} \qquad (69)$$

Derivation of Equation 70

The differential equation of New Model 2 is expressed as:

$$\frac{dn_1}{dt} = -\frac{k_0}{n_{10}} G n_1^2 + k_b G^2 n_{10}$$

Combining it with the mass balance equation 48 for CSTR system at the steady state that $dn_1/dt = 0$, we have:

$$Q n_{10} - Q n_1 = \left(\frac{k_0 G}{n_{10}} n_1^2 - k_b G^2 n_{10}\right) V$$

$$\because \quad V/Q = t$$

$$\therefore \quad n_{10} - n_1 = \left(\frac{k_0 G}{n_{10}} n_1^2 - k_b G^2 n_{10}\right) t$$

$$\therefore \quad \frac{k_0 G t}{n_{10}} n_1^2 + n_1 - (1 + k_b G^2 t)\, n_{10} = 0$$

This is a quadratic equation for n_1. A quadratic function in the form of $aX^2 + bX + c = 0$ can be solved by

$$X = \frac{-b \pm \sqrt{b^2 - 4ac}}{2a}$$

Therefore, the quadratic equation of n_1 can be solved as:

$$n_1 = \frac{-1 \pm \sqrt{1 + 4 \frac{k_0 G t}{n_{10}} (1 + k_b G^2 t)\, n_{10}}}{2 \frac{k_0 G t}{n_{10}}}$$

Only the positive sign is adopted, therefore we have:

$$n_1 = \frac{-1 + \sqrt{1 + 4 k_0 G t (1 + k_b G^2 t)}}{2 \frac{k_0 G t}{n_{10}}}$$

$$n_1 = \frac{n_{10} \left(-1 + \sqrt{1 + 4 k_0 G t (1 + k_b G^2 t)}\right)}{2 k_0 G t}$$

$$\therefore \quad \frac{n_{10}}{n_1} = \frac{2k_0Gt}{\sqrt{1+4k_0Gt(1+k_bG^2t)}-1}$$

$$\frac{n_{10}}{n_1} = \frac{2k_0Gt}{\sqrt{1+4k_0Gt(1+k_bG^2t)}-1} * \frac{\sqrt{1+4k_0Gt(1+k_bG^2)}+1}{\sqrt{1+4k_0Gt(1+k_bG^2t)}+1}$$

Since $(a+b)(a-b) = a^2 - b^2$, we have:

$$\therefore \quad \frac{n_{10}}{n_1} = \frac{2k_0Gt(1+\sqrt{1+4k_0Gt(1+k_bG^2t)}}{(1+4k_0Gt(1+k_bG^2t))-1}$$

Therefore, equation 70 is derived:

$$\therefore \quad \frac{n_{10}}{n_1} = \frac{1+\sqrt{1+4k_0Gt(1+k_bG^2t)}}{2(1+k_bG^2t)} \qquad (70)$$

APPENDIX C. GLM PROGRAM FOR ANALYSIS OF VARIANCE FOR DATA SET 1

```
 1.      // JOB
 2.      // EXEC SAS
 3.      OPTIONS LS=65;
 4.      DATA EXPT;
 5.      INPUT TIME RPM Y;
 6.      CARD;
 7.      0 10 1
 8.      0 10 1
 9.      0 10 1
10.      0 10 1
11.      0 30 1
12.      0 30 1
13.      0 30 1
14.      0 45 1
15.      0 45 1
16.      0 45 1
17.      0 60 1
18.      0 60 1
19.      0 60 1
20.      0 60 1
21.      0 100 1
22.      0 100 1
23.      0 100 1
24.      3 10 1.279
25.      3 10 1.014
26.      3 10 1.12
27.      3 10 1.053
28.      3 30 0.998
29.      3 30 1.076
30.      3 30 1.152
31.      3 45 1.315
32.      3 45 1.009
33.      3 45 1.527
34.      3 60 0.942
35.      3 60 1.212
36.      3 60 1.109
37.      3 60 1.168
38.      3 100 1.585
39.      3 100 1.192
40.      3 100 1.273
```

41.	5	10	1.143
42.	5	10	1.075
43.	5	10	1.019
44.	5	30	1.182
45.	5	30	1.056
46.	5	30	1.06
47.	5	45	1.286
48.	5	45	1.033
49.	5	45	1.577
50.	5	60	1.05
51.	5	60	1.229
52.	5	60	1.215
53.	5	60	1.263
54.	5	100	1.442
55.	5	100	1.183
56.	5	100	1.394
57.	10	10	1.177
58.	10	10	0.957
59.	10	10	1.443
60.	10	10	1.214
61.	10	30	1.18
62.	10	30	1.4
63.	10	30	1.129
64.	10	45	1.505
65.	10	45	1.201
66.	10	45	1.446
67.	10	60	1.085
68.	10	60	1.668
69.	10	60	1.448
70.	10	60	1.324
71.	10	100	1.737
72.	10	100	1.25
73.	10	100	1.636
74.	15	10	1.077
75.	15	10	1.074
76.	15	10	1.231
77.	15	10	1.315
78.	15	30	1.614
79.	15	30	1.204
80.	15	45	1.635

81.	15	45	1.222
82.	15	45	1.542
83.	15	60	1.359
84.	15	60	1.722
85.	15	60	1.937
86.	15	60	1.773
87.	15	100	1.883
88.	15	100	1.786
89.	15	100	2.117
90.	20	10	1.561
91.	20	10	1.14
92.	20	10	1.807
93.	20	10	1.418
94.	20	30	1.644
95.	20	30	1.196
96.	20	45	1.917
97.	20	45	1.401
98.	20	45	1.745
99.	20	60	1.289
100.	20	60	1.815
101.	20	60	2.632
102.	20	60	1.749
103.	20	100	2.082
104.	20	100	1.691
105.	20	100	1.678
106.	25	10	1.28
107.	25	10	1.199
108.	25	10	2.334
109.	25	10	1.443
110.	25	30	1.735
111.	25	30	1.55
112.	25	30	1.468
113.	25	45	2.591
114.	25	45	1.456
115.	25	45	1.98
116.	25	60	1.452
117.	25	60	1.961
118.	25	60	2.311
119.	25	60	2.313
120.	25	100	2.461

121.	25	100	2.486
122.	25	100	2.361
123.	30	10	1.282
124.	30	10	1.417
125.	30	10	2.474
126.	30	10	1.483
127.	30	30	2.141
128.	30	30	1.573
129.	30	30	1.854
130.	30	45	2.689
131.	30	45	1.161
132.	30	45	1.992
133.	30	60	1.903
134.	30	60	2.273
135.	30	60	2.637
136.	30	60	2.476
137.	30	100	2.299
138.	30	100	2.546
139.	30	100	2.656
140.	45	10	1.558
141.	45	10	1.473
142.	45	10	1.828
143.	45	10	1.562
144.	45	30	2.879
145.	45	30	1.85
146.	45	30	2.086
147.	45	45	4.017
148.	45	45	2.17
149.	45	45	3.572
150.	45	60	2.168
151.	45	60	2.445
152.	45	60	4.514
153.	45	60	3.013
154.	45	100	3.371
155.	45	100	3.6
156.	90	10	1.683
157.	90	10	2.777
158.	90	30	6.001
159.	90	30	3.792
160.	90	45	5.443

```
90 45 3.67
90 60 7.525
90 60 6.286
90 100 3.502
90 100 3.929
90 100 3.72
PROC GLM;
CLASS TIME RPM;
MODEL Y=TIME RPM TIME*RPM;
MEANS TIME*RPM;
PROC PRINT;
//
```

APPENDIX D. N_{10}/N_1 VERSUS TIME FOR EACH EXPERIMENT IN DATA SET 1

* indicates the data was lost.

Date of the flocculation test

G = 4.2 s

Time (min.)	FEB/13	JAN/30	JAN/25	Mar/26
0.00	1	1	1	1
3.00	1.279	1.014	1.12	1.053
5.00	1.143	1.075	*	1.019
10.00	1.177	0.957	1.443	1.214
15.00	1.077	1.074	1.231	1.315
20.00	1.561	1.14	1.807	1.418
25.00	1.28	1.199	2.334	1.443
30.00	1.282	1.417	2.474	1.483
45.00	1.558	1.473	1.828	1.562
90.00	1.683	*	*	2.777

G = 22.6 s

	MAR/10	FEB/6	JAN/29
0.00	1	1	1
3.00	0.998	1.076	1.152
5.00	1.182	1.056	1.06
10.00	1.18	1.4	1.129
15.00	1.614	1.204	*
20.00	1.644	*	1.196
25.00	1.735	1.55	1.468
30.00	2.141	1.573	1.854
45.00	2.879	1.85	2.086
90.00	6.001	3.762	*

G = 42.2 s

	FEB/22	FEB/12	JAN/31
0.00	1	1	1
3.00	1.315	1.009	1.527
5.00	1.286	1.033	1.577
10.00	1.505	1.201	1.446
15.00	1.635	1.222	1.542
20.00	1.917	1.401	1.745
25.00	2.591	1.456	1.98
30.00	2.689	1.161	1.992
45.00	4.017	2.17	3.572
90.00	5.443	3.67	*

Date of the flocculation test

G = 65.7 s

Time (min.)	JAN/23	JAN/24	MAR/11	mar/22
0.00	1	1	1	1
3.00	0.942	1.212	1.109	1.168
5.00	1.055	1.229	1.215	1.263
10.00	1.085	1.668	1.448	1.324
15.00	1.359	1.722	1.937	1.773
20.00	1.289	1.815	2.632	1.749
25.00	1.452	1.961	2.311	2.313
30.00	1.903	2.273	2.637	2.476
45.00	2.168	2.445	4.514	3.013
90.00	*	*	7.525	6.286

G = 144.2 s

	FEB/19	FEB/26	MAR/8
0.00	1	1	1
3.00	1.585	1.192	1.273
5.00	1.442	1.183	1.394
10.00	1.737	1.25	1.636
15.00	1.883	1.786	2.117
20.00	2.082	1.691	1.678
25.00	2.461	2.486	2.361
30.00	2.299	2.546	2.656
45.00	3.371	3.6	*
90.00	3.502	3.929	3.72

APPENDIX E. N_{10}/N_1 VERSUS TIME FOR EACH EXPERIMENT IN DATA SET 2, DATA FROM HANSON (1989)

Time (min.)	G s-1	n10/n1
0.00	22.6	1.000
0.00	65.7	1.000
1.00	22.6	1.025
3.00	22.6	0.985
5.00	22.6	1.142
10.00	22.6	1.432
15.00	22.6	1.655
20.00	22.6	2.949
25.00	22.6	3.738
30.00	22.6	4.338
1.00	22.6	1.051
3.00	22.6	0.993
5.00	22.6	1.150
15.00	22.6	1.920
20.00	22.6	2.539
25.00	22.6	3.883
30.00	22.6	3.669
1.00	22.6	1.247
3.00	22.6	1.318
5.00	22.6	1.655
10.00	22.6	1.586
15.00	22.6	1.809
20.00	22.6	2.835
25.00	22.6	4.796
30.00	22.6	5.878
1.00	65.7	0.997
3.00	65.7	1.195
5.00	65.7	1.834
15.00	65.7	3.667
20.00	65.7	6.138
30.00	65.7	7.874
1.00	65.7	1.307
3.00	65.7	1.304
5.00	65.7	1.874
10.00	65.7	3.231
15.00	65.7	4.068
20.00	65.7	6.063
25.00	65.7	10.060
30.00	65.7	9.034
1.00	65.7	1.394
3.00	65.7	1.547
5.00	65.7	2.003
10.00	65.7	3.082
15.00	65.7	4.500
20.00	65.7	7.651
25.00	65.7	10.333
30.00	65.7	11.341

APPENDIX F. N_{10}/N_1 VERSUS TIME FOR EACH EXPERIMENT IN DATA SET 3, SINGLE CSTR DATA OF ARGAMAN AND KAUFMAN (1968)

Time (min.)	G s-1	n10/n1
8.00	30.00	1.74
8.00	45.00	1.91
8.00	60.00	2.07
8.00	90.00	2.24
8.00	120.00	2.36
8.00	180.00	1.84
8.00	240.00	1.01
12.00	30.00	2.00
12.00	45.00	2.22
12.00	60.00	2.12
12.00	90.00	2.38
12.00	120.00	2.18
12.00	180.00	1.74
12.00	240.00	1.50
16.00	30.00	2.04
16.00	45.00	2.09
16.00	60.00	2.29
16.00	90.00	2.51
16.00	120.00	2.03
16.00	180.00	1.79
16.00	240.00	1.52
24.00	30.00	2.35
24.00	45.00	2.54
24.00	60.00	2.72
24.00	90.00	2.52
24.00	120.00	2.12
24.00	180.00	2.07
24.00	240.00	1.47

APPENDIX G. NLIN PROGRAMS FOR ARGAMAN AND KAUFMAN'S MODEL

The following is the summary of the NLIN programs utilized for the regression of Argaman and Kaufman's model to three sets of data.

NLIN Program Based on Equation 47 for Data Set 1

```
 1.      //NLINR JOB
 2.      /*JOBPARM JCL=NO
 3.      //STEP1 EXEC SAS
 4.      //SYSIN DD *
 5.      DATA O13;
 6.      INPUT T G Y;
 7.      CARD;
 8.      0 4.2 1
 9.      0 4.2 1
10.      0 4.2 1
11.      0 4.2 1
12.      0 22.6 1
13.      0 22.6 1
14.      0 22.6 1
15.      0 42.2 1
16.      0 42.2 1
17.      0 42.2 1
18.      0 65.7 1
19.      0 65.7 1
20.      0 65.7 1
21.      0 65.7 1
22.      0 144.3 1
23.      0 144.3 1
24.      0 144.3 1
25.      3 4.2 1.279
26.      3 4.2 1.014
27.      3 4.2 1.12
28.      3 4.2 1.053
29.      3 22.6 0.998
30.      3 22.6 1.076
31.      3 22.6 1.152
32.      3 42.2 1.315
33.      3 42.2 1.009
34.      3 42.2 1.527
35.      3 65.7 0.942
36.      3 65.7 1.212
37.      3 65.7 1.109
38.      3 65.7 1.168
39.      3 144.3 1.585
40.      3 144.3 1.192
```

41. 3 144.3 1.273
42. 5 4.2 1.143
43. 5 4.2 1.075
44. 5 4.2 1.019
45. 5 22.6 1.182
46. 5 22.6 1.056
47. 5 22.6 1.06
48. 5 44.2 1.286
49. 5 44.2 1.033
50. 5 44.2 1.577
51. 5 65.7 1.05
52. 5 65.7 1.229
53. 5 65.7 1.215
54. 5 65.7 1.263
55. 5 144.3 1.442
56. 5 144.3 1.183
57. 5 144.3 1.394
58. 10 4.2 1.177
59. 10 4.2 0.957
60. 10 4.2 1.443
61. 10 4.2 1.214
62. 10 22.6 1.18
63. 10 22.6 1.4
64. 10 22.6 1.129
65. 10 42.2 1.505
66. 10 42.2 1.201
67. 10 42.2 1.446
68. 10 65.7 1.085
69. 10 65.7 1.668
70. 10 65.7 1.448
71. 10 65.7 1.324
72. 10 144.3 1.737
73. 10 144.3 1.25
74. 10 144.3 1.636
75. 15 4.2 1.077
76. 15 4.2 1.074
77. 15 4.2 1.231
78. 15 4.2 1.315
79. 15 22.6 1.614
80. 15 22.6 1.204

81.	15	22.6	1.635
82.	15	42.2	1.222
83.	15	42.2	1.542
84.	15	65.7	1.359
85.	15	65.7	1.722
86.	15	65.7	1.937
87.	15	65.7	1.773
88.	15	144.3	1.883
89.	15	144.3	1.786
90.	15	144.3	2.117
91.	20	4.2	1.561
92.	20	4.2	1.14
93.	20	4.2	1.807
94.	20	4.2	1.418
95.	20	22.6	1.644
96.	20	22.6	1.196
97.	20	42.2	1.917
98.	20	42.2	1.401
99.	20	42.2	1.745
100.	20	65.7	1.289
101.	20	65.7	1.815
102.	20	65.7	2.632
103.	20	65.7	1.749
104.	20	144.3	2.082
105.	20	144.3	1.691
106.	20	144.3	1.678
107.	25	4.2	1.28
108.	25	4.2	1.199
109.	25	4.2	2.334
110.	25	4.2	1.443
111.	25	22.6	1.735
112.	25	22.6	1.55
113.	25	22.6	1.468
114.	25	42.2	2.591
115.	25	42.2	1.456
116.	25	42.2	1.98
117.	25	65.7	1.452
118.	25	65.7	1.961
119.	25	65.7	2.311
120.	25	65.7	2.313

121.	25	144.3	2.461
122.	25	144.3	2.486
123.	25	144.3	2.361
124.	30	4.2	1.282
125.	30	4.2	1.417
126.	30	4.2	2.474
127.	30	4.2	1.483
128.	30	22.6	2.141
129.	30	22.6	1.573
130.	30	22.6	1.854
131.	30	42.2	2.689
132.	30	42.2	1.161
133.	30	42.2	1.992
134.	30	65.7	1.903
135.	30	65.7	2.273
136.	30	65.7	2.637
137.	30	65.7	2.476
138.	30	144.3	2.299
139.	30	144.3	2.546
140.	30	144.3	2.656
141.	45	4.2	1.558
142.	45	4.2	1.473
143.	45	4.2	1.828
144.	45	4.2	1.562
145.	45	22.6	2.879
146.	45	22.6	1.85
147.	45	22.6	2.086
148.	45	42.2	4.017
149.	45	42.2	2.17
150.	45	42.2	3.572
151.	45	65.7	2.168
152.	45	65.7	2.445
153.	45	65.7	4.514
154.	45	65.7	3.013
155.	45	144.3	3.371
156.	45	144.3	3.6
157.	90	4.2	1.683
158.	90	4.2	2.777
159.	90	22.6	6.001
160.	90	22.6	3.792

```
161.      90 42.2 5.443
162.      90 42.2 3.67
163.      90 65.7 7.525
164.      90 65.7 6.286
165.      90 144.3 3.502
166.      90 144.3 3.929
167.      90 144.3 3.72
168.      PROC NLIN PLOT METHOD=MARQUARDT;
169.      PARAMETERS KA=1.0E-6 TO 1.0E-4
170.      BY 1.0E-6 KB=1.0E-8 TO 1.0E-7;
171.      A=-KA*G+KB*G*G*(1-EXP(KA*G*T*60));
172.      B=-G-KB*G*G*G*T*60*EXP(KA*G*T*60);
173.      C=-KA*G*EXP(KA*G*T*60);
174.      D=-G*EXP(KA*G*T*60)-KA*G*G*T*60
175.      *EXP(KA*G*T*60);
176.      E=G*G*(1-EXP(KA*G*T*60));
177.      MODEL Y=C/A;
178.      DER.KA=(D*A-C*B)/(A*A);
179.      DER.KB=(-C*E)/(A*A);
180.      //
```

NLIN Program Based on Equation 47 for Data Set 2

```
 1.      //NLINR JOB
 2.      /*JOBPARM JCL=NO
 3.      //STEP1 EXEC SAS
 4.      //SYSIN DD *
 5.      DATA AHO11;
 6.      INPUT T G Y;
 7.      CARD;
 8.      0 22.6 1
 9.      0 22.6 1
10.      0 22.6 1
11.      0 65.7 1
12.      0 65.7 1
13.      0 65.7 1
14.      1 22.6 1.025
15.      3 22.6 0.985
16.      5 22.6 1.142
17.      10 22.6 1.432
18.      15 22.6 1.655
19.      20 22.6 2.949
20.      25 22.6 3.738
21.      30 22.6 4.338
22.      1 22.6 1.051
23.      3 22.6 0.993
24.      5 22.6 1.150
25.      15 22.6 1.92
26.      20 22.6 2.539
27.      25 22.6 3.883
28.      30 22.6 3.669
29.      1 22.6 1.247
30.      3 22.6 1.318
31.      5 22.6 1.655
32.      10 22.6 1.586
33.      15 22.6 1.809
34.      20 22.6 2.835
35.      25 22.6 4.796
36.      30 22.6 5.878
37.      1 65.7 0.997
38.      3 65.7 1.195
39.      5 65.7 1.834
40.      15 65.7 3.667
```

```
41.      20 65.7 6.138
42.      30 65.7 7.874
43.      1 65.7 1.307
44.      3 65.7 1.304
45.      5 65.7 1.874
46.      10 65.7 3.231
47.      15 65.7 4.068
48.      20 65.7 6.063
49.      25 65.7 10.060
50.      30 65.7 9.034
51.      1 65.7 1.394
52.      3 65.7 1.547
53.      5 65.7 2.003
54.      10 65.7 3.082
55.      15 65.7 4.5
56.      20 65.7 7.651
57.      25 65.7 10.333
58.      30 65.7 11.341
59.      PROC NLIN PLOT METHOD=MARQUARDT;
60.      PARAMETERS KA=1.0E-6 TO 1.0E-4
61.      BY 1.0E-6 KB=1.0E-8 TO 1.0E-7;
62.      A=-KA*G+KB*G*G*(1-EXP(KA*G*T*60));
63.      B=-G-KB*G*G*G*T*60*EXP(KA*G*T*60);
64.      C=-KA*G*EXP(KA*G*T*60);
65.      D=-G*EXP(KA*G*T*60)-KA*G*G*T*60
66.      *EXP(KA*G*T*60);
67.      E=G*G*(1-EXP(KA*G*T*60));
68.      MODEL Y=C/A;
69.      DER.KA=(D*A-C*B)/(A*A);
70.      DER.KB=(-C*E)/(A*A);
71.      //
```

NLIN Program Based on Equation 46 for Data Set 3

```
1.      //NLINR JOB
2.      /*JOBPARM JCL=NO
3.      //STEP1 EXEC SAS
4.      //SYSIN DD *
5.      DATA AKO11;
6.      INPUT T G Y;
7.      CARD;
8.      8 30 1.74
9.      8 45 1.91
10.     8 60 2.07
11.     8 90 2.24
12.     8 120 2.36
13.     8 180 1.84
14.     8 240 1.01
15.     12 30 2
16.     12 45 2.22
17.     12 60 2.12
18.     12 90 2.38
19.     12 120 2.18
20.     12 180 1.74
21.     12 240 1.50
22.     16 30 2.04
23.     16 45 2.09
24.     16 60 2.29
25.     16 90 2.51
26.     16 120 2.03
27.     16 180 1.79
28.     16 240 1.52
29.     24 30 2.35
30.     24 45 2.54
31.     24 60 2.72
32.     24 90 2.52
33.     24 120 2.12
34.     24 180 2.07
35.     24 240 1.47
36.     PROC NLIN PLOT METHOD=MARQUARDT;
37.     PARAMETERS KA=1.0E-6 TO 1.0E-4
38.     BY 1.0E-6 KB=1.0E-8 TO 1.0E-7;
39.     A=1+KA*G*T*60;
40.     B=1+KB*G*G*T*60;
41.     MODEL Y=A/B;
42.     DER.KA=G*T*60/B;
43.     DER.KB=-G*G*T*60*A/(B*B);
44.     //
```

APPENDIX H. NLIN AND REG PROGRAMS FOR NEW MODEL 1

The following is the summary of the NLIN and REG programs utilized for the regression of New Model 1 to three sets of data. REG program is used for data yielding Gt $\leq$ 36,000. NLIN program is used for data yielding Gt > 36,000.

REG Program Based on Equation 55 (New Model 1, Stage 1) for Data Set 1

```
 1.      //NLINR JOB
 2.      /*JOBPARM JCL=NO
 3.      //STEP1 EXEC SAS
 4.      //SYSIN DD *
 5.      DATA N14;
 6.      INPUT T G Y;
 7.      X=G*T*60;
 8.      CARD;
 9.      0 4.2 1
10.      0 4.2 1
11.      0 4.2 1
12.      0 4.2 1
13.      0 22.6 1
14.      0 22.6 1
15.      0 22.6 1
16.      0 42.2 1
17.      0 42.2 1
18.      0 42.2 1
19.      0 65.7 1
20.      0 65.7 1
21.      0 65.7 1
22.      0 65.7 1
23.      0 144.3 1
24.      0 144.3 1
25.      0 144.3 1
26.      3 4.2 1.279
27.      3 4.2 1.014
28.      3 4.2 1.12
29.      3 4.2 1.053
30.      3 22.6 0.998
31.      3 22.6 1.076
32.      3 22.6 1.152
33.      3 42.2 1.315
34.      3 42.2 1.009
35.      3 42.2 1.527
36.      3 65.7 0.942
37.      3 65.7 1.212
38.      3 65.7 1.109
39.      3 65.7 1.168
40.      3 144.3 1.585
```

41. 3 144.3 1.192
42. 3 144.3 1.273
43. 5 4.2 1.143
44. 5 4.2 1.075
45. 5 4.2 1.019
46. 5 22.6 1.182
47. 5 22.6 1.056
48. 5 22.6 1.06
49. 5 44.2 1.286
50. 5 44.2 1.033
51. 5 44.2 1.577
52. 5 65.7 1.05
53. 5 65.7 1.229
54. 5 65.7 1.215
55. 5 65.7 1.263
56. 5 144.3 1.442
57. 5 144.3 1.183
58. 5 144.3 1.394
59. 10 4.2 1.177
60. 10 4.2 0.957
61. 10 4.2 1.443
62. 10 4.2 1.214
63. 10 22.6 1.18
64. 10 22.6 1.4
65. 10 22.6 1.129
66. 10 42.2 1.505
67. 10 42.2 1.201
68. 10 42.2 1.446
69. 10 65.7 1.085
70. 10 65.7 1.668
71. 10 65.7 1.448
72. 10 65.7 1.324
73. 15 4.2 1.077
74. 15 4.2 1.074
75. 15 4.2 1.231
76. 15 4.2 1.315
77. 15 22.6 1.614
78. 15 22.6 1.204
79. 15 22.6 1.635
80. 15 42.2 1.222

```
 81.      15 42.2 1.542
 82.      20 4.2 1.561
 83.      20 4.2 1.14
 84.      20 4.2 1.807
 85.      20 4.2 1.418
 86.      20 22.6 1.644
 87.      20 22.6 1.196
 88.      25 4.2 1.28
 89.      25 4.2 1.199
 90.      25 4.2 2.334
 91.      25 4.2 1.443
 92.      25 22.6 1.735
 93.      25 22.6 1.55
 94.      25 22.6 1.468
 95.      30 4.2 1.282
 96.      30 4.2 1.417
 97.      30 4.2 2.474
 98.      30 4.2 1.483
 99.      45 4.2 1.558
100.      45 4.2 1.473
101.      45 4.2 1.828
102.      45 4.2 1.562
103.      90 4.2 1.683
104.      90 4.2 2.777
105.      PROC REG;
106.      MODEL Y=X;
107.      RESTRICT INTERCEPT=1;
108.      //
```

REG Program Based on Equation 55 (New Model 1, Stage 1) for Data Set 2

```
1.      //NLINR JOB
2.      /*JOBPARM JCL=NO
3.      //STEP1 EXEC SAS
4.      //SYSIN DD *
5.      DATA AHN11;
6.      INPUT T G Y;
7.      X=G*T*60;
8.      CARD;
9.      0 22.6 1
10.     0 22.6 1
11.     0 22.6 1
12.     0 65.7 1
13.     0 65.7 1
14.     0 65.7 1
15.     1 22.6 1.025
16.     3 22.6 0.985
17.     5 22.6 1.142
18.     10 22.6 1.432
19.     15 22.6 1.655
20.     20 22.6 2.949
21.     25 22.6 3.738
22.     1 22.6 1.051
23.     3 22.6 0.993
24.     5 22.6 1.150
25.     15 22.6 1.92
26.     20 22.6 2.539
27.     25 22.6 3.883
28.     1 22.6 1.247
29.     3 22.6 1.318
30.     5 22.6 1.655
31.     10 22.6 1.586
32.     15 22.6 1.809
33.     20 22.6 2.835
34.     25 22.6 4.796
35.     1 65.7 0.997
36.     3 65.7 1.195
37.     5 65.7 1.834
38.     1 65.7 1.307
39.     3 65.7 1.304
40.     5 65.7 1.874
41.     10 65.7 3.231
42.     1 65.7 1.394
43.     3 65.7 1.547
44.     5 65.7 2.003
45.     10 65.7 3.082
46.     PROC REG;
47.     MODEL Y=X;
48.     RESTRICT INTERCEPT=1;
49.     //
```

NLIN Program Based on Equation 61 (New Model 1, Stage 1) for Data Set 3

```
 1.     //NLINR JOB
 2.     /*JOBPARM JCL=NO
 3.     //STEP1 EXEC SAS
 4.     //SYSIN DD *
 5.     DATA AKN11;
 6.     INPUT T G Y;
 7.     CARD;
 8.     8 30 1.74
 9.     8 45 1.91
10.     8 60 2.07
11.     12 30 2
12.     12 45 2.22
13.     16 30 2.04
14.     PROC NLIN PLOT METHOD=MARQUARDT;
15.     PARAMETERS K0=1.0E-6 TO 1.0E-4 BY 1.0E-6;
16.     A=SQRT(1+4*K0*G*T*60);
17.     MODEL Y=(1+A)/2;
18.     DER.K0=G*T*60/A;
19.     //
```

NLIN Program Based on Equation 67 (New Model 1, Stage 2) for Data Set 1

```
 1.     //NLINR JOB
 2.     /*JOBPARM JCL=NO
 3.     //STEP1 EXEC SAS
 4.     //SYSIN DD *
 5.     DATA N121;
 6.     INPUT T G Y;
 7.     CARD;
 8.     10 144.3 1.737
 9.     10 144.3 1.25
10.     10 144.3 1.636
11.     15 65.7 1.359
12.     15 65.7 1.722
13.     15 65.7 1.937
14.     15 65.7 1.773
15.     15 144.3 1.883
16.     15 144.3 1.786
17.     15 144.3 2.117
18.     20 42.2 1.917
19.     20 42.2 1.401
20.     20 42.2 1.745
21.     20 65.7 1.289
22.     20 65.7 1.815
23.     20 65.7 2.632
24.     20 65.7 1.749
25.     20 144.3 2.082
26.     20 144.3 1.691
27.     20 144.3 1.678
28.     25 42.2 2.591
29.     25 42.2 1.456
30.     25 42.2 1.98
31.     25 65.7 1.452
32.     25 65.7 1.961
33.     25 65.7 2.311
34.     25 65.7 2.313
35.     25 144.3 2.461
36.     25 144.3 2.486
37.     25 144.3 2.361
38.     30 22.6 2.141
39.     30 22.6 1.573
40.     30 22.6 1.854
```

```
41.      30 42.2 2.689
42.      30 42.2 1.161
43.      30 42.2 1.992
44.      30 65.7 1.903
45.      30 65.7 2.273
46.      30 65.7 2.637
47.      30 65.7 2.476
48.      30 144.3 2.299
49.      30 144.3 2.546
50.      30 144.3 2.656
51.      45 22.6 2.879
52.      45 22.6 1.85
53.      45 22.6 2.086
54.      45 42.2 4.017
55.      45 42.2 2.17
56.      45 42.2 3.572
57.      45 65.7 2.168
58.      45 65.7 2.445
59.      45 65.7 4.514
60.      45 65.7 3.013
61.      45 144.3 3.371
62.      45 144.3 3.6
63.      90 22.6 6.001
64.      90 22.6 3.792
65.      90 42.2 5.443
66.      90 42.2 3.67
67.      90 65.7 7.525
68.      90 65.7 6.286
69.      90 144.3 3.502
70.      90 144.3 3.929
71.      90 144.3 3.72
72.      PROC NLIN PLOT METHOD=MARQUARDT;
73.      PARAMETERS KA=1.0E-6 TO 1.0E-4
74.      KB=1.0E-8 TO 1.0E-7;
75.      C0=36000;
76.      K0=0.000015896;
77.      X=EXP(KA*(G*T*60-C0));
78.      A=-(KA*G)/(1+K0*C0)+KB*G*G*(1-X);
79.      B=-G/(1+K0*C0)-KB*G*G*(G*T*60-C0)*X;
80.      C=-KA*G*X;
81.      D=-G*X*(1+KA*(G*T*60-C0));
82.      E=G*G*(1-X);
83.      MODEL Y=C/A;
84.      DER.KA=(D*A-C*B)/(A*A);
85.      DER.KB=(-C*E)/(A*A);
86.      //
```

NLIN Program Based on Equation 67 (New Model 1, Stage 2) for Data Set 2

```
1.      //NLINR JOB
2.      /*JOBPARM JCL=NO
3.      //STEP1 EXEC SAS
4.      //SYSIN DD *
5.      DATA AHN12;
6.      INPUT T G Y;
7.      CARDS;
8.      30 22.6 4.338
9.      30 22.6 3.669
10.     30 22.6 5.878
11.     15 65.7 3.667
12.     20 65.7 6.138
13.     30 65.7 7.874
14.     15 65.7 4.068
15.     20 65.7 6.063
16.     25 65.7 10.060
17.     30 65.7 9.034
18.     15 65.7 4.5
19.     20 65.7 7.651
20.     25 65.7 10.333
21.     30 65.7 11.341
22.     PROC NLIN PLOT METHOD=MARQUARDT;
23.     PARAMETERS KA=1.0E-6 TO 1.0E-4
24.     KB=1.0E-9 TO 1.0E-7;
25.     C0=36000;
26.     K0=0.00006335;
27.     X=EXP(KA*(G*T*60-C0));
28.     A=-(KA*G)/(1+K0*C0)+KB*G*G*(1-X);
29.     B=-G/(1+K0*C0)-KB*G*G*(G*T*60-C0)*X;
30.     C=-KA*G*X;
31.     D=-G*X*(1+KA*(G*T*60-C0));
32.     E=G*G*(1-X);
33.     MODEL Y=C/A;
34.     DER.KA=(D*A-C*B)/(A*A);
35.     DER.KB=(-C*E)/(A*A);
36.     //
37.
```

NLIN Program Based on Equation 46 (New Model 1, Stage 2) for Data Set 3

```
1.      //NLINR JOB
2.      /*JOBPARM JCL=NO
3.      //STEP1 EXEC SAS
4.      //SYSIN DD *
5.      DATA AKN12;
6.      INPUT T G Y;
7.      CARD;
8.      8 90 2.24
9.      8 120 2.36
10.     8 180 1.84
11.     8 240 1.01
12.     12 60 2.12
13.     12 90 2.38
14.     12 120 2.18
15.     12 180 1.74
16.     12 240 1.50
17.     16 45 2.09
18.     16 60 2.29
19.     16 90 2.51
20.     16 120 2.03
21.     16 180 1.79
22.     16 240 1.52
23.     24 30 2.35
24.     24 45 2.54
25.     24 60 2.72
26.     24 90 2.52
27.     24 120 2.12
28.     24 180 2.07
29.     24 240 1.47
30.     PROC NLIN PLOT METHOD=MARQUARDT;
31.     PARAMETERS KA=1.0E-6 TO 1.0E-4
32.     BY 1.0E-6 KB=1.0E-8 TO 1.0E-7;
33.     A=1+KA*G*T*60;
34.     B=1+KB*G*G*T*60;
35.     MODEL Y=A/B;
36.     DER.KA=G*T*60/B;
37.     DER.KB=-G*G*T*60*A/(B*B);
38.     //
```

APPENDIX I. NLIN PROGRAMS FOR NEW MODEL 2

The following is the summary of the NLIN programs utilized for the regression of New Model 2 to three sets of data.

NLIN Program Based on Equation 69 for Data Set 1

```
 1.     //NLINR JOB
 2.     /*JOBPARM JCL=NO
 3.     //STEP1 EXEC SAS
 4.     //SYSIN DD *
 5.     DATA N22;
 6.     INPUT T G Y;
 7.     CARDS;
 8.     0 4.2 1
 9.     0 4.2 1
10.     0 4.2 1
11.     0 4.2 1
12.     0 22.6 1
13.     0 22.6 1
14.     0 22.6 1
15.     0 42.2 1
16.     0 42.2 1
17.     0 42.2 1
18.     0 65.7 1
19.     0 65.7 1
20.     0 65.7 1
21.     0 65.7 1
22.     0 144.3 1
23.     0 144.3 1
24.     0 144.3 1
25.     3 4.2 1.279
26.     3 4.2 1.014
27.     3 4.2 1.12
28.     3 4.2 1.053
29.     3 22.6 0.998
30.     3 22.6 1.076
31.     3 22.6 1.152
32.     3 42.2 1.315
33.     3 42.2 1.009
34.     3 42.2 1.527
35.     3 65.7 0.942
36.     3 65.7 1.212
37.     3 65.7 1.109
38.     3 65.7 1.168
39.     3 144.3 1.585
40.     3 144.3 1.192
```

41. 3 144.3 1.273
42. 5 4.2 1.143
43. 5 4.2 1.075
44. 5 4.2 1.019
45. 5 22.6 1.182
46. 5 22.6 1.056
47. 5 22.6 1.06
48. 5 44.2 1.286
49. 5 44.2 1.033
50. 5 44.2 1.577
51. 5 65.7 1.05
52. 5 65.7 1.229
53. 5 65.7 1.215
54. 5 65.7 1.263
55. 5 144.3 1.442
56. 5 144.3 1.183
57. 5 144.3 1.394
58. 10 4.2 1.177
59. 10 4.2 0.957
60. 10 4.2 1.443
61. 10 4.2 1.214
62. 10 22.6 1.18
63. 10 22.6 1.4
64. 10 22.6 1.129
65. 10 42.2 1.505
66. 10 42.2 1.201
67. 10 42.2 1.446
68. 10 65.7 1.085
69. 10 65.7 1.668
70. 10 65.7 1.448
71. 10 65.7 1.324
72. 10 144.3 1.737
73. 10 144.3 1.25
74. 10 144.3 1.636
75. 15 4.2 1.077
76. 15 4.2 1.074
77. 15 4.2 1.231
78. 15 4.2 1.315
79. 15 22.6 1.614
80. 15 22.6 1.204

81.	15	22.6	1.635
82.	15	42.2	1.222
83.	15	42.2	1.542
84.	15	65.7	1.359
85.	15	65.7	1.722
86.	15	65.7	1.937
87.	15	65.7	1.773
88.	15	144.3	1.883
89.	15	144.3	1.786
90.	15	144.3	2.117
91.	20	4.2	1.561
92.	20	4.2	1.14
93.	20	4.2	1.807
94.	20	4.2	1.418
95.	20	22.6	1.644
96.	20	22.6	1.196
97.	20	42.2	1.917
98.	20	42.2	1.401
99.	20	42.2	1.745
100.	20	65.7	1.289
101.	20	65.7	1.815
102.	20	65.7	2.632
103.	20	65.7	1.749
104.	20	144.3	2.082
105.	20	144.3	1.691
106.	20	144.3	1.678
107.	25	4.2	1.28
108.	25	4.2	1.199
109.	25	4.2	2.334
110.	25	4.2	1.443
111.	25	22.6	1.735
112.	25	22.6	1.55
113.	25	22.6	1.468
114.	25	42.2	2.591
115.	25	42.2	1.456
116.	25	42.2	1.98
117.	25	65.7	1.452
118.	25	65.7	1.961
119.	25	65.7	2.311
120.	25	65.7	2.313

121.	25	144.3	2.461
122.	25	144.3	2.486
123.	25	144.3	2.361
124.	30	4.2	1.282
125.	30	4.2	1.417
126.	30	4.2	2.474
127.	30	4.2	1.483
128.	30	22.6	2.141
129.	30	22.6	1.573
130.	30	22.6	1.854
131.	30	42.2	2.689
132.	30	42.2	1.161
133.	30	42.2	1.992
134.	30	65.7	1.903
135.	30	65.7	2.273
136.	30	65.7	2.637
137.	30	65.7	2.476
138.	30	144.3	2.299
139.	30	144.3	2.546
140.	30	144.3	2.656
141.	45	4.2	1.558
142.	45	4.2	1.473
143.	45	4.2	1.828
144.	45	4.2	1.562
145.	45	22.6	2.879
146.	45	22.6	1.85
147.	45	22.6	2.086
148.	45	42.2	4.017
149.	45	42.2	2.17
150.	45	42.2	3.572
151.	45	65.7	2.168
152.	45	65.7	2.445
153.	45	65.7	4.514
154.	45	65.7	3.013
155.	45	144.3	3.371
156.	45	144.3	3.6
157.	90	4.2	1.683
158.	90	4.2	2.777
159.	90	22.6	6.001
160.	90	22.6	3.792

```
161.      90 42.2 5.443
162.      90 42.2 3.67
163.      90 65.7 7.525
164.      90 65.7 6.286
165.      90 144.3 3.502
166.      90 144.3 3.929
167.      90 144.3 3.72
168.      PROC NLIN PLOT METHOD=MARQUARDT;
169.      PARAMETERS K0=1.0E-5 TO 1.0E-4
170.      KB=1.0E-8 TO 1.0E-7;
171.      X1=SQRT(K0*KB*G);
172.      X2=(SQRT((KB*G)/K0))/(2);
173.      X3=(SQRT((K0*G)/KB))/(2);
174.      X=EXP(2*X1*G*T*60);
175.      A=X1-KB*G+(KB*G+X1)*X;
176.      B=X2+X2*X+(X1+KB*G)*X*2*X2*G*T*60;
177.      C=X1-K0+(K0+X1)*X;
178.      D=X2-1+(1+X2)*X+(K0+X1)*X*G*T*60*2*X2;
179.      E=X3-G+(G+X3)*X+(KB*G+X1)*X*G*T*60*2*X3;
180.      F=X3+X3*X+(K0+X1)*X*G*T*60*2*X3;
181.      MODEL Y=C/A;
182.      DER.K0=(D*A-C*B)/(A*A);
183.      DER.KB=(F*A-C*E)/(A*A);
184.      //
```

NLIN Program Based on Equation 69 for Data Set 2

```
 1.      //NLINR JOB
 2.      /*JOBPARM JCL=NO
 3.      //STEP1 EXEC SAS
 4.      //SYSIN DD *
 5.      DATA AHN21;
 6.      INPUT T G Y;
 7.      CARDS;
 8.      0 22.6 1
 9.      0 22.6 1
10.      0 22.6 1
11.      0 65.7 1
12.      0 65.7 1
13.      0 65.7 1
14.      1 22.6 1.025
15.      3 22.6 0.985
16.      5 22.6 1.142
17.      10 22.6 1.432
18.      15 22.6 1.655
19.      20 22.6 2.949
20.      25 22.6 3.738
21.      30 22.6 4.338
22.      1 22.6 1.051
23.      3 22.6 0.993
24.      5 22.6 1.150
25.      15 22.6 1.92
26.      20 22.6 2.539
27.      25 22.6 3.883
28.      30 22.6 3.669
29.      1 22.6 1.247
30.      3 22.6 1.318
31.      5 22.6 1.655
32.      10 22.6 1.586
33.      15 22.6 1.809
34.      20 22.6 2.835
35.      25 22.6 4.796
36.      30 22.6 5.878
37.      1 65.7 0.997
38.      3 65.7 1.195
39.      5 65.7 1.834
40.      15 65.7 3.667
```

```
41.      20 65.7 6.138
42.      30 65.7 7.874
43.      1 65.7 1.307
44.      3 65.7 1.304
45.      5 65.7 1.874
46.      10 65.7 3.231
47.      15 65.7 4.068
48.      20 65.7 6.063
49.      25 65.7 10.060
50.      30 65.7 9.034
51.      1 65.7 1.394
52.      3 65.7 1.547
53.      5 65.7 2.003
54.      10 65.7 3.082
55.      15 65.7 4.5
56.      20 65.7 7.651
57.      25 65.7 10.333
58.      30 65.7 11.341
59.      PROC NLIN PLOT METHOD=MARQUARDT;
60.      PARAMETERS K0=1.0E-6 TO 1.0E-5
61.      KB=1.0E-8 TO 1.0E-7;
62.      X1=SQRT(K0*KB*G);
63.      X2=(SQRT((KB*G)/K0))/(2);
64.      X3=(SQRT((K0*G)/KB))/(2);
65.      X=EXP(2*X1*G*T*60);
66.      A=X1-KB*G+(KB*G+X1)*X;
67.      B=X2+X2*X+(X1+KB*G)*X*2*X2*G*T*60;
68.      C=X1-K0+(K0+X1)*X;
69.      D=X2-1+(1+X2)*X+(K0+X1)*X*G*T*60*2*X2;
70.      E=X3-G+(G+X3)*X+(KB*G+X1)*X*G*T*60*2*X3;
71.      F=X3+X3*X+(K0+X1)*X*G*T*60*2*X3;
72.      MODEL Y=C/A;
73.      DER.K0=(D*A-C*B)/(A*A);
74.      DER.KB=(F*A-C*E)/(A*A);
75.      //
76.
77.
78.
```

NLIN Program Based on Equation 70 for Data Set 3

```
 1.     //NLINR JOB
 2.     /*JOBPARM JCL=NO
 3.     //STEP1 EXEC SAS
 4.     //SYSIN DD *
 5.     DATA AKN21;
 6.     INPUT T G Y;
 7.     CARD;
 8.     8 30 1.74
 9.     8 45 1.91
10.     8 60 2.07
11.     8 90 2.24
12.     8 120 2.36
13.     8 180 1.84
14.     8 240 1.01
15.     12 30 2
16.     12 45 2.22
17.     12 60 2.12
18.     12 90 2.38
19.     12 120 2.18
20.     12 180 1.74
21.     12 240 1.50
22.     16 30 2.04
23.     16 45 2.09
24.     16 60 2.29
25.     16 90 2.51
26.     16 120 2.03
27.     16 180 1.79
28.     16 240 1.52
29.     24 30 2.35
30.     24 45 2.54
31.     24 60 2.72
32.     24 90 2.52
33.     24 120 2.12
34.     24 180 2.07
35.     24 240 1.47
36.     PROC NLIN PLOT METHOD=MARQUARDT;
37.     PARAMETERS K0=1.0E-6 TO 1.0E-4
38.     BY 1.0E-6 KB=1.0E-8 TO 1.0E-7;
39.     A=2*(1+KB*G*G*T*60);
40.     B=SQRT(1+4*K0*G*T*60*(1+KB*G*G*T*60));
41.     MODEL Y=(1+B)/A;
42.     DER.K0=G*T*60/B;
43.     DER.KB=(2*K0*G*G*G*T*T*60*60
44.     /B-2*G*G*T*60*(1+B))/(A*A);
45.     //
```